AN ABSTRACT OF THE THESIS OF

Jonathan Mackey Hanson for the degree of Doctor of Philosophy

in Geophysics presented on November 1, 1977

Title: HEAT TRANSFER EFFECTS IN FORCED GEOHEAT RECOVERY SYSTEMS

Abstract approved: Redacted for Privacy

Current investigations into forced geoheat recovery are based on hydraulic fracturing of impermeable hot dry rock formations. Forced recovery using naturally occurring fluid conductors, viz., fault zones, basaltic dikes, and open formation contacts, presents an alternate approach that may circumvent some of the difficulties associated with the hydraulic fracturing method. The latter type of system is considered in terms of the system physical-economic feasibility. The heat transfer surface area required for an economically viable forced recovery system for direct contact heating applications is estimated based on various geologic and economic parameters. The heat transfer surface area reflects the required dimensions of the subsurface system and therefore serves as an indicator of the feasibility of the system.

Heat extraction from a hot rock formation based on sheet-like flow involves a balance of the total heat transport of the heat extracting

fluid with the conductive heat transport within the rock. The heat recovery efficiency is considered in terms of an idealized flow model in order to estimate the required heat transfer surface area. Various flow characteristics adverse to heat recovery efficiency are likely to occur within the fluid conductors under consideration. These include primarily non-uniform flow within the conductor and fluid losses due to leakage from the conductor. The first order effects of these adverse flow conditions are considered in terms of the idealized flow model using analytic and semi-analytic methods. Furthermore, a significant change in fracture permeability can occur within the conductor due to the thermoelastic response of the rock formation upon cooling. This effect is estimated in terms of the idealized flow model under various flow conditions within the conductor.

The results of this work indicate that, under current economic conditions and regional geothermal gradients of 50°C/km or more, the minimum heat transfer surface area per injection/production borehole pair required for an economically viable direct-contact heating system with a 10 to 20 year system lifetime is less than 1 km^2. Under the same conditions, it is found that the minimum required heat transfer surface area for electrical power production systems is 2 to 4 times this figure.

Heat Transfer Effects in Forced Geoheat Recovery Systems

by

Jonathan Mackey Hanson

A THESIS

submitted to

Oregon State University

in partial fulfillment of
the requirements for the
degree of

Doctor of Philosophy

Completed November 1977

Commencement June 1978

APPROVED:

Redacted for Privacy

Professor of Geophysics and Mathematics

in charge of major

Redacted for Privacy

Acting Dean of School of Oceanography

Redacted for Privacy

Dean of Graduate School

Date thesis is presented November 1, 1977

Typed by Clover Redfern for Jonathan Mackey Hanson

ACKNOWLEDGMENTS

I wish to thank my major professor, Dr. Gunnar Bodvarsson, for the help and encouragement he provided throughout the preparation of this thesis and for the insight into geophysics and applied mathematics he has given during my graduate studies.

I thank Dr. F. Tom Lindstrom, Dr. Richard Couch, and Dr. David Griffiths for their helpful suggestions and comments regarding this thesis.

Discussions with fellow students Chuen-Tien Shyu, Paul Jones, Keith Wrolstad, Fran Boler, and Tom Plawman were quite valuable to my research and education.

This research was supported by the United States Energy Research and Development Administration, Contract E(45-1)-2227, Task Agreement No. 21.

TABLE OF CONTENTS

Chapter | Page

LIST OF FIGURES

LIST OF TABLES

HEAT TRANSFER EFFECTS IN FORCED GEOHEAT RECOVERY SYSTEMS

I. INTRODUCTION

During the formation and evolution of the Earth to its present state, vast quantities of heat energy have been released by several processes. Gravitational collapse of the original diffuse dust cloud, decay of radioactive isotopes, core-mantle differentiation, and tidal effects have contributed to the creation of a very large reservoir of primitive heat. It has been estimated that, in the coterminous United States alone, the outer 10 km of the Earth's crust contains 3.3×10^{25} J of thermal energy relative to the mean annual surface temperature (White and Williams, 1975). From the point of view of human energy consumption, this figure is enormous. For comparison the entire energy consumption of the United States in 1968 amounted to 6.3×10^{19} J (Stanford Research Institute, 1972). Most of the heat is buried too deeply or spread too diffusely for commercial exploitation. However, analogous to the case of petroleum and mineral resources, the near-surface distribution of heat energy is not uniform and there exist regions of sufficient heat concentration for economic recovery.

Technological advancement and increasing demand for energy during the last several decades have brought the worldwide geothermal

power generating capacity to over 1100 MWe (Kruger and Ramey, 1975). However, in spite of the advantages, development of geothermal energy in the United States has been slow. As Armstead (1973) points out, the reluctance in the past to embark upon fairly costly geothermal exploration projects is attributable, in part, to the "risk capital" associated with geothermal resource exploration. Not all geothermal fields are necessarily amenable to economic development, and in order to determine whether a field can be profitably put to use, it is necessary to expend fairly large sums in carrying out exploration. Thus, analogous with costs associated with petroleum exploration, the costs of geothermal exploration may be regarded as risk capital.

Assuming a successful geothermal field has been located and developed, one market for the energy is electrical power production. Electrical power, however, can be developed by conventional means (oil and coal fired plants, hydroelectric plants) without the need to extend risk capital.

The other possible market is non-electrical applications such as space and district heating. District heating systems per se have not been implemented to any significant degree in the United States. This reflects the condition that consumers have in the past been able to meet their space and hot water needs more cheaply with individual heating systems than with district heating systems (Karkheck et al.,

1977). Furthermore, these systems are very capital intensive, and though there exists a margin for profit, it is unlikely that extensive development of district heating will occur without some involvement by corporate or governmental bodies. The primary benefit of such systems will be the conservation of scarce conventional energy resources.

Development of Non-Electrical Applications of Geothermal Energy in the United States

The recent large increases in the cost of fossil fuels have made district heating systems and other non-electrical applications much more attractive and this trend will continue as conventional energy supplies become scarcer. Demographic projections show the urbanization trend continuing in the United States which will also favor a change to district heating (Karkheck et al., 1977). Geothermal energy used for non-electrical applications is a thermodynamically more efficient use of the resource than is electricity production. This is due to the fact that Carnot efficiency dominates power production but is not involved in direct-contact heating. As a result, a lower grade (lower temperature) resource is economically better suited for exploitation for non-electrical uses than for power production. Geographic distribution and relative occurrence of lower grade resources in the United States are much greater than higher grade resources suitable for power production (White and Williams, 1975).

It is commonly agreed that the geothermal resources that exist at a low to medium temperature (< 150°C) are at least an order of magnitude larger than those which exist at temperatures high enough to be economically used for electricity generation. As a consequence, the risk associated with exploration for low to medium temperature resources will be substantially less than for the higher grade resources.

The potential for non-electrical application of geothermal energy in the United States is large. Reistad (1975b) has estimated that 40% of the total energy requirements of the United States could be satisfied from geothermal resources within direct-contact heating at maximum temperatures of 200°C. This estimate assumes that the resource is available at each application site. The percentages for temperatures of 150°C and 100°C are 30 and 20% respectively. Detailed summaries of low-temperature applications of geoheat are presented by Reistad (1975a, 1975b), Armstead (1973), and Lienau and Lund (1974).

Forced Geoheat Recovery

Geothermal energy extraction systems fall roughly into three types: (1) free flow, (2) partially forced, or stimulated, and (3) forced recovery systems. The free flow technique is based on free flowing boreholes in naturally occurring hydrothermal systems. The driving force is thermoartesian pressure that results from density

differences due to thermal expansion and phase (liquid, gaseous, or a mixture) of the fluid within the conductor. The method is applicable where the resulting pressure head is sufficient to maintain the required borehole flow. The migration of meteoric water from the surface to the reservoir replaces the fluid lost from the system. The most notable examples of free flow systems are The Geysers, California (dry steam); Larderello, Italy (dry steam); and Wairakei, New Zealand (mixture). All three of these systems are exploited for electrical power production.

The partially forced, or stimulated, system involves down-hole pumping to compliment the natural pressure head of the system to maintain or increase the borehole flow. The Reykjavik District Heating System, which now supplies energy for domestic heating for more than 100,000 people in the capital of Iceland, is a low temperature operation where large scale resource stimulation by borehole pumping is being applied. This system has been in operation for more than three decades and represents one of the most successful commercial applications of geoheat. As in the case of free convective systems, the stimulated system relies on a natural fluid recharge to the system.

The third type of geoheat recovery, and the most recent to come under investigation, is the forced geoheat production system. This type of system relies on an artificial recharge of the heat extracting fluid into the reservoir. Unlike the free and stimulated systems, in

which the fluid flows through natural fluid conducting openings, the forced recovery system relies, at least partially, on artificial openings created by hydraulic fracturing or other pressurizing operations. As the forced recovery system does not rely on the occurrence of a naturally convecting system, there exists the possibility of extracting heat at suitable temperatures over much wider areas than has been possible so far. The advantages of such a system are obvious when one considers the low transportability of thermal waters and steam. Steam can be transported economically over distances on the order of only a few kilometers. Thermal water can be transported at most a few tens of kilometers.

The Hot Dry Rock Concept

The main investigation into forced geoheat recovery currently being undertaken is the "hot dry rock" project at the Los Alamos Scientific Laboratory (LASL) in New Mexico. The method is based on drilling two holes into hot, relatively impermeable rock, connecting them at depth through a large crack produced by hydraulic fracturing, and then circulating pressurized water through this connected system to recover heat from the rock. In 1971, a field investigation was undertaken to determine a suitable drilling site. The chosen site, at Fenton Hill, is situated just west of the Valles Caldera in northern New Mexico. Drilling and hydraulic fracturing were completed at the

site, with a measurable flow connection between the two boreholes, in 1977. The boreholes are approximately 3000 m deep. A detailed description of the engineering aspects of the experiment is given by Blair et al. (1976). The LASL project is directed toward electrical power production.

The economic viability of such a system, which remains to be shown, depends on the feasibility of creating a sufficient fracture permeability and fluid-rock contact area required to extract the total heat energy necessary to amortize the initial capital investment and to cover the recurring costs associated with operation and maintenance. The viability of the process is highly dependent on the occurrence of thermal stress cracking at the fracture boundary for fracture extension into the hot rock mass. Theoretical results (Harlow and Pracht, 1972) indicate that thermal stress cracking will occur in this type of system. Testing at the Fenton Hill site is in a very early stage at the time of this writing, and as yet, it is uncertain whether thermal stress cracking is occurring in this system.

An Alternate Approach to Forced Geoheat Recovery

The use of natural fluid conductors presents an alternate approach to forced geoheat extraction that may circumvent some of the difficulties associated with the hydraulic fracture method (Bodvarsson, 1976; Bodvarsson and Hanson, 1976, 1977). Four types of structures

are of primary interest, viz., quasi-vertical conductors such as (1) fault zones and (2) basaltic dikes with longitudinal fluid conductivity and quasi-horizontal structures such as (3) open formation contacts, mainly between basaltic lava beds and (4) permeable sedimentary horizons. Extensive use of sedimentary horizons in forced geoheat recovery for district heating is in progress in France (DGRST, 1976; Coulbois and Herault, 1975).

The present work investigates the feasibility of using the fluid conductors of the types (1) through (3) listed above in forced geoheat recovery for low temperature, non-electrical applications. The efficiency of heat extraction from the hot rock formation is considered in terms of the heat transfer characteristics of a sheet-like flow system. The efficiency of the system will determine the total thermal energy produced over a given system lifetime. For such a system to be economically viable, the revenues must cover the costs of the system, which include capital costs (drilling, well head equipment, piping, etc.) and recurring costs (interest on capital expenditure, operation and maintenance, etc.). The purpose of this work is to estimate the required heat transfer surface area (i.e. fluid-rock contact area) for a forced recovery system based on various economic and geologic parameters. The heat transfer surface area reflects the required dimensions of the system and therefore serves as an indicator to the feasibility of the system.

The work is directed in general toward potential use in the western United States and specifically to the Pacific Northwest. This geographic area is characterized by relatively large areas of above normal crustal heat flow (Sass et al., 1971; White and Williams, 1975; Hull et al., 1977) and exhibits specific geologic conditions consistent with the type of forced geoheat recovery system under investigation.

The shaded region in Figure 1 represents the area of the western United States exhibiting above normal crustal heat flow. The world-wide average, or "normal", crustal heat flow for continental areas is 61.5 mW/m^2 (Lee, 1970) corresponding to a geothermal temperature gradient of roughly 30°C/km.

Chapter II discusses the geologic characteristics of the natural fluid conductors being considered. Attention is given primarily to the observed permeability characteristics of these structures. In Chapter III, the fundamental heat transport equations are developed. This is followed by the introduction of the "first-order" heat extraction model which is used throughout the remainder of the work. The chapter concludes with the derivation of the rock and fluid temperature field equations for a sheet-like flow system based on this model.

Chapter IV discusses the effect of adverse flow characteristics within the fluid conductor on the behavior of the temperature field of the fluid. Non-uniform flow within the conductor and fluid loss due to

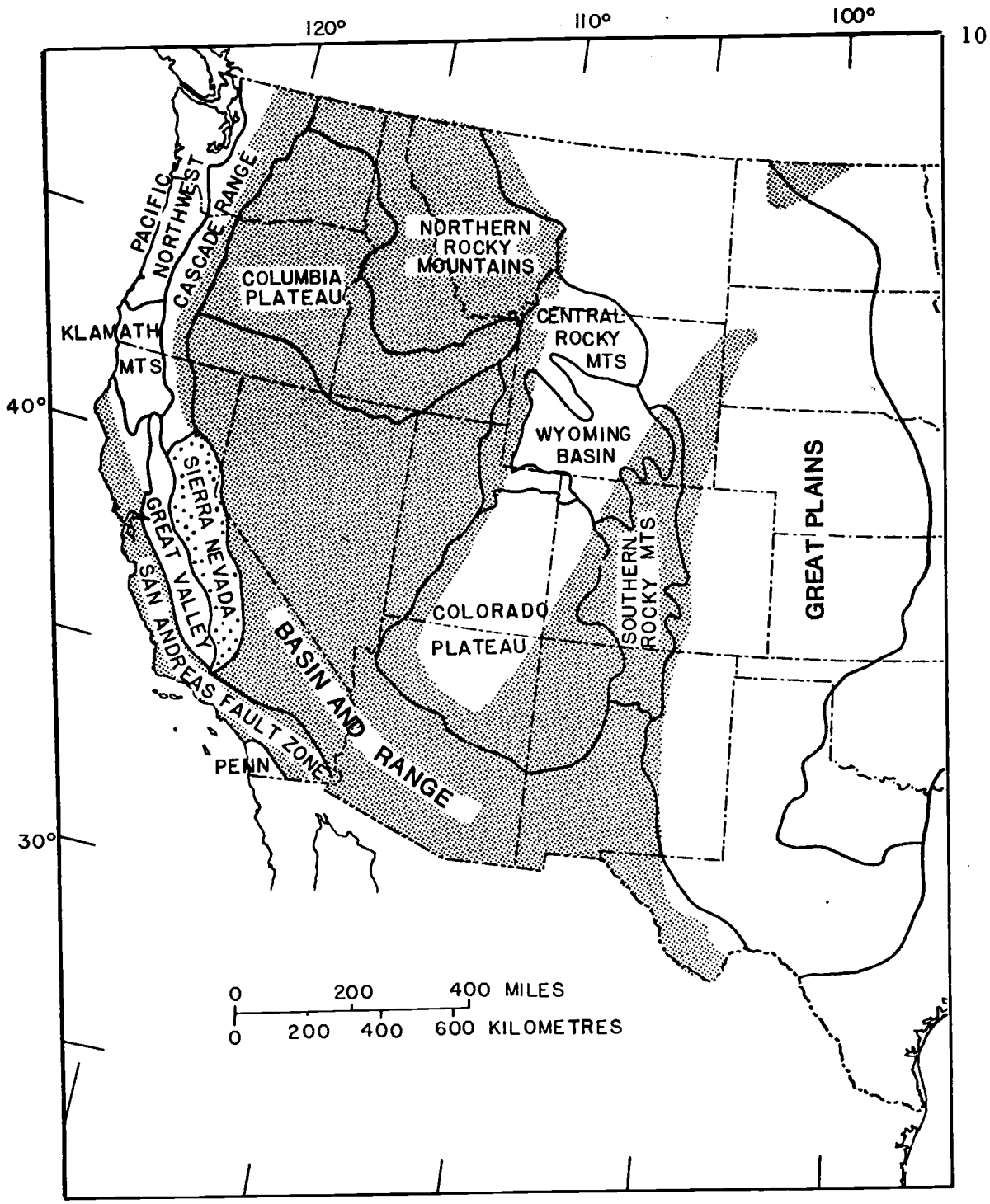

Figure 1. Map showing probable extent of above average crustal heat flow (shaded region) in the western United States. Physiographic provinces do not necessarily represent heat flow provinces (from White and Williams, 1975).

leakage from the conductor are considered in the analysis.

The ability of a forced recovery system based on sheet-like flow to meet a constant or seasonal power demand by varying well head flow rate is considered in Chapter V. Chapter VI derives the thermo-elastic response of an ideal fracture to cooling and the resulting effect on fracture permeability.

Heat recovery system design and economics, based on the first-order model, are discussed in Chapter VII. The absolute lower bound on the fluid-rock contact area required for an economically viable system is computed as a function of system lifetime, economic conditions, and geologic setting. This is followed by a discussion of adverse flow effects with regard to system feasibility.

II. NATURAL FLUID CONDUCTORS

Fault Zones

Many fault zones exhibit a substantial fluid conductivity. This is demonstrated quite well in the Basin and Range Province where a considerable number of geothermal convection systems appear to be associated with or controlled by normal master faults of the region (Hose and Taylor, 1974). Chemical and thermal alteration of the rock adjacent to and within fault zones containing active or historically active hydrothermal convection systems indicate that many systems have lifetimes on the order of thousands to tens of thousands of years. This observation suggests that the effective fluid-rock contact area within such systems may be quite large.

There is evidence in southern Idaho that in the past, extensive hot spring activity has occurred at the sites of a number of faults which transect siliceous volcanic areas. Current hot spring activity in this region is also associated with major fault zones (Warner, 1975; Williams et al., 1975).

Very little is known about the in situ permeability conditions of fault zones. Undoubtedly, intergranular type percolation through fault gouge or breccia and/or a fracture type percolation can occur depending on the characteristics of the fracture zone. There is some indication that normal faults contain gouge that consists of broken, crushed,

and finely ground rock material that changes in character with depth. In the shallow parts of large faults, the gouge is commonly several centimeters to a few meters thick and consists of sheared plastic clay and sheared breccia containing rolled pebble- and cobble-sized rock fragments. Within deeper parts of the same faults, the gouge is commonly only a few centimeters thick and consists mainly of clay that is hardened and brittle rather than plastic. There is little or no brecciation of the adjacent rock but a crude foliation may result from shearing (Proffett, 1977).

It is not known at what depth a fracture opening and/or fault gouge becomes impermeable to fluid flow. It is reasonable to assume that the increase in lithostatic pressure with depth and the regional tectonic stress will play a dominant role. Field data based on borehole pressure testing (Snow, 1968) supports the assumption that fracture permeability decreases with depth due to overburden stress.

Dikes in Flood Basalt Areas

The most extensive swarms of Cenozoic basaltic dikes in the United States occur in the adjoining parts of northeastern Oregon, southeastern Washington, and western Idaho. From the number of dikes that are visible in well exposed areas of pre-Tertiary rocks within the swarms, it has been estimated that at least 20,000 dikes occur at the level of the regional unconformity beneath the Columbia

River Basalt. Trends in dike orientation suggest that the same tectonic forces that prevailed throughout the Basin and Range Province were also responsible for dike emplacement in this area (Taubeneck, 1969). Little is known about the hydrology of dikes in the United States and there is no direct evidence that the mafic dikes of the Columbia River Basalt host hydrothermal circulation systems.

There is considerable field evidence that many basaltic dikes in north-central Iceland have a substantial fluid conductivity. Most of the natural hot springs in this region are controlled by dikes and a large number of boreholes have been drilled to extract thermal water from the dikes (Bodvarsson, 1961). The geologic characteristics of dikes associated with flood basalt areas in the United States appear to be similar to those of dikes in the flood basalt regions of Iceland. Thus, one may infer similarities in the permeability characteristics of dikes in the two regions.

Formation Contacts

The Columbia River and Snake River flood basalts in Oregon, Washington and Idaho consist of layered horizontal lava flows of individual thicknesses ranging on the order of meters to tens of meters. Contacts between individual lava beds quite frequently exhibit a high degree of fluid conductivity through an interconnected system of pipes and other related openings. This is evidenced in the

Snake River Canyon in Idaho (Tolman, 1937). There is also considerable field evidence in Iceland that open contacts found at various depths in flood basalt formations associated with geothermal systems allow the thermal water to flow along the lava-bed contacts over very great horizontal distances (Bodvarsson, 1961).

The lava sequence of quaternary basalts extruded on and near the flanks of stratovolcanoes of the southern Cascade Range in Washington form highly permeable strata. Individual flows range from 1 to 50 meters thick, the average being 2 meters in thickness. Contacts are rarely exposed except in postglacially incised valleys (Hammond et al., 1975).

III. FIRST-ORDER HEAT RECOVERY MODEL FOR SHEET-LIKE FLOW

Heat extraction from hot subsurface formations, for the type of system being considered, involves injection of water into suitable fluid conductors at one location and extraction of the thermal water at another location. Figure 2 shows two possible configurations. The boreholes are drilled to intersect the conductor at a sufficient depth and circulation is obtained by pumping. For the case of quasi-vertical conductors, circulation may be enhanced by buoyancy forces created by density differences between the cooler injected water and the hotter water within the conductor.

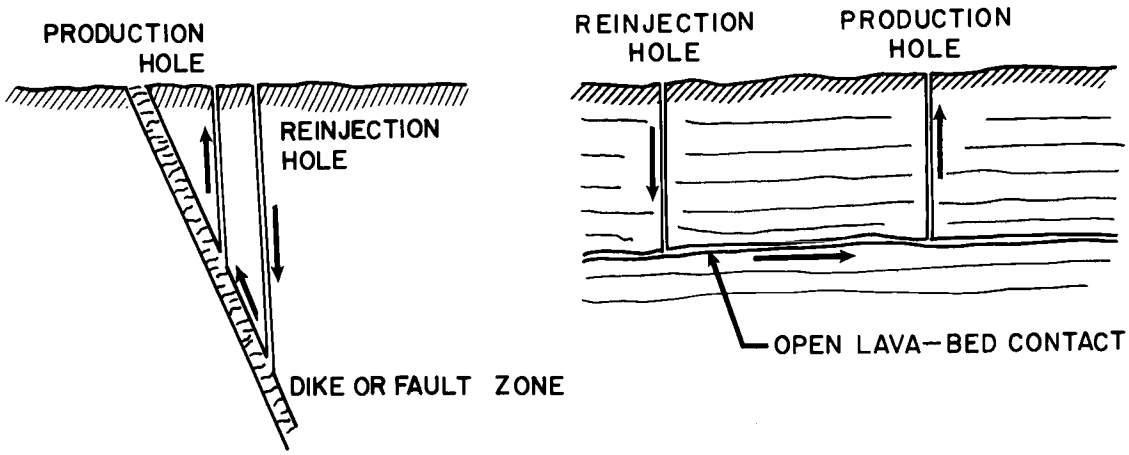

Figure 2. Two possible configurations for forced recovery using natural fluid conductors.

The flow geometry within the conductor depends on several factors and may be quite complex. These factors include the injection and production borehole location, borehole spacing, and the permeability characteristics of the fluid conductor. In addition, significant time dependent effects on permeability due to thermoelastic response of the fracture walls caused by temperature transients and/or chemical deposition or solution within the conductor openings are likely to occur. Because of the uncertainty of the permeability characteristics associated with natural fluid conductors, it is felt that an attempt at the present time to model the complex convective processes within such systems may be premature. Such an approach should be considered only after considerably more field data is available on these specific parameters. It is expected that the permeability characteristics will be, to some degree, site specific.

We have chosen instead to approach the problem of forced geoheat recovery more from the standpoint of physical-economic system feasibility. To cover capital and operational costs, a forced recovery system must produce a sufficient amount of energy in the form of thermal water during a prescribed system lifetime. The total produced thermal energy depends primarily on the effective fluid-rock contact area within the conductor. The effective contact area required reflects the dimensions of the subsurface heat extraction system, and consequently, serves as an indicator of the

feasibility of the operation. The physical-economic analysis presented in this work is based on a simplified flow geometry within the conductor. This leads to a useful approximate, or "first-order", heat extraction model for sheet-like flow.

The present chapter develops the equations governing heat transport for the sheet-like fluid flow system which serves as our first-order heat recovery model. The chapter concludes with the derivation of the production temperature equations assuming an optimal flow configuration. This particular model will maximize the total heat production and therefore will yield the lower bound on the required fluid-rock contact area necessary for the economic viability of the system. Following chapters consider deviations from such optimal flow conditions and the resulting effects on the system production characteristics.

Basic Heat Transport Theory

In the theoretical development of this and following chapters, we assume that the fluid conductor is quasi-flat and that the adjacent rock formation is homogeneous and isotropic. The geologic structures discussed in Chapter III, viz., fault zones, basaltic dikes and formation contacts, are generally found to have a planar geometry. Furthermore, the fluid is assumed to remain in the liquid phase within the conductor.

Heat Diffusion Equation

It is useful to highlight the derivation of the well known diffusion equation that governs energy transport within the rock mass bounding the fluid conductor. Assuming a stationary rock mass, the conservation of thermal energy in some arbitrary domain B bounded by the surface Σ requires that the rate of increase of enthalpy in B is equal to the heat flow into B across Σ plus the rate of heat production within B. In integral form

$$\partial_t \int_B \rho_r \sigma_r T dV = - \int_\Sigma \vec{h} \cdot \hat{n} dA + \int_B \rho_r S dV \qquad (3.1)$$

where ρ_r is the rock density, σ_r is the specific heat (at constant pressure) of the rock, $\vec{h}$ is the heat flow per unit area, and S is the specific source density per unit mass of the rock. The temperature field of the rock is given by T. The material constants ρ_r and σ_r are assumed to be independent of time.

Using Gauss' integral theorem the surface integral in equation (3.1) can be transformed to a volume integral, resulting in

$$\int_B \{\rho_r \sigma_r \partial_t T + \nabla \cdot \vec{h} - \rho_r S\} dV = 0 \qquad (3.2)$$

Since the domain B is arbitrary the integrand must be identically

zero, so that

$$\rho_r \sigma_r \partial_t T + \nabla \cdot \vec{h} - \rho_r S = 0 \tag{3.3}$$

Assuming the empirical Fourier heat conduction law, the heat flow $\vec{h}$ can be expressed in terms of T, or

$$\vec{h} = -k_r \nabla T \tag{3.4}$$

where k_r is the coefficient of thermal conductivity of the rock. In general k_r is a tensor. For an isotropic solid k_r reduces to a scalar.

Substituting expression (3.4) into equation (3.3) results in the second order partial differential equation governing the temperature field in the rock.

$$\rho_r \sigma_r \partial_t T - \nabla \cdot (k_r \nabla T) = \rho_r S \tag{3.5}$$

For a homogeneous isotropic solid in which there are no sources, the above expression reduces to the standard homogeneous form of the diffusion equation

$$\frac{1}{a_r} \partial_t T - \nabla^2 T = 0 \tag{3.6}$$

where a_r is the thermal diffusivity of the rock defined by

$$a_r = \frac{k_r}{\rho_r \sigma_r}$$

Heat Transfer Boundary Condition

The energy transfer between a fluid flowing in a fracture, or a similar structure, and the surrounding rock mass is governed by a balance between conductive heat flow in the rock and the total heat transport in the fluid.

The ratio of the convective to conductive transport in the fluid is given by the characteristic Péclet number defined by

$$Pe = \frac{\sigma_f q}{k_f}$$

where σ_f is the specific heat of the fluid, q is the mass flow per unit length of fracture, and k_f is the thermal conductivity of the fluid. For fracture flow rates greater than 0.01 kg/(m. sec), the Péclet number is greater than 70. Consequently, the convective transport of the fluid dominates the conductive transport within the fluid by a factor of almost 10^2. The conductive transport within the fluid is therefore ignored for flow rates of this magnitude.

Figure 3 shows a small fluid element flowing within a fracture opening of width w. The velocity of the fluid averaged over the fracture width is $\vec{v}$. To account for the effect of debris filling the

fracture spaces, we assume a constant volume porosity θ within the region between the fracture walls. Referring to this figure, the balance of convective heat transport in the fluid with the conductive transport in the rock, required by the conservation of energy, is given by

$$\{\rho_f \sigma_f \theta + \rho_r \sigma_r (1-\theta)\}\partial_t (wT_f) + \rho_f \sigma_f \theta \vec{v} \cdot \nabla_2 (wT_f) = 2k_r \partial_y T\big|_{y\downarrow 0} \qquad (3.7)$$

where

$$\nabla_2 = \hat{x}\partial_x + \hat{z}\partial_z$$

and T_f is the temperature of the fluid averaged across the fracture width and ρ_f is the density of the fluid. An open fracture, in which there is no debris, corresponds to $\theta = 1$.

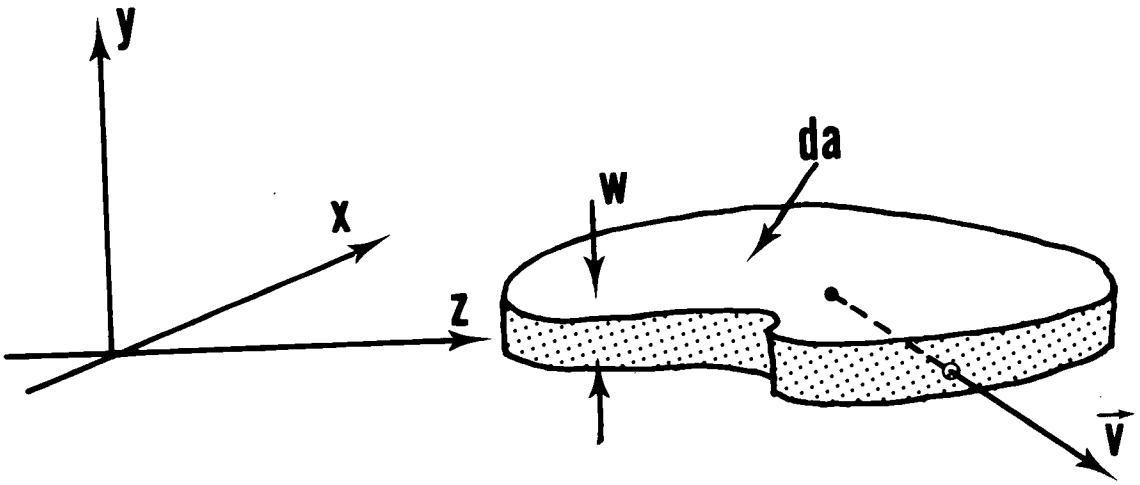

Figure 3. Fluid element within conductor, showing Cartesian coordinate system.

The right hand side of equation (3.7) is the conductive heat flow per unit area from the rock to the fluid and implicitly assumes that the rock temperature field is symmetric with respect to the plane of the fluid conductor. The left hand side of this expression represents the net rate of change of enthalpy per unit fracture wall area of the volume element of fluid and debris. The second term on the left hand side is the change in enthalpy associated with the mass transfer of the fluid into or out of the element. The temperature of the solid debris within the fracture spaces is assumed to be equal to the temperature of the interstitial fluid.

We will limit the discussion to fracture widths on the order of millimeters to tens of millimeters. The thermal relaxation time for water then varies from several seconds to several minutes (see Appendix D). Considering the fluid velocities involved for flow rates on the order of 0.01 to 0.1 kg/(m. sec), these relaxation times correspond to thermal relaxation distances of several centimeters to a few meters. Thus, to good approximation, the temperature of the fluid can be taken to be isothermal with respect to the y coordinate and can be set equal to the temperature of the adjacent rock, or

$$T_f(x, z, t) = T(x, y, z, t)\Big|_{y \downarrow 0}$$

With the simplification of a constant fracture width, equation (3.7) becomes

$$\{\rho_f\theta + \frac{\rho_r\sigma_r}{\sigma_f}(1-\theta)\}w\partial_t T + \vec{q}\cdot\nabla_2 T = \frac{2k_r}{\sigma_f}\partial_y T, \quad y \downarrow 0 \tag{3.8}$$

where the mass flow per unit length of fracture is defined by

$$\vec{q} = w\theta\rho_f\vec{v}$$

The coordinate system shown in Figure 3 will be used in all subsequent calculations.

First-Order Heat Recovery Model

Fluid flow within sheet-like conductors will be of a non-uniform quasi-potential type. For the purpose of estimating the required fluid-rock contact area, we simplify the flow geometry by assuming a uni-directional flow between the injection and production ports. On this model, fluid at a constant temperature is injected into the conductor by a line source located at $x = 0$ and recovered at a line sink located at some position $x > 0$. We will refer to the source and sink as system "ports". The fluid flow is in the positive x direction. The initial rock formation temperature is assumed to be a function of the x coordinate only. Therefore, this first-order model can be represented mathematically by the following initial and boundary value problem.

$$\frac{1}{a_r}\partial_t T - \nabla^2 T = 0, \quad y > 0 \tag{3.9}$$

$$\{\rho_f\theta + \frac{\rho_r\sigma_r}{\sigma_f}(1-\theta)\}w\partial_t T + q(x,z,t)\partial_x T = \frac{2k_r}{\sigma_f}\partial_y T, \quad y \downarrow 0 \tag{3.10}$$

$$T(x,y,z,t)\big|_{t \leq 0} = f(x) \tag{3.11}$$

$$T(0,0,z,t)\big|_{t > 0} = T_i \tag{3.12}$$

The assumption of a constant injection temperature at the injection port $x = 0$ ignores the thermal interaction of the injected fluid with the rock mass through which the injection borehole passes. The consequences of this assumption are discussed in some detail in Appendix C. With the constraint on the flow rate, $q > 0.01$ kg/(m. sec), the heat transport within the rock in the direction of flow is negligible and can be ignored (see Appendix B).

Optimum Flow Configuration for the First-Order Model

The remainder of the present chapter considers a stationary and uniform fluid flow within the conductor--that is, $q(x,z,t) = \text{constant}$. For a sheet-like flow heat recovery system, this is the optimum flow configuration, in the sense of heat extraction efficiency. Therefore, the model will yield the absolute lower bound on the required fluid-rock contact area.

Due to the symmetry of the flow there is no conductive heat transport in the rock in the z direction. Thus the temperature field within the rock formation is governed, to good approximation, by the one-dimensional diffusion equation

$$\frac{1}{a_r}\partial_t T - \partial_{yy} T = 0, \quad y > 0 \tag{3.13}$$

Furthermore, the heat transfer boundary condition (3.10) becomes, for this case,

$$\beta\partial_t T + \partial_x T = \alpha\partial_y T, \quad y \downarrow 0 \tag{3.14}$$

where

$$\beta = \{\rho_f\theta + \frac{\rho_r\sigma_r}{\sigma_f}(1-\theta)\}\frac{w}{q}$$

and where the dimensionless parameter α is defined by

$$\alpha = \frac{2k_r}{\sigma_f q}$$

For an open fracture, where $\theta = 1$, β is simply the reciprocal of the fluid velocity.

The two additional initial and boundary conditions required to complete the statement of the problem are given by

$$T(x, y, t)\big|_{t \leq 0} = f(x) \tag{3.15}$$

$$T(0, 0, t)\big|_{t \geq 0} = T_i \tag{3.16}$$

The solution to the initial and boundary value problem represented by equations (3.13) through (3.16) is obtained analytically using integral transform methods. The Laplace transform operator and its inverse are defined by (Abramowitz and Stegun, 1964)

$$\hat{g}(s) = \mathbb{L}_t[g(t)] = \int_0^{\infty} e^{-st} g(t)dt$$

$$g(t) = \mathbb{L}_s^{-1}[\hat{g}(s)] = \frac{1}{2\pi i} \int_{c-i\infty}^{c+i\infty} e^{st} \hat{g}(s)ds$$

where s is the transform variable corresponding to t.

Applying the Laplace transform to equations (3.13) and (3.14),

$$\frac{1}{a_r}\{s\hat{T} - f(x)\} - \partial_{yy}\hat{T} = 0, \quad y > 0 \tag{3.17}$$

$$\beta\{s\hat{T} - f(x)\} + \partial_x \hat{T} = \alpha \partial_y \hat{T}, \quad y \downarrow 0 \tag{3.18}$$

The general solution of equation (3.17) that remains finite as $y \to \infty$ is

$$\hat{T}(x, y, s) = \hat{A}(x, s)\exp\left(-\sqrt{\frac{s}{a_r}}\, y\right) + \frac{f(x)}{s}, \quad y > 0 \tag{3.19}$$

Inserting expression (3.19) into equation (3.18), a first order differential equation for $\hat{A}(x,s)$ is obtained

$$\partial_x \hat{A}(x,s) + K(s)\hat{A}(x,s) = -\frac{f'(x)}{s} \tag{3.20}$$

where

$$K(s) = \alpha\sqrt{\frac{s}{a_r}} + \beta s$$

and

$$f'(x) = \frac{df}{dx}$$

The general solution of the above for $\hat{A}(x,s)$ is given by

$$\hat{A}(x,s) = \hat{B}(s)\exp(-K(s)x) - \frac{1}{s}\int_0^x \exp[-K(s)(x-x')]f'(x')dx' \tag{3.21}$$

where $\hat{B}(s)$ is a function yet to be determined.

Thus the Laplace transform of the rock temperature field is

$$\hat{T}(x,y,s) = \hat{B}(s)\exp\left(-K(s)x - \sqrt{\frac{s}{a_r}}\,y\right)$$

$$- \frac{\exp\left(-\sqrt{\frac{s}{a_r}}\,y\right)}{s}\int_0^x \exp[-K(s)(x-x')]f'(x')dx' + \frac{f(x)}{s} \tag{3.22}$$

Evaluating $\hat{T}(x,y,s)$ at $x = y = 0$ and using the Laplace transforms of equations (3.15) and (3.16), it is easily shown that

$$\hat{B}(s) = \frac{T_i - f(0)}{s} \tag{3.23}$$

Assuming a constant geothermal gradient in the upper few kilometers of the Earth's crust, the initial formation temperature $f(x)$ for quasi-vertical structures (e.g. dikes, fault zones) is a linear function of depth. For quasi-horizontal structures (e.g. formation contacts), the initial formation temperature is, to good approximation, constant. Thus, we consider the special case of the initial formation temperature

$$f(x) = c_1 + c_2 x \tag{3.24}$$

where c_1 and c_2 are constants.

Substituting expression (3.24) into equation (3.22), the Laplace transformed rock temperature field becomes

$$\hat{T}(x, y, s) = \frac{(T_i - c_1)}{s} \exp\left(-K(s)x - \sqrt{\frac{s}{a_r}}\, y\right) - \frac{c_2 \exp\left(-\sqrt{\frac{s}{a_r}}\, y\right)}{sK(s)} \{1 - \exp(-K(s))\} + \frac{c_1 + c_2 x}{s} \tag{3.25}$$

To determine the temperature of the water within the conductor, $\hat{T}(x, y, s)$ is to be evaluated at $y = 0$. Inverse Laplace transforming the resulting equation (Abramowitz and Stegun, 1964; Carslaw and Jaeger, 1959), the fluid temperature is found to be

$$T_f(x,t) = (T_i - c_1)\operatorname{erfc}\left(\frac{\alpha x}{2\sqrt{a_r \xi}}\right) U(\xi)$$

$$+ \frac{2c_2}{\alpha}\left[\sqrt{\frac{a_r \xi}{\pi}}\exp\left(-\frac{\alpha^2 x^2}{4a\xi}\right) - \frac{\beta a_r}{2\alpha}\left(1+\frac{\alpha^2 x}{\beta a_r}\right)\operatorname{erfc}\left(\frac{\alpha x}{2\sqrt{a_r \xi}}\right)\right.$$

$$\left. + \frac{\beta a_r}{2\alpha}\exp\left(\frac{\alpha^2 t}{\beta^2 a_r}\right)\operatorname{erfc}\left(\frac{\alpha x}{2\sqrt{a_r \xi}} + \frac{\alpha}{\beta a_r}\sqrt{a_r \xi}\right)\right] U(\xi)$$

$$- \frac{2c_2}{\alpha}\left[\sqrt{\frac{a_r t}{\pi}} - \frac{\beta a_r}{2\alpha} + \frac{\beta a_r}{2\alpha}\exp\left(\frac{\alpha^2 t}{\beta^2 a_r}\right)\operatorname{erfc}\left(\frac{\alpha\sqrt{a_r t}}{\beta a_r}\right)\right] U(t)$$

$$+ (c_1 + c_2 x) \qquad (3.26)$$

where $\xi = t - \beta x$ and $U(\xi)$ is the unit step function defined by

$$U(\xi) = \begin{cases} 0, & \xi \leq 0 \\ 1, & \xi > 0 \end{cases}$$

The complimentary error function is defined as (Abramowitz and Stegun, 1964)

$$\operatorname{erfc}(x) = 1 - \operatorname{erf}(x) = 1 - \sqrt{\frac{2}{\pi}}\int_0^x e^{-y^2}\, dy$$

The error function erf(x) is evaluated numerically using a rational approximation (Abramowitz and Stegun, 1964) and is presented in function subprogram form ERF(X) in Appendix E.

At this point, it is useful to introduce the "zero fracture width" approximation. The thermal inertia of the fluid and debris within fracture openings on the order of millimeters wide is small and can be neglected. We therefore set the fracture width $w = 0$ but keep the flow q finite. Hence, the zero fracture width approximation for the case under consideration is equivalent to taking the limit of equation (3.26) as $\beta \to 0$. The limit is easily shown to be

$$T_f^*(x,t) = \lim_{\beta \to 0} T_f(x,t)$$

$$= (T_i - c_1 - c_2 x)\operatorname{erfc}\left(\frac{\alpha x}{2\sqrt{a_r t}}\right) \tag{3.27}$$

$$+ \frac{2c_2}{\alpha}\left[\sqrt{\frac{a_r t}{\pi}}\ \exp\left(-\frac{\alpha^2 x^2}{4a_r t}\right) - 1\right] + (c_1 + c_2 x), \quad t > 0$$

The above equation reduces to the solution obtained by Bodvarsson (1969) for the case in which the initial formation temperature is uniform ($c_2 = 0$).

Some examples of the magnitude of the error due to the zero fracture width approximation are shown in Figure 4. These examples assume that water is injected at 30°C with a flow rate of 0.05 kg/(m. sec) into a conductor with porosity $\theta = 1$. The value of the flow rate is considered representative for a sheet-like flow recovery system. We note that the volume specific heat of rock is

roughly the same as that of water. Thus, to first approximation,

$$\beta = \rho_f\{\theta + \frac{\rho_r \sigma_r}{\rho_f \sigma_f}(1-\theta)\}\frac{w}{q} \approx \rho_f \frac{w}{q} \qquad (3.28)$$

The results obtained will therefore be approximately valid for porosities less than 1. The rock formation temperature is initially 150°C and the fracture width is 10 millimeters. The error ΔT is calculated according to $\Delta T = T_f - T_f^*$. The values of the physical parameters for the rock and fluid (water) used in this and later computations are given in Appendix E.

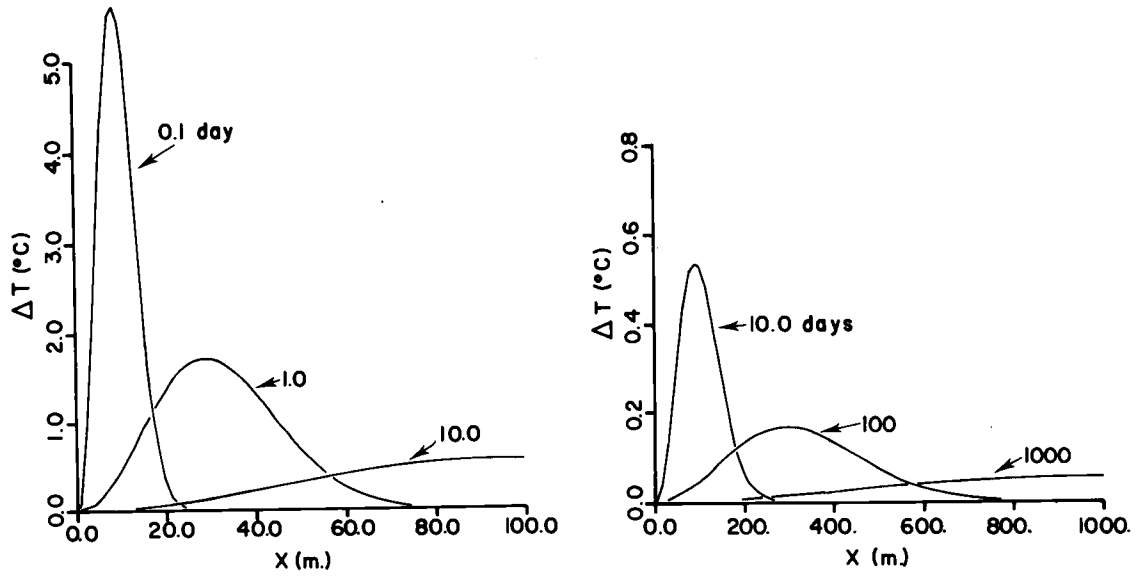

Figure 4. Error in fluid temperature due to zero fracture width approximation. Injection port is at $x = 0$ and the fluid flow is in the positive x direction (note change of scale).

It is evident from these examples that the error incurred by the zero fracture width approximation damps out rapidly with increasing time and distance from the injection port. Since the characteristic dimensions of a forced geoheat recovery system will be on the order of a kilometer, the error in temperature at the production port is negligible and the zero width approximation is quite good. The same applies for initially non-uniform formation temperatures.

The two basic flow options for a quasi-vertical conductor are shown in Figure 5. For the purpose of definition, the case in which the fluid flows upward within the conductor is referred to as an "upflow" system. For the case in which the fluid flow is downward, the configuration is referred to as "downflow" (Bodvarsson, 1976; Bodvarsson and Hanson, 1976, 1977).

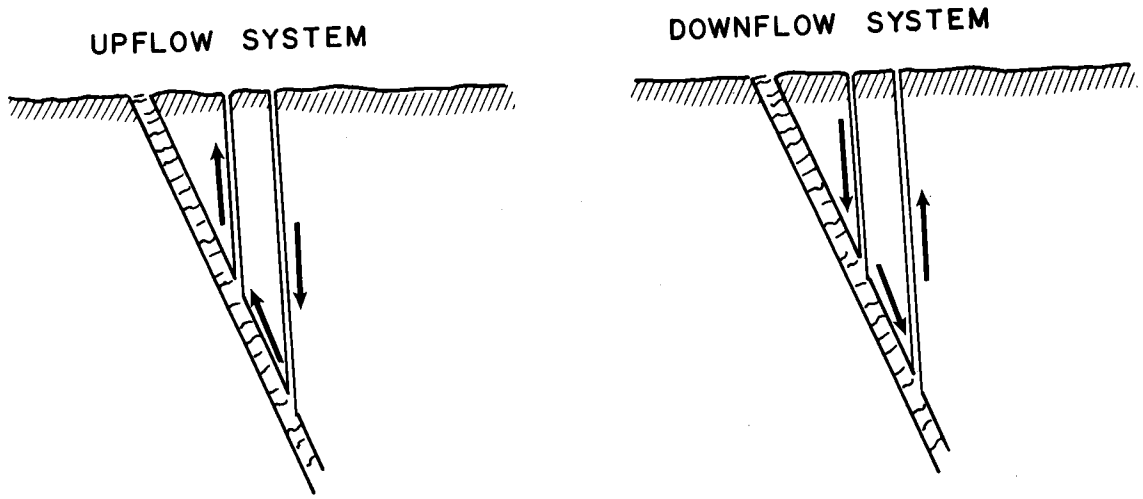

Figure 5. Upflow and downflow system configurations for quasi-vertical fluid conductors.

Figure 6 shows the time evolution of the water temperature distribution within the fluid conductor based on equation (3.27) for three different initial formation temperature situations. The dotted lines represent the initial formation temperatures and the curves are labeled according to the length of time, measured in years, after initiation of flow. All three cases assume that the water injected into the fluid conductor has a constant temperature of 30°C at a constant mass flow rate of 0.05 kg/(m.sec). The initial formation temperatures are as follows:

$$T(x, y, t)\big|_{t \leq 0} = f(x) = \begin{cases} 175 - 50x \ ^\circ C \text{ (Case A)} & (3.29) \\ 125 + 50x \ ^\circ C \text{ (Case B)} & (3.30) \\ 150 \ ^\circ C \text{ (Case C)} & (3.31) \end{cases}$$

Assuming a 25°C ambient surface temperature, Figure 6A represents an ideal flow configuration within an upflow system in which the injection port is at a depth of 3 km. Figure 6B represents a downflow configuration where the injection port is at a depth of 2 km. Figure 6C assumes fluid is injected into a quasi-horizontal conductor embedded in a rock formation that has an initial uniform temperature of 150°C. As time increases, it is seen that the temperature distributions of the three cases considered approach the same value. This reflects the fact that the initial average temperature of the rock in the domain $(0 \leq x \leq 1) \times (0 < y < \infty)$ is identical for all three cases.

For the purpose of notational economy, the asterisk denoting the zero width approximation will be dropped. Unless otherwise stated, the remainder of this work will use this approximation.

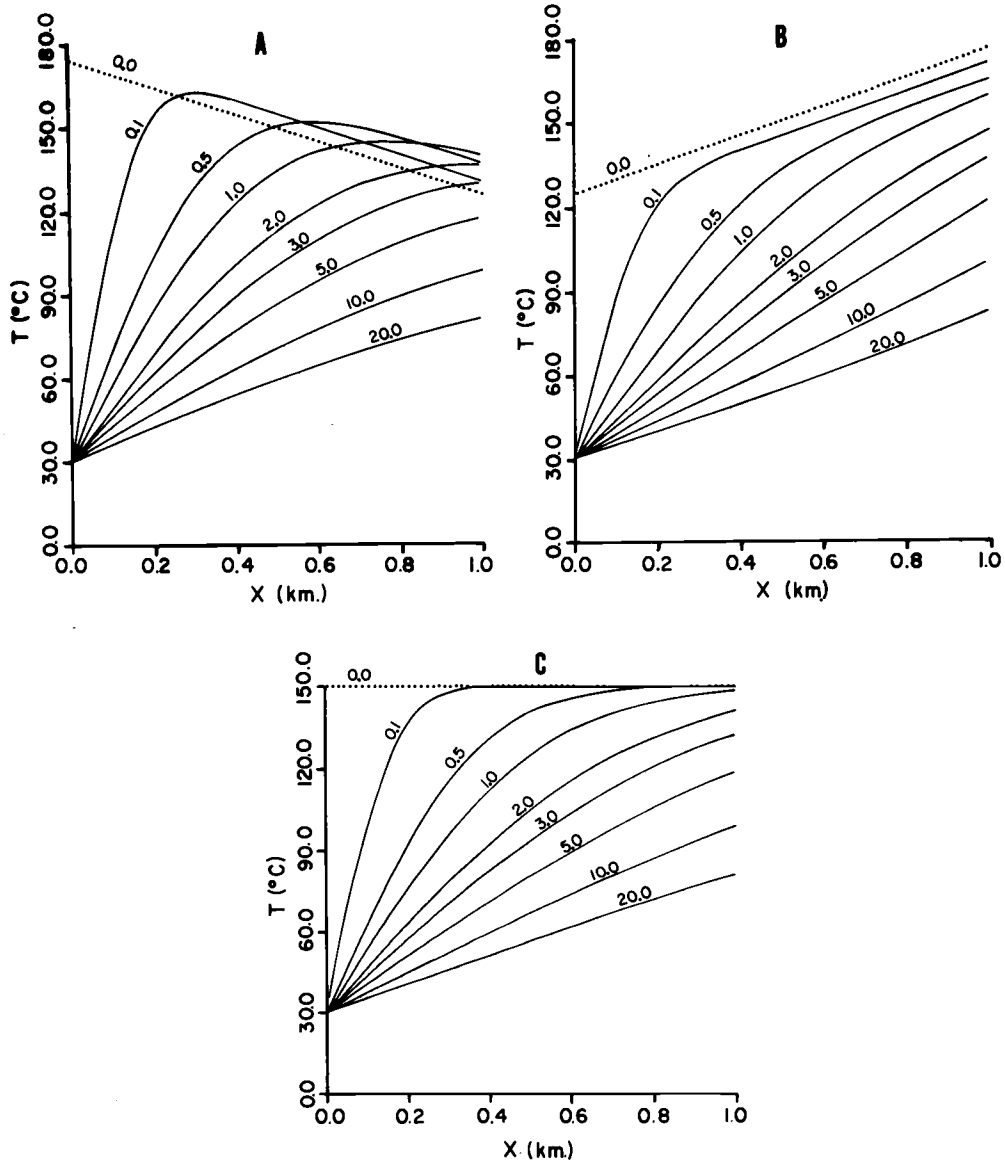

Figure 6. Fluid temperature distributions within the conductor for upflow (A), downflow (B), and initial uniform formation temperature (C) configurations. Individual curves labeled according to time (years) after initiation of flow. All cases assume $q = 0.05$ kg/(m.sec) and $T_i = 30°C$. Initial formation temperature distributions are given by dotted lines.

IV. EFFECTS OF NON-IDEAL FLOW ON PRODUCTION TEMPERATURE

The flow geometry within an actual recovery system may deviate substantially from the ideal case considered in the previous chapter. Non-uniform flow within the fluid conductor as well as fluid losses from the system due to leakage are likely to be the two main adverse flow characteristics that will degrade the system heat extraction efficiency. The present chapter considers these in terms of the first-order heat extraction model and discusses the resulting effects on the production temperature of the system.

Flow-Channelling

Non-uniform flow within a fluid conductor can arise as a result of several processes. These include borehole location and spacing, spatial variation of permeability prior to initiation of flow, and the time dependent effects of thermoelastic, chemical and convective processes on permeability. The present section estimates the effect of non-uniform flow (which will be referred to as "flow-chanelling") on the fluid temperature within the conductor based on the first-order heat extraction model.

The first part of the present section is concerned with estimating the dependence of the fluid temperature on the flow-channel wave-length. In the present context wavelength refers to the characteristic

distance over which a significant change in flow rate occurs. A parameter perturbation method is used in the analysis. The second part of the section applies the Fourier-Galerkin variational approach to generalize the solution to allow for arbitrarily severe flow-channel configurations.

Perturbation Method

The first-order heat extraction model is based on a line source and line sink connected by a uni-directional flow. Using this concept, a stationary non-uniform flow between the injection and production ports of the system, assuming no fluid losses, translates to a flow configuration of the form $\vec{q} = q(z)\hat{x}$. Thus, the mathematical problem can be stated, analogous to equations (3.9) through (3.12), as

$$\frac{1}{a_r}\partial_t T - \partial_{yy} T - \partial_{zz} T = 0, \quad y > 0 \tag{4.1}$$

$$2k_r \partial_y T = \sigma_f q(z) \partial_x T, \quad y \downarrow 0 \tag{4.2}$$

$$T(x, y, t)\big|_{t \leq 0} = f(x) \tag{4.3}$$

$$T(0, 0, t)\big|_{t > 0} = T_i \tag{4.4}$$

The zero fracture width approximation in heat transfer boundary condition (4.2) has been made. Furthermore, conductive heat transport in the rock in the direction transverse to the flow direction is included

in equation (4. 1) to allow for thermal communication between the flow channels.

The perturbation method is based on the idea of approximating a given system by a simpler ideal system which deviates only slightly from the system under consideration. The perturbation theory (for linear operators) was originated by Rayleigh and Schrodinger (Rayleigh, 1926; Schrodinger, 1928). Criteria have been given for the validity of the perturbation method and the reader is referred to Titchmarsh (1949, 1950) and Kato (1951, 1966).

The perturbation method used in the present analysis assumes that the flow rate $q(z)$ can be represented by a constant flow rate perturbed by a small spatial flow variation, or

$$q(z) = q_0 + \nu \epsilon(z) \tag{4.5}$$

where

$$\left| \frac{\epsilon(z)}{q_0} \right| \ll 1 \tag{4.6}$$

and ν is a dimensionless perturbation parameter. The introduction of the parameter ν allows one to group terms of comparable degrees of approximation in a methodical and convenient fashion.

We look for a solution of the rock temperature field of the form

$$T(x, y, z, t) = T_1(x, y, z, t) + f(x) \tag{4.7}$$

where $f(x)$ is the initial formation temperature. The deviation T_1 from the initial configuration is represented by the perturbation series

$$T_1(x, y, z, t) = T_1^{(0)}(x, y, t) + \nu T_1^{(1)}(x, y, z, t) + \nu^2 T_1^{(2)}(x, y, z, t) + \ldots + \nu^n T_1^{(n)}(x, y, z, t) + \ldots \tag{4.8}$$

Defining the operators H and $V(z)$ as

$$H = \sigma_f q_0 \partial_x - 2k_r \partial_y$$

$$V(z) = \sigma_f \epsilon(z) \partial_x$$

the heat transfer boundary condition (4.2) can be written as

$$[H+\nu V(z)]T_1(x, y, z, t)\big|_{y \downarrow 0} = -\sigma_f q(z) f'(x) \tag{4.9}$$

Inserting expression (4.8) into equation (4.9) and equating equal powers of ν, one obtains

$$\begin{aligned}
HT_1^{(0)} &= -\sigma_f q_0 f'(x) , && y \downarrow 0 \\
HT_1^{(1)} + V(z)T_1^{(0)} &= -\sigma_f \epsilon(z) f'(x) , && y \downarrow 0 \\
HT_1^{(2)} + V(z)T_1^{(1)} &= 0 , && y \downarrow 0 \\
&\vdots \\
HT_1^{(n)} + V(z)T_1^{(n-1)} &= 0 , && y \downarrow 0 \\
&\vdots
\end{aligned} \tag{4.10}$$

Furthermore, substituting expressions (4.7) and (4.8) into equation (4.1), we find that the elements of the perturbation series must satisfy

$$\begin{aligned}
&\frac{1}{a_r}\partial_t T_1^{(0)} - \partial_{yy} T_1^{(0)} = 0, \quad y > 0 \\
&\frac{1}{a_r}\partial_t T_1^{(1)} - \partial_{yy} T_1^{(1)} - \partial_{zz} T_1^{(1)} = 0, \quad y > 0 \\
&\qquad\qquad \vdots \\
&\frac{1}{a_r}\partial_t T_1^{(n)} - \partial_{yy} T_1^{(n)} - \partial_{zz} T_1^{(n)} = 0, \quad y > 0 \\
&\qquad\qquad \vdots
\end{aligned} \tag{4.11}$$

The initial and boundary conditions on the elements $T_1^{(n)}$ of the perturbation series are easily shown to be

$$\begin{aligned}
&T_1^{(n)}(x, y, z, t)\big|_{t \leq 0} = 0, \quad n = 0, 1, \ldots \\
&T_1^{(n)}(0, 0, z, t)\big|_{t > 0} = \begin{cases} T_i - f(0), & n = 0 \\ 0, & n = 1, 2, \ldots \end{cases}
\end{aligned} \tag{4.12}$$

It is evident from this formulation that a solution for the nth term of the perturbation series can, in principle, be built up from the knowledge of the previous n-1 terms.

We simplify the present analysis by truncating the perturbation series (4.8) after the first two terms which results in a first order perturbation approximation. The solution will be sufficiently valid as long as constraint (4.6) is met. A discussion of the range of validity

of this approximation is given in the following section. Thus, we look for a solution of T_1 of the form

$$T_1(x, y, z, t) = T_1^{(0)}(x, y, t) + T_1^{(1)}(x, y, z, t)$$

where

$$\begin{aligned}
&\frac{1}{a_r}\,\partial_t T_1^{(0)} - \partial_{yy} T_1^{(0)} = 0, \qquad y > 0 \\
&HT_1^{(0)} = -\sigma_f q_0 f'(x), \qquad y \downarrow 0 \\
&T_1^{(0)}(x, y, t)\big|_{t \le 0} = 0 \\
&T_1^{(0)}(0, 0, t)\big|_{t > 0} = T_i - f(0)
\end{aligned} \tag{4.13}$$

and where

$$\begin{aligned}
&\frac{1}{a_r}\,\partial_t T_1^{(1)} - \partial_{yy} T_1^{(1)} - \partial_{zz} T_1^{(1)} = 0, \qquad y > 0 \\
&HT_1^{(1)} + V(z)T_1^{(0)} = -\sigma_f \epsilon(z) f'(x), \qquad y \downarrow 0 \\
&T_1^{(1)}(x, y, t)\big|_{t \le 0} = 0 \\
&T_1^{(1)}(0, 0, t)\big|_{t > 0} = 0
\end{aligned} \tag{4.14}$$

The solution of equations (4.13) and (4.14) is obtained by integral transform techniques.

The initial rock formation temperature $f(x)$ is again assumed to be a linear function of x, or

$$f(x) = c_1 + c_2 x$$

where c_1 and c_2 are constants.

Laplace transforming equations (4.13) with respect to time and solving the resulting set of equations for $T_1^{(0)}$ gives

$$\hat{T}_1^{(0)}(x, y, s) = \frac{(T_i - c_1)}{s} \exp\left[-\sqrt{\frac{s}{a_r}}(\alpha_0 x + y)\right]$$

$$- \frac{c_2 \exp\left(-\sqrt{\frac{s}{a_r}}\, y\right)}{\alpha_0 s \sqrt{\frac{s}{a_r}}} \left[1 - \exp\left(-\alpha_0 \sqrt{\frac{s}{a_r}}\, x\right)\right] \qquad (4.15)$$

where

$$\alpha_0 = \frac{2k_r}{\sigma_f q_0}$$

As expected, the unperturbed solution for the fluid temperature, $\hat{T}_1^{(0)} + f(x)/s$, is identical to equation (3.25) in the limit of zero fracture width, corresponding to the uniform component of flow q_0.

Noting that the operators H and $V(z)$ are time independent, the Laplace transform (with respect to time) applied to the first two equations of (4.14) followed by an exponential Fourier transform (with respect to z) gives

$$\partial_{yy} \hat{\hat{T}}_1^{(1)} - \left(\frac{s}{a_r} + \omega^2\right) \hat{\hat{T}}_1^{(1)} = 0, \quad y > 0 \qquad (4.16)$$

and

$$H\hat{\hat{T}}_1^{(1)} + \tilde{V}(\omega)\hat{T}_1^{(0)} = -\frac{\sigma_f \tilde{\epsilon}(\omega) f'(x)}{s} \tag{4.17}$$

where the "$\hat{\hat{\ }}$" indicates a Laplace followed by a Fourier transform and the "$\sim$" denotes the Fourier transform. The (exponential) Fourier transform and its inverse are defined, in symmetric form, by (Magnus and Oberhettinger, 1966)

$$\tilde{g}(\omega) = \mathbb{F}_t[g(t)] = \frac{1}{\sqrt{2\pi}} \int_{-\infty}^{\infty} e^{i\omega t} g(t)\,dt$$

$$g(t) = \mathbb{F}_\omega^{-1}[g(\omega)] = \frac{1}{\sqrt{2\pi}} \int_{-\infty}^{\infty} e^{-i\omega t} \tilde{g}(\omega)\,d\omega$$

The solution of equation (4.16) that remains finite as $y \to \infty$ is

$$\hat{\hat{T}}_1^{(1)}(x, y, \omega, s) = \hat{\hat{A}}(x, \omega, s)\exp\left(-\sqrt{\frac{s}{a_r} + \omega^2}\, y\right) \tag{4.18}$$

Substitution of expression (4.17) into equation (4.18) yields a first order differential equation for $\hat{\hat{A}}(x, \omega, s)$

$$\partial_x \hat{\hat{A}} + \alpha_0 \sqrt{\frac{s}{a_r} + \omega^2}\, \hat{\hat{A}} = -\frac{\tilde{\epsilon}(\omega)}{q_0}\left\{\partial_x \hat{T}_1^{(0)}\Big|_{y \downarrow 0} + f'(x)\right\} \tag{4.19}$$

With the solution of $\hat{T}_1^{(0)}$ given by equation (4.15) and the homogeneous boundary conditions at $x = 0$ given in equations (4.14), it

can be shown that

$$\hat{\hat{A}}(x, \omega, s) = \frac{\tilde{\epsilon}(\omega)}{q_0} R(x, s, \omega) \tag{4.20}$$

where

$$R(x, s, \omega) = \left[\frac{\alpha_0 \sqrt{\frac{s}{a_r}} (c_1 - T_i) - c_2}{s} \right] \cdot \left[\frac{\exp(-\alpha_0 \sqrt{\frac{s}{a_r} + \omega^2} x) - \exp(-\alpha_0 \sqrt{\frac{s}{a_r}} x)}{\alpha_0 \sqrt{\frac{s}{a_r} + \omega^2} - \alpha_0 \sqrt{\frac{s}{a_r}}} \right]$$

$$- \frac{c_2}{s} \left[\frac{1 - \exp(-\alpha_0 \sqrt{\frac{s}{a_r} + \omega^2} x)}{\alpha_0 \sqrt{\frac{s}{a_r} + \omega^2}} \right] \tag{4.21}$$

The analysis to this point has assumed, of course, that the Fourier transform of $\epsilon(z)$ exists.

Expressions (4.20) and (4.21) will in general be quite difficult to invert analytically. The problem is simplified by assuming that the flow perturbation can be represented by a pure harmonic function with amplitude q_1.

$$\epsilon(z) = q_1 \cos(\omega_0 z)$$

With this simplification the inverse Fourier transform is immediate, and

$$\hat{T}_1^{(1)}(x, 0, z, s) = \hat{A}(x, z, s)$$

$$= \frac{q_1}{q_0} \cos(\omega_0 z) R(x, \omega_0, s) \qquad (4.22)$$

We are primarily concerned with the temperature variation in the fluid due to the flow perturbation. To this end, we evaluate the peak-to-peak temperature variation as a function of channel wavelength using equation (4.22), or

$$\Delta T(x, t, \lambda) = \frac{2q_1}{q_0} \left| \mathbb{L}_s^{-1}\left[R(x, \frac{2\pi}{\lambda}, s)\right] \right| \qquad (4.23)$$

where λ is the channel wavelength. The indicated inverse is done numerically using a method described in Appendix A.

Figure 7 shows several examples of the peak-to-peak fluid temperature variation due to a sinusoidal flow perturbation. The examples assume a constant 30°C injection temperature and an initial uniform formation temperature of 150°C. The magnitude of the unperturbed flow q_0 is 0.05 kg/(m.sec) and the flow perturbation amplitude q_1 is 20% of this value, or 0.01 kg/(m.sec). Cases a, b and c represent channel wavelengths of 100 m, 50 m, and 10 m respectively. The dotted lines represent $\Delta T(x, t, \lambda)$ based on equation (4.23). The solid lines assume that there is no conductive transport in the rock in the z coordinate and are computed on the basis of equation (3.27).

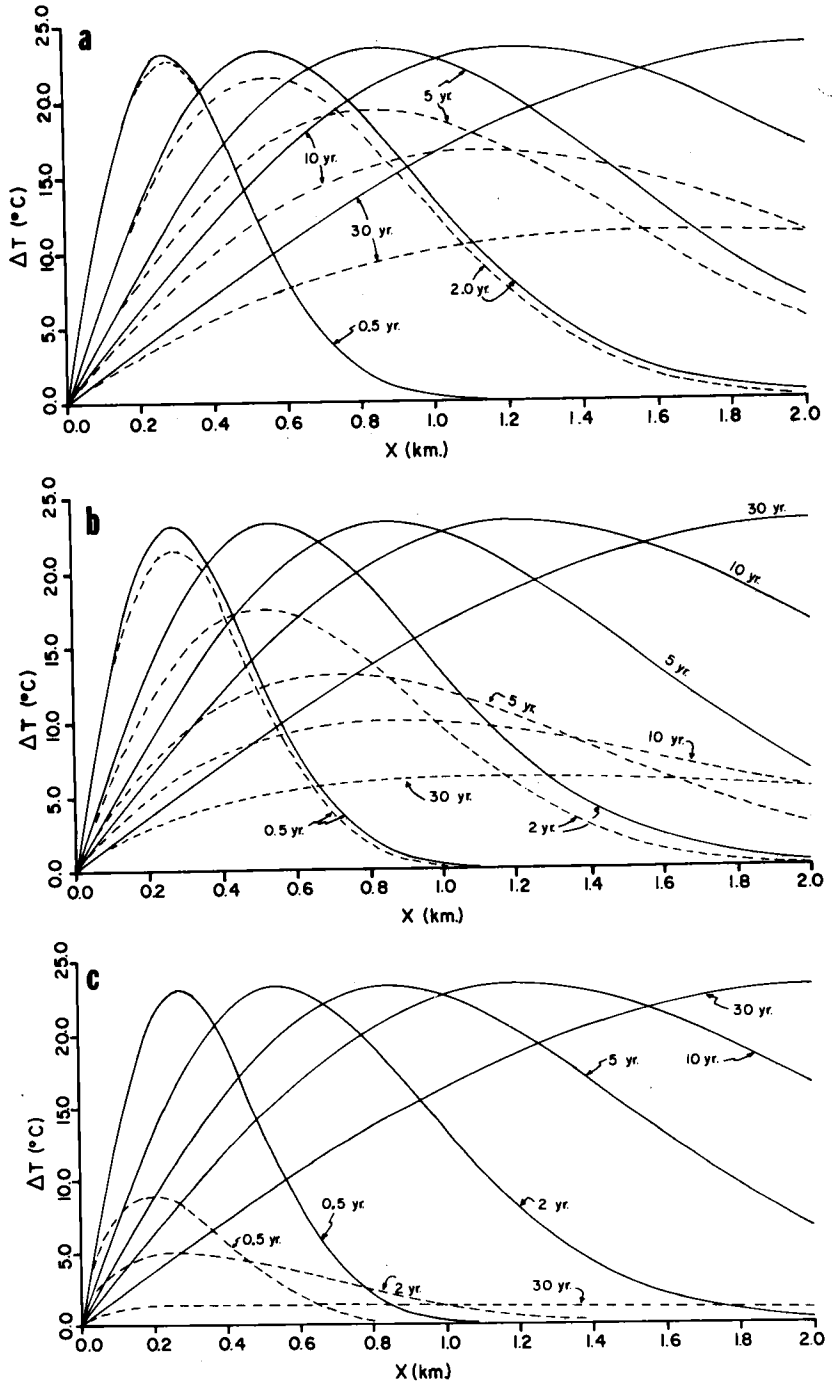

Figure 7. Peak-to-peak fluid temperature difference within the conductor in the direction transverse to flow assuming a sinusoidal spatial flow variation. Channel wavelengths are 100 m, 50 m, and 10 m for cases a, b, and c respectively.

It is evident that the effect of non-uniform flow is most significant for long wavelengths and damps out rapidly for shorter wavelengths. This is due to the greater thermal communication between flow channels for the shorter wavelengths and the resulting "smearing out" of the temperature differences in the transverse (z) coordinate. For the case in which there is no thermal communication between channels (solid lines) the maximum peak-to-peak temperature difference moves away from the injection port with increasing time with no change in amplitude.

The results of this simple perturbation model show that a substantial error in fluid temperature can occur by ignoring the conductive transport in the rock in the direction transverse to the flow under non-uniform flow conditions. The consequences of ignoring this term of the diffusion equation for wavelengths on the order of 100 m or less can be quite severe in terms of heat extraction efficiency. For the shorter wavelengths ($\lambda < 10$ m) the temperature field of the fluid approaches that obtained for the uniform flow case--that is, ΔT becomes small. Therefore, the heat extraction efficiency, in the limit of small flow channel wavelength, approaches the optimum value. However, by ignoring transverse conduction, there is no approach to this optimum.

Fourier-Galerkin Method

The perturbation method is quite instructive in regard to the overall effect of flow channelling. However, constraint (4.6) severely limits the range of applicability of the method. We therefore recast the problem of flow channelling into an equivalent variational problem.

The Galerkin variational method (Galerkin, 1915) is formulated as follows. Assume that we are given an equation $Bu - f = 0$, where B is a linear operator defined on some Hilbert space. The Galerkin method requires us to select the sequence of orthogonal elements $\varphi_n \in D_B$ (domain of B) and the sequence of orthogonal elements $\psi_n \in D_B$ and then to attempt to find an approximate solution, or "trial" solution, of the form

$$u_n = \sum_{k=0}^{n} a_k \varphi_k$$

The coefficients a_k are determined from the condition that $(Bu_n, \psi_i) = 0$, $i = 0, 1, \ldots, n$. This leads to the set of equations

$$\sum_{k=0}^{n} a_k (B\varphi_k, \psi_i) = (f, \psi_i), \quad i = 0, 1, \ldots, n$$

from which the a_k's and consequently u_n can be obtained. The above formulation is Petrov's generalization of Galerkin's method. It

is sometimes convenient to restrict the sets $\{\varphi_i\}$ and $\{\psi_i\}$ to be identical, which yields the Bubnov-Galerkin method (Mikhlin and Smolitskiy, 1967). It is the latter method that will be used in the following analysis.

For the problem under consideration, we let the flow rate $q(z)$ be a given periodic function of z with period $2L$. Furthermore, $q(z) > 0$ and is even on the interval $-L \leq z \leq L$. Thus, the dimensionless parameter α can be expressed by the Fourier cosine series

$$\alpha(z) = \frac{2k_r}{\sigma_f q(z)} = \sum_{\ell=0}^{2N} c_\ell \cos \frac{\ell \pi z}{L} \tag{4.24}$$

The choice of the upper summation index will become apparent as the analysis develops. A periodicity in flow implies a periodicity in the temperature field, so we look for a solution for the temperature field of the form

$$T(x, y, z, t) = T_1(x, y, z, t) + f(x) \tag{4.25}$$

where

$$T_1(x, y, z, t) = \sum_{n=0}^{N} a_n(x, y, t) \cos \frac{n\pi z}{L} \tag{4.26}$$

and where $f(x)$ is the initial formation temperature.

The above equations can be thought of as the "trial solution" that approximates the true temperature field. The set of coefficients $\{a_n, n = 0, 1, \ldots, N\}$ are chosen using the method of Galerkin such that expression (4.26) is the "best" solution (in the least squares sense) for the true temperature field. Since the basis functions for the trial solution are simply the set of trigonometric cosine functions, the method is termed the Fourier-Galerkin method.

Laplace transforming equations (4.1) and (4.26) with respect to time, we obtain

$$\frac{s}{a_r}\hat{T}_1 - \partial_{yy}\hat{T}_1 - \partial_{zz}\hat{T}_1 = 0, \quad y > 0 \tag{4.27}$$

and

$$\hat{T}_1(x, y, z, s) = \sum_{n=0}^{N} \hat{a}_n(x, y, s) \cos \frac{n\pi z}{L} \tag{4.28}$$

Substituting expression (4.28) into equation (4.27) and using the orthogonality of the basis functions on the interval $-L \leq z \leq L$, one obtains

$$\partial_{yy}\hat{a}_n(x, y, s) - (\frac{s}{a_r} + \beta_n^2)\hat{a}_n(x, y, s) = 0, \quad y > 0 \tag{4.29}$$

$$n = 0, 1, \ldots, N$$

where

$$\beta_n = \frac{n\pi}{L}$$

The solution for $\hat{a}_n(x, y, s)$ that remains finite as $y \to \infty$ is

$$\hat{a}_n(x, y, s) = \hat{b}_n(x, s)\exp\left(-\sqrt{\frac{s}{a_r} + \beta_n^2}\, y\right), \quad n = 0, 1, \ldots, N \tag{4.30}$$

and therefore,

$$\hat{T}_1(x, y, z, s) = \sum_{n=0}^{N} \hat{b}_n(x, s)\exp\left(-\sqrt{\frac{s}{a_r} + \beta_n^2}\, y\right) \cos\frac{n\pi z}{L} \tag{4.31}$$

The heat transfer boundary condition is now recast in terms of the set of coefficients $\{\hat{b}_n(x, s),\ n = 0, 1, \ldots, N\}$ by means of the Fourier-Galerkin method. Laplace transforming the boundary condition (4.2) with respect to time and using expression (4.25), one obtains

$$B[\hat{T}_1] = 0 \tag{4.32}$$

where the operator B is defined as

$$B[\ ] = \frac{2k_r}{\sigma_f q(z)}\, \partial_y[\ ] - \partial_x[\ ] - \frac{f'(x)}{s}, \quad y \downarrow 0 \tag{4.33}$$

The Fourier Galerkin method requires that the coefficients $\hat{b}_n(x, s)$ be selected so that the $N+1$ algebraic equations

$$\frac{2}{L}\int_0^L B[\hat{T}_1] \cos\frac{m\pi z}{L}\, dz = 0, \quad m = 0, 1, \ldots, N \tag{4.34}$$

be satisfied.

For the purpose of notational economy, the multiple inner product of the basis functions is defined as

$$(n, \ell, m, \ldots, j) = \frac{2}{L}\int_0^L \cos\frac{n\pi z}{L}\cos\frac{\ell\pi z}{L}\cos\frac{m\pi z}{L}\ldots\cos\frac{j\pi z}{L}\,dz$$

Using expressions (4.24), (4.31) and (4.34), it can be shown that the $\hat{b}_n$'s satisfy the set of equations

$$\sum_{n=0}^{N}\sum_{\ell=0}^{2N}(m, \ell, n)\sqrt{\frac{s}{a_r}+\beta_n^2}\,c_\ell\hat{b}_n(x, s)$$

$$+\sum_{n=0}^{N}(m, n)\partial_x\hat{b}_n(x, s) + (m, 0)\frac{f'(x)}{s} = 0, \qquad (4.35)$$

$$m = 0, 1, \ldots, N$$

With the use of a common trigonometric identity, it is evident that

$$(n, \ell, m) = \frac{1}{2}(\ell, m+n) + \frac{1}{2}(\ell, m-n)$$

Furthermore, the orthogonality of the basis functions on the interval $-L \leq z \leq L$ requires that

$$(n, m) = \begin{cases} 0, & n \neq m \\ 1, & n = m \neq 0 \\ 2, & n = m = 0 \end{cases}$$

Using these addition and orthogonality properties, the problem can be reduced to solving the set of $N+1$ first order coupled ordinary differential equations

$$\partial_x \hat{b}_m(x, s) + \sum_{n=0}^{N} \hat{\Lambda}_{mn}(s)\hat{b}_n(x, s) = -\hat{\xi}_m(x, s), \qquad (4.36)$$

$$m = 0, 1, \ldots, N$$

where

$$\hat{\Lambda}_{mn}(s) = \frac{\sqrt{\frac{s}{a_r} + \beta_n^2}}{2}\left[\frac{(n+m, n+m)}{(m, m)} c_{m+n} + \frac{(m-n, m-n)}{(m, m)} c_{|m-n|}\right] \qquad (4.37)$$

and where

$$\hat{\xi}_m(x, s) = \begin{cases} \dfrac{f'(x)}{s}, & m = 0 \\ 0, & m > 0 \end{cases} \qquad (4.38)$$

It is instructive to cast the above equations in matrix form.

$$\partial_x \vec{\hat{b}}(x, s) + \hat{\Lambda}(s)\vec{\hat{b}}(x, s) = -\vec{\hat{\xi}}(x, s) \qquad (4.39)$$

where

$$\vec{\hat{b}}(x, s) = \begin{bmatrix} \hat{b}_0(x, s) \\ \hat{b}_1(x, s) \\ \vdots \\ \hat{b}_N(x, s) \end{bmatrix} \qquad \vec{\hat{\xi}}(x, s) = \begin{bmatrix} f'(x)/s \\ 0 \\ 0 \\ \vdots \\ 0 \end{bmatrix} \leftarrow (N+1)\text{th entry}$$

and where

$$\hat{\Lambda}(s) = \begin{bmatrix} \hat{\Lambda}_{00}(s) & \hat{\Lambda}_{01}(s) & \cdots & \hat{\Lambda}_{0N}(s) \\ \hat{\Lambda}_{10}(s) & \hat{\Lambda}_{11}(s) & \cdots & \vdots \\ \vdots & & & \vdots \\ \hat{\Lambda}_{N0}(s) & & \cdots & \hat{\Lambda}_{NN}(s) \end{bmatrix}$$

It is not unexpected that there is a striking similarity between equations (4.39) and (3.20). The thermal coupling between the flow channels and the temperature field is quite explicit in expression (4.36), where the matrix $\hat{\Lambda}(s)$ couples the Fourier coefficients of the temperature field with the Fourier coefficients of the flow configuration. Furthermore, it is at this point evident from equation (4.37) why $2N+1$ terms were retained in the expansion of $\alpha(z)$. We note that in t-space, the coupling matrix $\hat{\Lambda}(s)$ will be time dependent. The final requirement for the solution of equations (4.36) through (4.38) is the value of $\hat{b}(x, s)$ at $x = 0$. This is easily shown to be

$$\vec{\hat{b}}(0, s) = \begin{bmatrix} \dfrac{T_i - f(0)}{s} \\ 0 \\ 0 \\ \vdots \\ 0 \end{bmatrix} \leftarrow (N+1)\text{th entry}$$

Equation (4.39) is integrated numerically using the Backward Difference Approximation (BDA) method (Varga, 1962). The BDA method approximates the differential equation (4.39) with the finite difference equation

$$\frac{\vec{\hat{b}}(x_{k+1}, s)-\vec{\hat{b}}(x_k, s)}{\Delta x_k} + \hat{\Lambda}(s)\vec{\hat{b}}(x_{k+1}, s) = -\vec{\hat{\xi}}(x_{k+1}, s) \qquad (4.40)$$

where the real line $x > 0$ has been partioned into the set of sub-intervals $\Delta x_k = x_{k+1} - x_k$ where $x_0 < x_1 < \ldots$. The injection port at $x = 0$ corresponds to x_0. Rewriting equation (4.40) in terms of a computational marching scheme, we obtain

$$\vec{\hat{b}}(x_{k+1}, s) = (I+\Delta x_k \Lambda(s))^{-1}\{\vec{\hat{b}}(x_k, s)-\Delta x_k \vec{\hat{\xi}}(x_{k+1}, s)\}, \qquad (4.41)$$

$$k = 0, 1, 2, \ldots$$

where I is the identity matrix. The above method will yield $\vec{\hat{b}}(x_k, s)$, $k > 0$ given the "starting" vector $\vec{\hat{b}}(x_0, s)$. The number of matrix inversions required in the computational procedure is minimized by letting the grid spacing Δx_k be constant. The matrix inversion indicated above is carried out using the point Jacobi iterative procedure (Varga, 1962). Having integrated the equation to the desired value of x, the resulting set of $N+1$ coefficients $\hat{b}_n(x,s)$ are numerically inverse Laplace transformed by a method described

in Appendix A. The temperature of the fluid, $T(x, 0, z, t)$, is then evaluated by expression (4.25). A computer program, CHFLO, based on the above procedure is given in Appendix E.

An important question to be addressed at this point is the existence of the above indicated matrix inverse under the Jacobi iterative procedure. A necessary and sufficient condition for the convergence of the sequence of elements in the iteration is that the spectral radius of the Jacobi matrix M be less than 1, where the spectral radius is defined as

$$\rho(M) = \max_i |\lambda_i|$$

and the λ_i are the eigenvalues of M. For the case under consideration, the Jacobi matrix is given by $M = D^{-1}(UTM+LTM)$, where D, UTM, and LTM are the diagonal, upper triangular matrix, and lower triangular matrix of $I + \Delta x\hat{\Lambda}(s)$ respectively. A closed form solution for the eigenvalues will in general be quite difficult to obtain. However, if any norm $\|M\|$ of the Jacobi matrix can be shown to be less than 1, it follows that $\rho(M) < 1$, since $\rho(M) \leq \|M\|$ (Isaacson and Keller, 1966). The matrix norm used in the present analysis is

$$\|M\|_\infty = \max_i \sum_{\substack{j=0 \\ j\neq i}}^{N} \left| \frac{d_{ij}}{d_{ii}} \right|$$

where the d_{ij}'s are the elements of $I + \Delta x\hat{\Lambda}(s)$. The values of this norm for the specific examples of the Fourier-Galerkin solution to be considered are given in Appendix E. For all cases considered, the spectral radius of the Jacobi matrix was less than one and therefore the iteration sequence converged.

A flow channel configuration on the interval $0 \leq z \leq L$ of the form

$$q(z) = \begin{cases} q_0, & 0 \leq z \leq z_L \\ \frac{(q_0 - q_1)}{2}\left[1 - \cos\left(\frac{z_H - z}{w}\pi\right)\right] + q_1, & z_L < z < z_H \\ q_1, & z_H \leq z \leq L \end{cases}$$

is used in the analysis, where q_0, q_1, z_L and z_H are constants and where $z_H > z_L$. The "taper width" w is given by $z_H - z_L$. The cosine taper function gives a very smooth $q(z)$, which is advantageous in minimizing the number of terms required in expansion (4.24).

Figure 8 shows three flow channel configurations of varying degrees of severity considered in the present analysis and in later

discussions of non-uniform flow. All have a mean flow (averaged over the interval $0 \leq z \leq L$) of 0.05 kg/(m.sec). The choice of these specific configurations was arbitrary. The range of severity of the channelling goes from the uniform flow case (curve c) to a configuration that varies by a factor of ten (curve a). It is felt that this range of flow variations may be representative of the degree of flow non-uniformity to be expected in an actual recovery system. The periodicity of the channelling, 2L, is probably the most uncertain parameter.

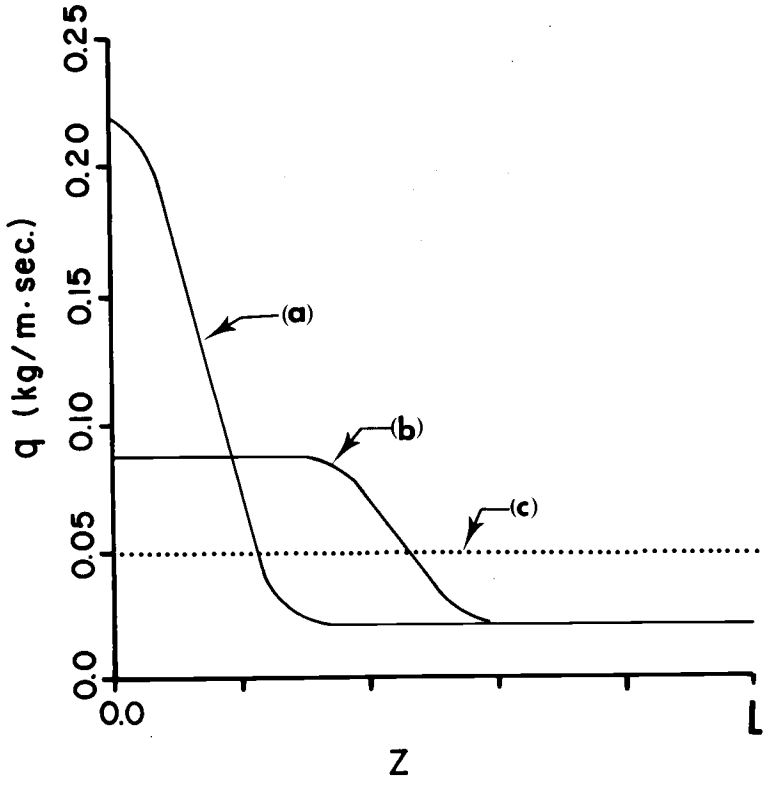

Figure 8. Flow channel configurations used in the Fourier-Galerkin analysis. Channels have a periodicity of 2L and a mean flow (averaged over the interval $0 \leq z \leq L$) of 0.05 kg/(m.sec).

For the purpose of example, we consider two initial rock formation temperature distributions, corresponding to an upflow system and an initial uniform temperature configuration. The formation temperature distributions for these cases are given by equations (3.29) and (3.31) respectively. Figure 9 shows the fluid temperature distribution for the upflow configuration and Figure 10 for the initial uniform temperature case. The flow configuration (a) in Figure 8 is used in the computations, where L is assumed to be 10 m. The temperature distributions are plotted at 100 m intervals from the injection port $(x = 0)$ of the system to a maximum distance of 1 km. The curves on the left hand side of the figures correspond to the Fourier-Galerkin solution ("coupled" model) and those on the right hand side correspond to the case where conductive transport in the z coordinate is ignored ("uncoupled" model), i.e., equation (3.27) with q replaced with $q(z)$. The latter is given for comparison in order to observe the degree of inter-channel communication. The injection temperature assumed for both figures is 30°C.

It is evident from Figures 9 and 10 that, for early time $(t < 0.1$ yr), there is little difference in the uncoupled and coupled models. However, for later times, the difference becomes quite significant. This observation is also substantiated by the simple perturbation model discussed previously.

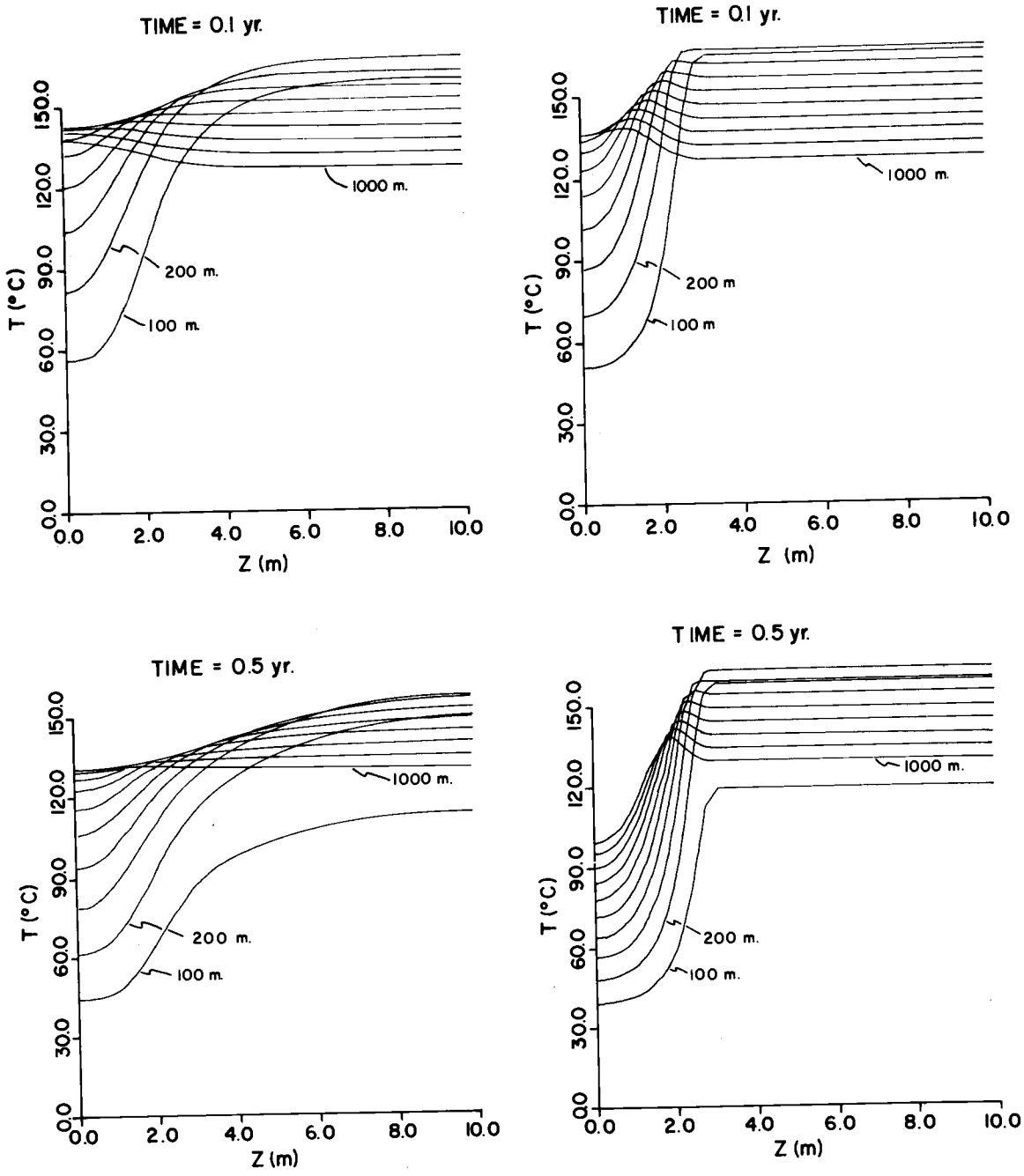

Figure 9. Time development of fluid temperature distribution in an upflow system under severely non-uniform flow. Curves on the left hand side correspond to Fourier-Galerkin solution and those on the right hand side correspond to uncoupled solution.

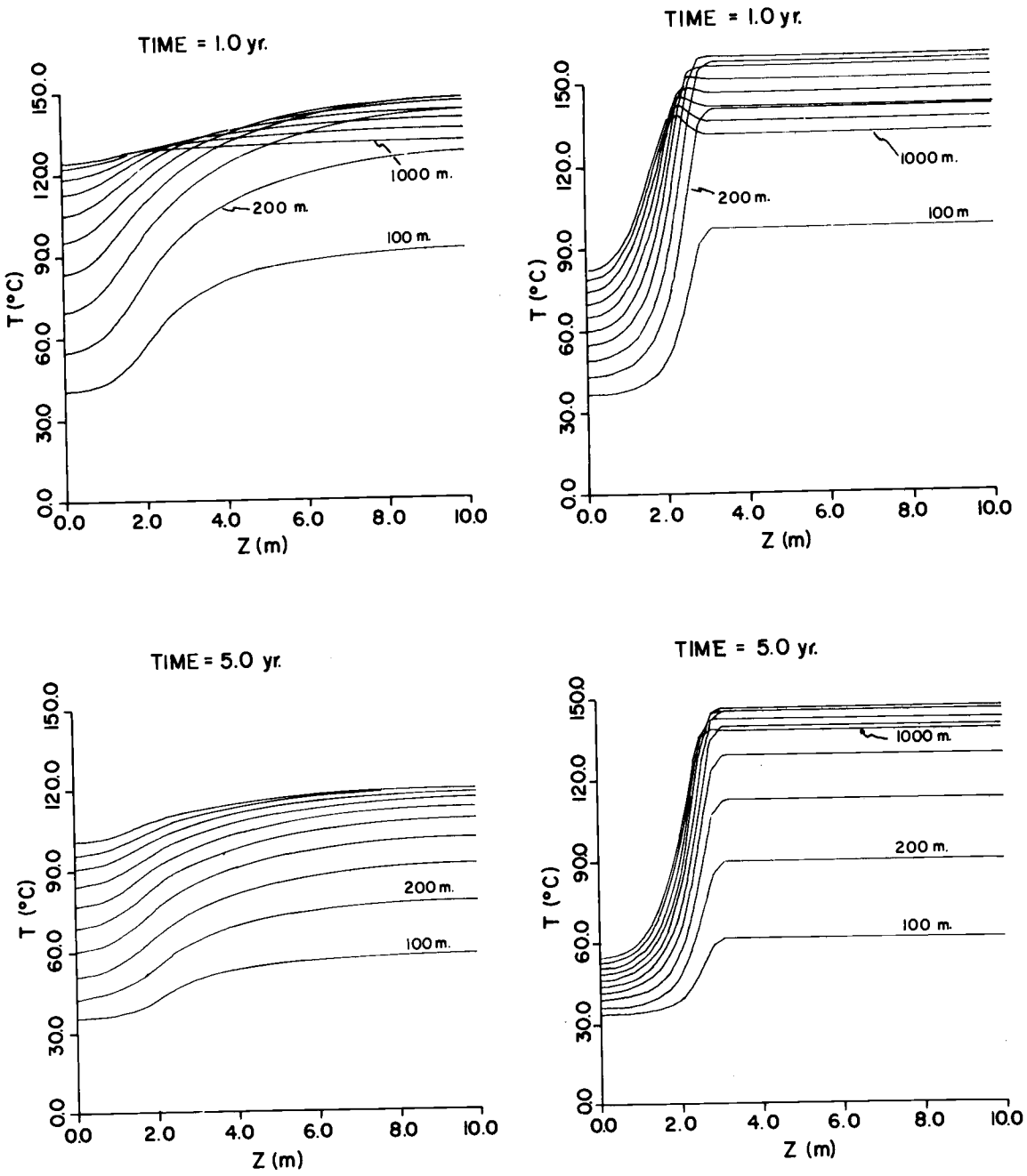

Figure 9. Continued.

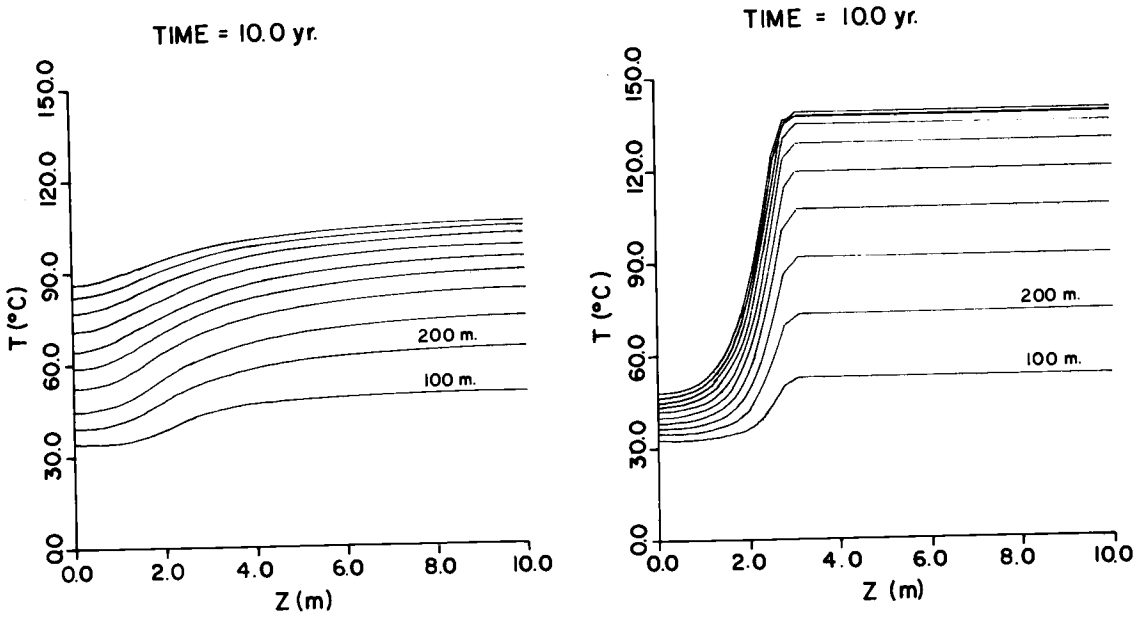

Figure 9. Continued.

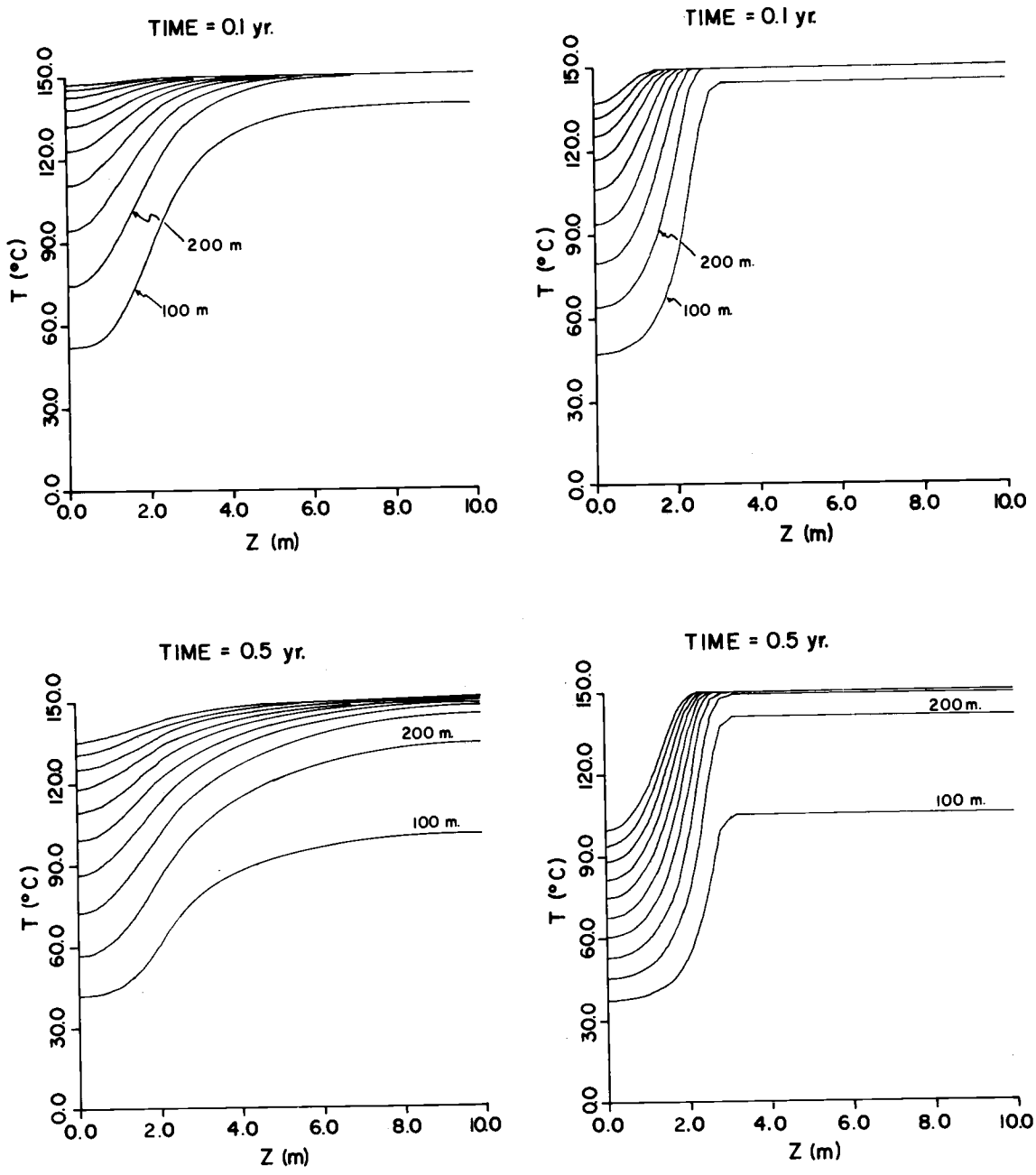

Figure 10. Time development of fluid temperature distribution for the case of an initial uniform rock formation temperature under severely non-uniform flow. Curves on the left hand side correspond to Fourier-Galerkin solution and those on the right hand side correspond to uncoupled solution.

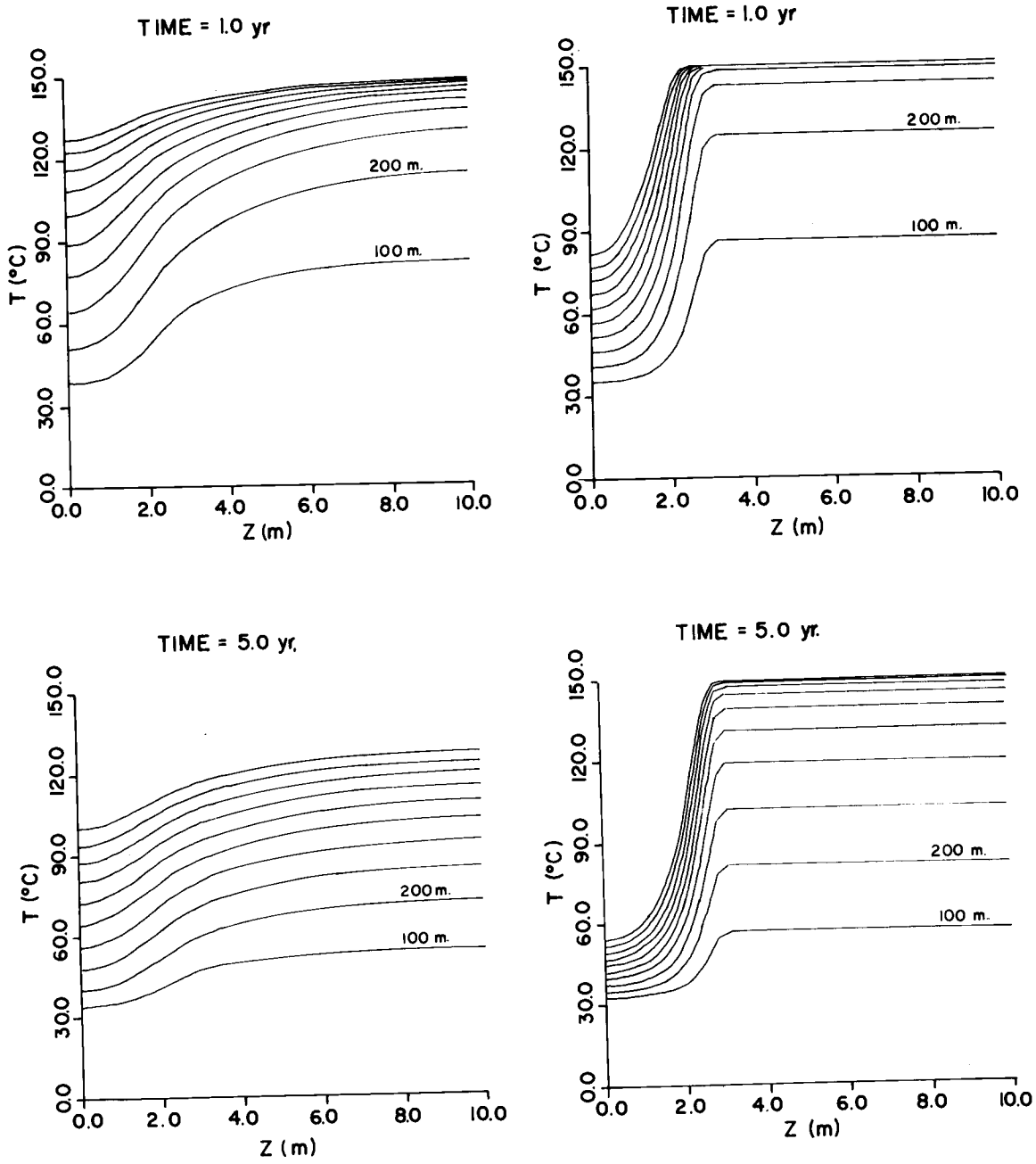

Figure 10. Continued.

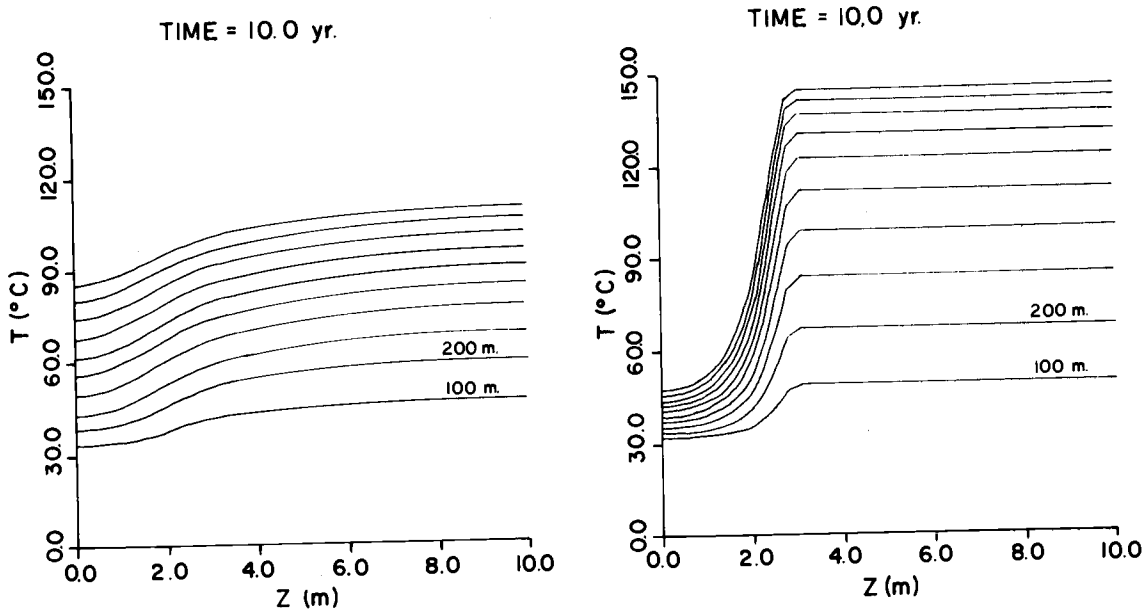

Figure 10. Continued.

At this juncture, it is of some interest to compare the Fourier-Galerkin solution with the perturbation solution to determine at what point the perturbation solution breaks down. That is, as the flow perturbation amplitude q_1 (see equation 4.22) is increased, at what point does the perturbation theory deviate "substantially" from the Fourier-Galerkin solution. Since the perturbation method discussed in the previous section was developed specifically for a pure harmonic flow variation (see equation 4.22), the Fourier-Galerkin solution is computed on the basis of an identical flow geometry. This is accomplished by setting $z_L = 0$ and $z_H = L$ in the above expression for $q(z)$. Letting T_P be the perturbation solution and T_{F-G} be the Fourier-Galerkin solution, the rms error of the perturbation solution is computed as

$$|T_P - T_{F-G}|_{rms} = \frac{1}{L}\left[\int_0^L (T_P - T_{F-G})^2 dz\right]^{1/2}$$

where the indicated integration is accomplished numerically using Simpson's Rule.

Figure 11 shows an example of the rms error of the perturbation method as a function of distance from the injection port and time based on a channel wavelength $\lambda = 10$ m. Two flow perturbations, $q_1/q_0 = 0.5$ and $q_1/q_0 = 0.75$, were considered, where q_0 was taken to be 0.05 kg/(m. sec). The injection temperature is 30°C and

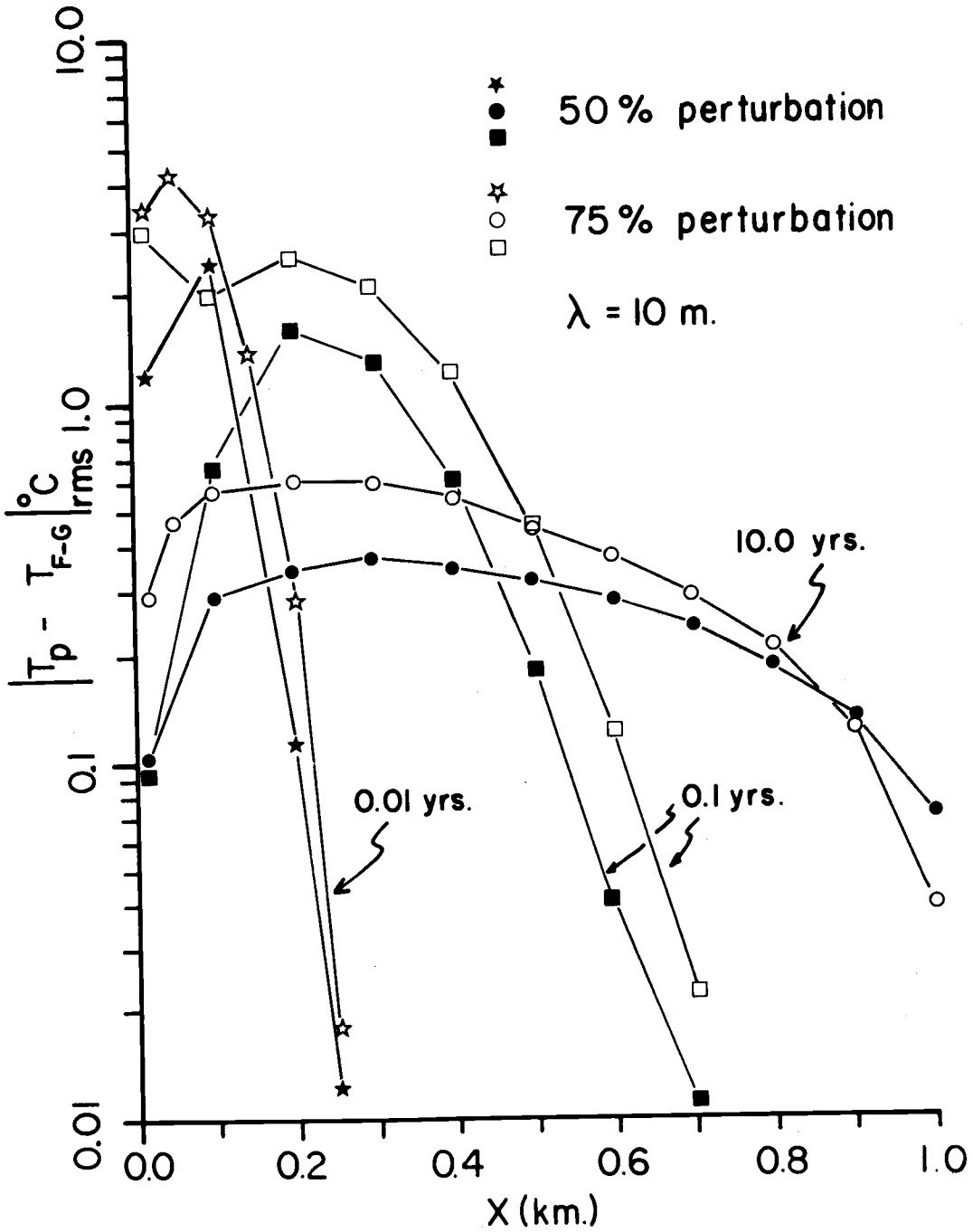

Figure 11. Error in the perturbation method as a function of distance from the injection port and time. Error is calculated by comparison with Fourier-Galerkin method.

the initial formation temperature is 150°C. It is seen that, even for these large perturbations, the first-order theory does a very good job of approximating the true fluid temperature for the particular flow geometry under consideration. It is furthermore noted that the shapes of the error distributions in Figure 11 correspond roughly to the shapes of the peak-to-peak temperature curves of Figure 7. This reflects the condition that the magnitude of error in the perturbation method is correlated strongly with the transverse temperature gradient. For the most part, the true temperature field of the fluid is a pure harmonic function of the z coordinate, as indicated by the relatively small rms error shown in Figure 11. The maximum deviations from a pure harmonic field occur in regions of the conductor where the transverse temperature gradient is the largest. Additional computations have been carried out that show that the error associated with the perturbation method for $\lambda > 10$ m is smaller than that indicated in Figure 11 for $\lambda = 10$ m.

The above analysis indicates that, for rather large flow perturbations, solutions for an arbitrary uni-directional flow configuration based on a linear combination of terms of the form indicated by equation (4. 22) can serve as a good approximation to the true fluid temperature field.

Fluid Losses

Fluid losses due to leakage from a natural fluid conductor may significantly reduce the total produced thermal energy of a recovery system. As a rock cools, fracture openings will enlarge due to the thermoelastic contraction of the adjacent formation. The increased permeability combined with the preferential downward convective penetration of cold water within the system may serve to channel the injected water out of the heating zone. It is evident that a fluid can be injected between the contact planes of a closed conductor only if the fluid pressure exceeds the local contact pressure. The magnitude of the lithostatic (overburden) and regional tectonic stresses may be such that in order to obtain the required flow rate, an increased well head pumping pressure may be necessary. It is likely that the elevated pumping pressure required for conductors exhibiting very small natural permeability will increase fluid losses from the system.

The present section describes the effects of a distributed fluid loss within the conductor on the production temperature of the system.

Fluid Loss Model

We will investigate the case where the fluid flow is a function only of the distance between the injection and production ports of the system. Using the first-order heat extraction model, the problem can

be stated mathematically, analogous to equations (3.9) through (3.12), as

$$\frac{1}{a_r}\partial_t T - \partial_{yy} T = 0, \quad y > 0 \tag{4.42}$$

$$2k_r \partial_y T = \sigma_f q(x) \partial_x T, \quad y \downarrow 0 \tag{4.43}$$

$$T(x, y, t)\big|_{t \leq 0} = f(x) \tag{4.44}$$

$$T(0, 0, t)\big|_{t > 0} = T_i \tag{4.45}$$

The zero fracture width approximation has been used in the heat transfer boundary condition (4.43).

The solution to the above initial and boundary value problem is obtained using integral transform methods in a manner similar to that discussed in Chapter III. Applying the Laplace transform with respect to time to equations (4.42) and (4.43), we obtain

$$2k_r \partial_y \hat{T} = \sigma_f q(x) \partial_x \hat{T}, \quad y \downarrow 0 \tag{4.46}$$

$$\frac{1}{a_r}\{s\hat{T} - f(x)\} - \partial_{yy} \hat{T} = 0, \quad y > 0 \tag{4.47}$$

The general solution for $\hat{T}$ that remains finite as $y \to \infty$ is

$$\hat{T}(x, y, s) = \hat{A}(x, s)\exp\left(-\sqrt{\frac{s}{a_r}}\, y\right) + \frac{f(x)}{s} \tag{4.48}$$

Inserting expression (4.48) into equation (4.46), a first order differential equation for $\hat{A}(x, s)$ is obtained

$$\partial_x \hat{A}(x, s) + \alpha_0 \sqrt{\frac{s}{a_r}} \frac{q(0)}{q(x)} \hat{A}(x, s) = - \frac{1}{s} f'(x) \tag{4.49}$$

where

$$\alpha_0 = \frac{2k_r}{\sigma_f q(0)}$$

Using standard techniques for the solution of non-homogeneous differential equations with variable coefficients (Leighton, 1966), the general solution for $\hat{A}(x, s)$ is

$$\hat{A}(x, s) = \exp\left[-\alpha_0 \sqrt{\frac{s}{a_r}} \int_0^x \frac{q(0)}{q(x')} dx' \right] \times \left[\hat{B}(s) - \frac{1}{s} \int_0^x f'(x'') \exp\left[\alpha_0 \sqrt{\frac{s}{a_r}} \int_0^{x''} \frac{q(0)}{q(x')} dx' \right] dx'' \right] \tag{4.50}$$

where $\hat{B}(s)$ is a function yet to be determined. Thus, the Laplace transform of the rock temperature field can be written as

$$\hat{T}(x, y, s) = \exp\left[- \sqrt{\frac{s}{a_r}} \left[y + \alpha_0 \int_0^x \frac{q(0)}{q(x')} dx' \right] \right] \times \left[\hat{B}(s) - \frac{1}{s} \int_0^x f'(x'') \exp\left[\alpha_0 \sqrt{\frac{s}{a_r}} \int_0^{x''} \frac{q(0)}{q(x')} dx' \right] dx'' \right] + \frac{f(x)}{s} \tag{4.51}$$

Evaluating $\hat{T}$ at $x = y = 0$ and using the Laplace transforms of equation (4.44) and (4.45),

$$\hat{B}(s) = \frac{T_i - f(0)}{s}$$

For the present analysis, we choose the simplest distributed fluid loss between the injection and production ports of the system--namely, a uniform loss. Thus, the flow rate can be written as

$$q(x) = q_1 + q_2 x \tag{4.52}$$

where q_1 and q_2 are constants and $q_2 < 0$. The initial rock formation temperature is again assumed to be a linear function of x, or

$$f(x) = c_1 + c_2 x$$

where c_1 and c_2 are constants. With these requirements, equation (4.51) reduces to

$$\hat{T}(x, y, s) = \exp\left[-\sqrt{\frac{s}{a_r}}\left[y + \frac{\alpha_0}{\gamma} \ln(1+\gamma x) \right] \right] \times \left[\frac{(T_i - c_1)}{s} - \frac{c_2}{s}\left[\frac{1}{\gamma + \alpha_0 \sqrt{\frac{s}{a_r}}} \right] (1+\gamma x) \exp\left[\frac{\alpha_0}{\gamma} \sqrt{\frac{s}{a_r}} \ln(1+\gamma x) \right] - 1 \right] + \frac{(c_1 + c_2 x)}{s} \tag{4.53}$$

where

$$\gamma = \frac{q_2}{q_1}$$

To determine the temperature of the water within the fluid conductor, $\hat{T}(x, y, s)$ is evaluated at $y = 0$. Inverse Laplace transforming the resulting equation (Abramowitz and Stegun, 1964; Carslaw and Jaeger, 1959), the fluid temperature is found to be

$$\begin{aligned} T_f(x,t) &= \mathbb{L}_s^{-1}[\hat{T}(x,0,s)] \\ &= (T_i - c_1)\operatorname{erfc}\left[\frac{\alpha_0 \ln(1+\gamma x)}{2\gamma\sqrt{a_r t}}\right] - \frac{c_2(1+\gamma x)}{\gamma}\left[1-\exp\left(\frac{\gamma^2 a_r t}{\alpha_0^2}\right)\operatorname{erfc}\left(\frac{\gamma\sqrt{a_r t}}{\alpha_0}\right)\right] \\ &\quad + \frac{c_2}{\gamma}\left[\operatorname{erfc}\left(\frac{\alpha_0 \ln(1+\gamma x)}{2\gamma\sqrt{a_r t}}\right) - (1+\gamma x)\exp\left(\frac{\gamma^2 a_r t}{\alpha_0^2}\right)\right. \\ &\quad \left.\times \operatorname{erfc}\left[\frac{\gamma\sqrt{a_r t}}{\alpha_0} + \frac{\alpha_0 \ln(1+\gamma x)}{2\gamma\sqrt{a_r t}}\right]\right] + (c_1 + c_2 x), \quad t > 0 \end{aligned} \tag{4.54}$$

It can be shown that the above solution for the fluid temperature reduces to equation (3.27) in the limit of zero fluid loss within the conductor $(q_1 = 0)$.

We define a fluid loss parameter δ as

$$\delta = \frac{q(0) - q(x_p)}{q(0)}$$

where $q(0)$ is the injection flow rate and $q(x_p)$ is the production flow rate.

Figure 12 shows several examples of the effect of a distributed fluid loss on the temperature of the fluid in the conductor based on equation (4.54). These particular examples assume a constant injection temperature of 30°C and a constant production flow rate of 0.05 kg/(m. sec). The production port is 1 km from the injection port. Three initial formation temperature situations, represented by the dotted lines, are considered. As in Figure 5, these represent an upflow (case A), downflow (case B) and initial uniform temperature (case C) configuration. A 50°C/km geotemperature grandient has been used for the calculation of cases A and B. The fluid temperature distribution has been calculated for 1 year and 10 years after flow start up and for 0%, 25%, and 50% fluid loss between the injection and production ports. Therefore, the injection flow rates corresponding to the 0%, 25%, and 50% losses are 0.05 kg/(m. sec), 0.067 kg/(m.sec), and 0.10 kg/(m. sec) respectively.

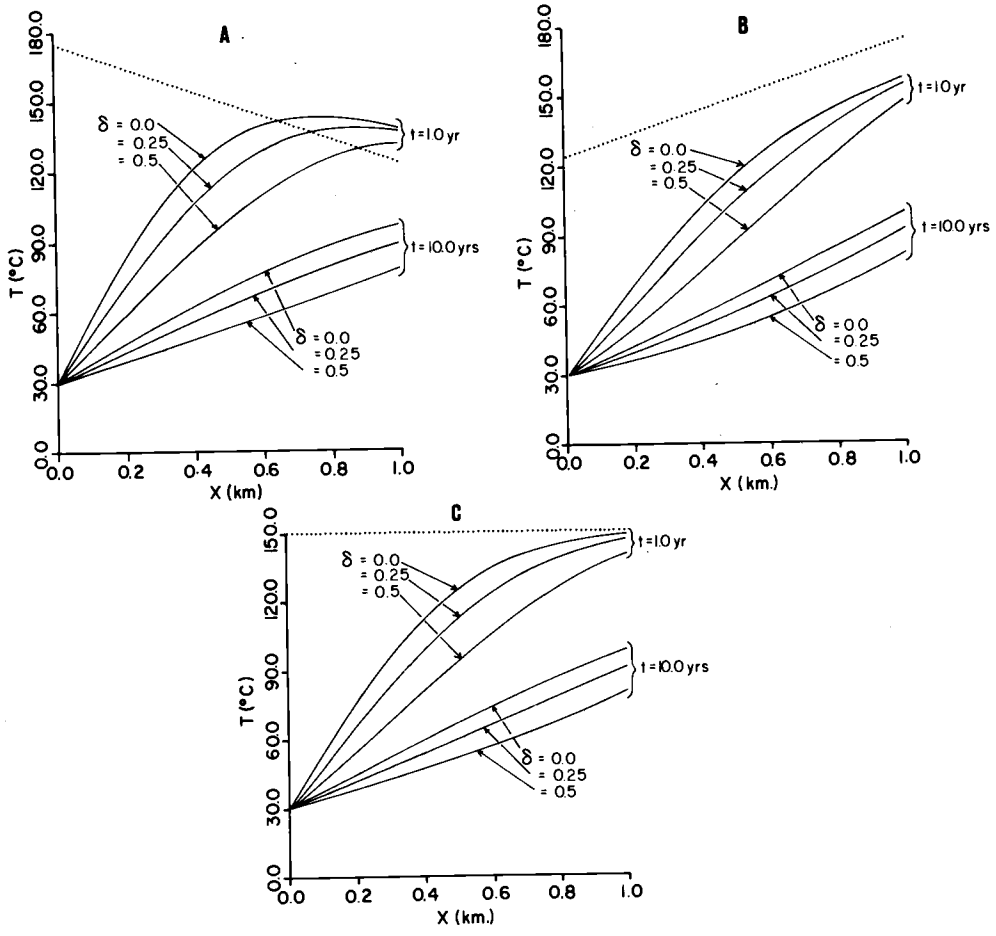

Figure 12. Fluid temperature distributions within the conductor for 0%, 25%, and 50% distributed fluid losses from the conductor.

V. VARIATION OF FLOW RATE TO MEET CONSTANT AND SEASONAL POWER LOADS

The results of Chapters III and IV are based on the assumption that the system flow is stationary in time. The effective power $P = \sigma_f q \Delta T$, where ΔT is the effective utilized temperature span, will vary according to the variation in ΔT. In many commercial applications of geoheat, there will be an interest in a specific power variation--for example, a seasonally varying output in the case of domestic heating. In order to meet these types of loads, the flow rate q must be varied in time in some manner. The present chapter considers two cases of power loads; (1) constant and (2) seasonally varying. A parameter perturbation method is used to determine the required flow rate to meet a constant power load. A numerical approach is used to address the question of a seasonally varying power demand.

Constant Power Demand

The present section investigates the effect of a small time dependent flow rate perturbation on the power output of a forced recovery system. The perturbation method is analogous to that discussed in Chapter IV. The analysis is based on the first-order heat recovery model. Therefore, we consider a uniform and unidirectional flow connecting the injection and production ports of the

system. Referring to Figure 2, a flow rate of the form $\vec{q} = q(t)\hat{x}$ is required.

The mathematical problem can be stated, corresponding to equations (3.9) through (3.12) as

$$\frac{1}{a_r}\partial_t T - \partial_{yy} T = 0, \quad y > 0 \tag{5.1}$$

$$2k_r \partial_y T = \sigma_f q(t) \partial_x T, \quad y \downarrow 0 \tag{5.2}$$

$$T(x, y, t)\Big|_{t \leq 0} = f(x) \tag{5.3}$$

$$T(0, 0, t)\Big|_{t > 0} = T_i \tag{5.4}$$

Again, the zero fracture width approximation has been used in the heat transfer boundry condition (5.2).

The perturbation method used in the present analysis assumes that the flow rate $q(t)$ can be represented by a constant flow rate perturbed by a small temporal flow variation, or

$$q(t) = q_0 + \nu \epsilon(t) \tag{5.5}$$

where

$$\left| \frac{\epsilon(t)}{q_0} \right| \ll 1, \quad t > 0 \tag{5.6}$$

and where ν is the perturbation parameter (see Chapter IV).

We look for a solution of the rock temperature field of the form

$$T(x, y, t) = T_1(x, y, t) + f(x) \tag{5.7}$$

where $f(x)$ is the initial formation temperature and where T_1 is represented by the perturbation series

$$T_1(x, y, t) = T_1^{(0)}(x, y, t) + \nu T_1^{(1)}(x, y, t) + \nu^2 T_1^{(2)}(x, y, t) + \ldots \tag{5.8}$$

Defining the operators H and $V(t)$ as

$$H = \sigma_f q_0 \partial_x - 2k_r \partial_y$$

$$V(t) = \sigma_f \epsilon(t) \partial_x$$

heat transfer boundary condition (5.2) can be written as

$$[H+\nu V(t)]T_1(x, y, t)\big|_{y\downarrow 0} = -\sigma_f q(t) f'(x) \tag{5.9}$$

Inserting expression (5.8) into equation (5.9) and equating equal powers of ν, a set of equations analogous to equations (4.10), (4.11), and (4.12) is obtained. As in Chapter IV, we simplify the analysis by truncating the series (5.8) after the first two terms. Thus, the problem is reduced to solving the following initial and boundary value problem.

$$\frac{1}{a_r}\partial_t T_1^{(0)} - \partial_{yy} T_1^{(0)} = 0, \quad y > 0$$

$$HT_1^{(0)} = -\sigma_f q_0 f'(x), \quad y \downarrow 0$$

$$T_1^{(0)}(x, y, t)\big|_{t \leq 0} = 0 \tag{5.10}$$

$$T_1^{(0)}(0, 0, t)\big|_{t > 0} = T_i - f(0)$$

and

$$\frac{1}{a_r}\partial_t T_1^{(1)} - \partial_{yy} T_1^{(1)} = 0, \quad y > 0$$

$$HT_1^{(1)} + V(t)T_1^{(0)} = -\sigma_f \epsilon(t) f'(x), \quad y \downarrow 0$$

$$T_1^{(1)}(x, y, t)\big|_{t \leq 0} = 0 \tag{5.11}$$

$$T_1^{(1)}(0, 0, t)\big|_{t > 0} = 0$$

The solution of equations (5.10) for the unperturbed solution $T_1^{(0)}$ has been obtained previously. Using the unperturbed solution, equations (5.11) are solved for the first-order perturbation solution $T_1^{(1)}$ using integral transform techniques.

The flow rate perturbation $\epsilon(t)$ is represented by a polynomial in t, or

$$\epsilon(t) = \sum_{n=0}^{N} (-1)^n a_n t^n \tag{5.12}$$

where the a_n's are given numerical coefficients. The reason for including the factor $(-1)^n$ will become apparent as the analysis develops.

The diffusion equation in (5.11) is Laplace transformed with respect to time. The resulting solution for $\hat{T}_1^{(1)}$ that remains finite as $y \to \infty$ is

$$\hat{T}_1^{(1)}(x, y, s) = \hat{A}(x, s)\exp\left(-\sqrt{\frac{s}{a_r}}\, y\right) \tag{5.13}$$

Using the relation (Abramowitz and Stegun, 1964)

$$\mathbb{L}_t[(-1)^n t^n F(t)] = \frac{d^n}{ds^n}\hat{F}(s)$$

the heat transfer boundary condition in (5.11) can be shown, following the Laplace transformation in time, to be

$$H\hat{T}_1^{(1)} + \sigma_f \partial_x \sum_{n=0}^{N} a_n \partial_s^n \hat{T}_1^{(0)}(x, y, s) = -\sigma_f f'(x) \sum_{n=0}^{N} (-1)^n \frac{a_n n!}{s^{n+1}}, \tag{5.14}$$

$$y \downarrow 0$$

Inserting expression (5.13) into equation (5.14), we obtain a first order differential equation for $\hat{A}(x, s)$.

$$\partial_x \hat{A}(x, s) + \alpha_0 \sqrt{\frac{s}{a_r}}\, \hat{A}(x, s) = -\hat{G}(x, s) \tag{5.15}$$

where

$$\alpha_0 = \frac{2k_r}{\sigma_f q_0}$$

and where

$$\hat{G}(x, s) = \frac{1}{q_0} \partial_x \sum_{n=0}^{N} a_n \partial_s^n \hat{T}_1^{(0)}(x, y, s)\Big|_{y \downarrow 0} + \frac{f'(x)}{q_0} \sum_{n=0}^{N} (-1)^n a_n \frac{n!}{s^{n+1}}$$

The general solution for $\hat{A}(x, s)$ that satisfies the homogeneous boundary condition at $x = 0$ is

$$\hat{A}(x, s) = -\int_0^x \exp\{\alpha_0 \sqrt{\frac{s}{a_r}} (x-x')\} \hat{G}(x', s) dx' \qquad (5.16)$$

We now make the simplification that the flow perturbation $\epsilon(t)$ can be represented by a second order polynomial, i.e., $N = 2$. Furthermore, the initial formation temperature $f(x)$ is assumed to have the form

$$f(x) = c_1 + c_2 x$$

where c_1 and c_2 are constants. Using the solution for $\hat{T}_1^{(0)}$ given by equation (3.25) (in the limit of zero fracture width, where $\beta = 0$) in the evaluation of expression (5.16), followed by an inverse transformation, and omitting considerable algebra, we obtain

$$T_1^{(1)}(x, 0, t) = \mathbb{L}_s^{-1}[\hat{A}(x, s)]$$

$$= (c_1 - T_i)\left[\frac{a_0}{q_0} g_0(\xi) + \frac{a_1 t}{q_0} g_1(\xi) + \frac{a_2 t^2}{q_0} g_2(\xi)\right] \qquad (5.17)$$

$$+ c_2 x\left[\frac{a_0}{q_0} h_0(\xi) + \frac{a_1 t}{q_0} h_1(\xi) + \frac{a_2 t^2}{q_0} h_2(\xi)\right]$$

where

$$g_0(\xi) = \frac{-2\xi}{\sqrt{\pi}} \exp(-\xi^2)$$

$$g_1(\xi) = 2\xi \, \text{ierfc}(\xi) + \xi^2 \text{erfc}(\xi)$$

$$g_2(\xi) = 12\,\xi\, i^3\text{erfc}(\xi) + 6\xi^2 i^2\text{erfc}(\xi) - \frac{4}{3}\xi^3 \text{ierfc}(\xi)$$

$$h_0(\xi) = -\frac{1}{\xi\sqrt{\pi}} + \frac{1}{\xi} \text{ierfc}(\xi) + \text{erfc}(\xi)$$

$$h_1(\xi) = -\frac{4}{3} i^3\text{erfc}(\xi) - 4i^2\text{erfc}(\xi) - \xi\text{ierfc}(\xi) + \frac{2}{3\xi\sqrt{\pi}}$$

$$h_2(\xi) = \frac{32}{\xi} i^5\text{erfc}(\xi) + 32i^4\text{erfc}(\xi) + 10\xi i^3\text{erfc}(\xi) + \frac{4\xi^2}{3} i^2\text{erfc}(\xi)$$

$$- \frac{3}{5\xi\sqrt{\pi}}$$

where

$$\xi = \frac{\alpha_0 t}{2\sqrt{a_r t}}$$

The repeated integral of the error function, $i^n\text{erfc}(\xi)$, is given by (Abramowitz and Stegun, 1964)

$$i^n\text{erfc}(\xi) = \int_{\xi}^{\infty} i^{n-1}\text{erfc}(t)dt$$

and satisfies the recurrence relation

$$i^n\text{erfc}(\xi) = -\frac{\xi}{n} i^{n-1}\text{erfc}(\xi) + \frac{1}{2n} i^{n-2}\text{erfc}(\xi)$$

where

$$i^{-1}\text{erfc}(\xi) = \frac{2}{\sqrt{\pi}} \exp(-\xi^2)$$

$$i^0\text{erfc}(\xi) = \text{erfc}(\xi)$$

Recalling from Chapter IV that for a harmonic spatial flow of the form

$$q(z) = q_1 + q_2\cos(\omega_0 z)$$

we obtained a fluid temperature perturbation (in Laplace transform space) of the form

$$\hat{T}_1^{(1)}(x, 0, z, s) = \frac{q_2}{q_1} \cos(\omega_0 z) R(x, \omega_0, s) \qquad (4.22)$$

where R is given by equation (4.21). Taking the limit of the above expression as $\omega_0 \to 0$ we obtain an expression for the temperature perturbation due to a small constant flow change, given by

$$\lim_{\omega_0 \to 0} \hat{T}_1^{(1)}(x, 0, z, s) = (c_1 - T_i) \frac{q_2}{q_1} \hat{g}_0^*(x, s) + c_2 x \frac{q_1}{q_0} \hat{h}_0^*(x, s)$$

where

$$\hat{g}_0^*(x, s) = - \frac{\alpha_0 \sqrt{\frac{s}{a_r}}\, x}{s} \exp(-\alpha_0 \sqrt{\frac{s}{a_r}}\, x)$$

$$\hat{h}_0^*(x, s) = \frac{1}{s} \exp(-\alpha_0 \sqrt{\frac{s}{a_r}}\, x)$$

$$- \frac{1}{\alpha_0 s \sqrt{\frac{s}{a_r}}\, x} \{1 - \exp(-\alpha_0 \sqrt{\frac{s}{a_r}}\, x)\}$$

It is easily shown that the inverse Laplace transforms of $\hat{g}_0^*$ and $\hat{h}_0^*$ are precisely g_0 and h_0 given in equation (5. 17). This expected result serves as a partial check on expression (5. 17).

As an example of the effect of a small flow perturbation on a forced recovery system, we consider the case of an initial uniform formation temperature of 150°C. Water is injected at a constant temperature of 30°C and recovered at a distance of 1. 5 km from the injection port. The power output is computed assuming that the enthalpy is useable down to 40°C with an overall efficiency of 80%. The power output history is varied in the model by adjusting the perturbation coefficients a_0, a_1 and a_2. Figure 13 shows the thermal power history for a 10 year system lifetime with and without

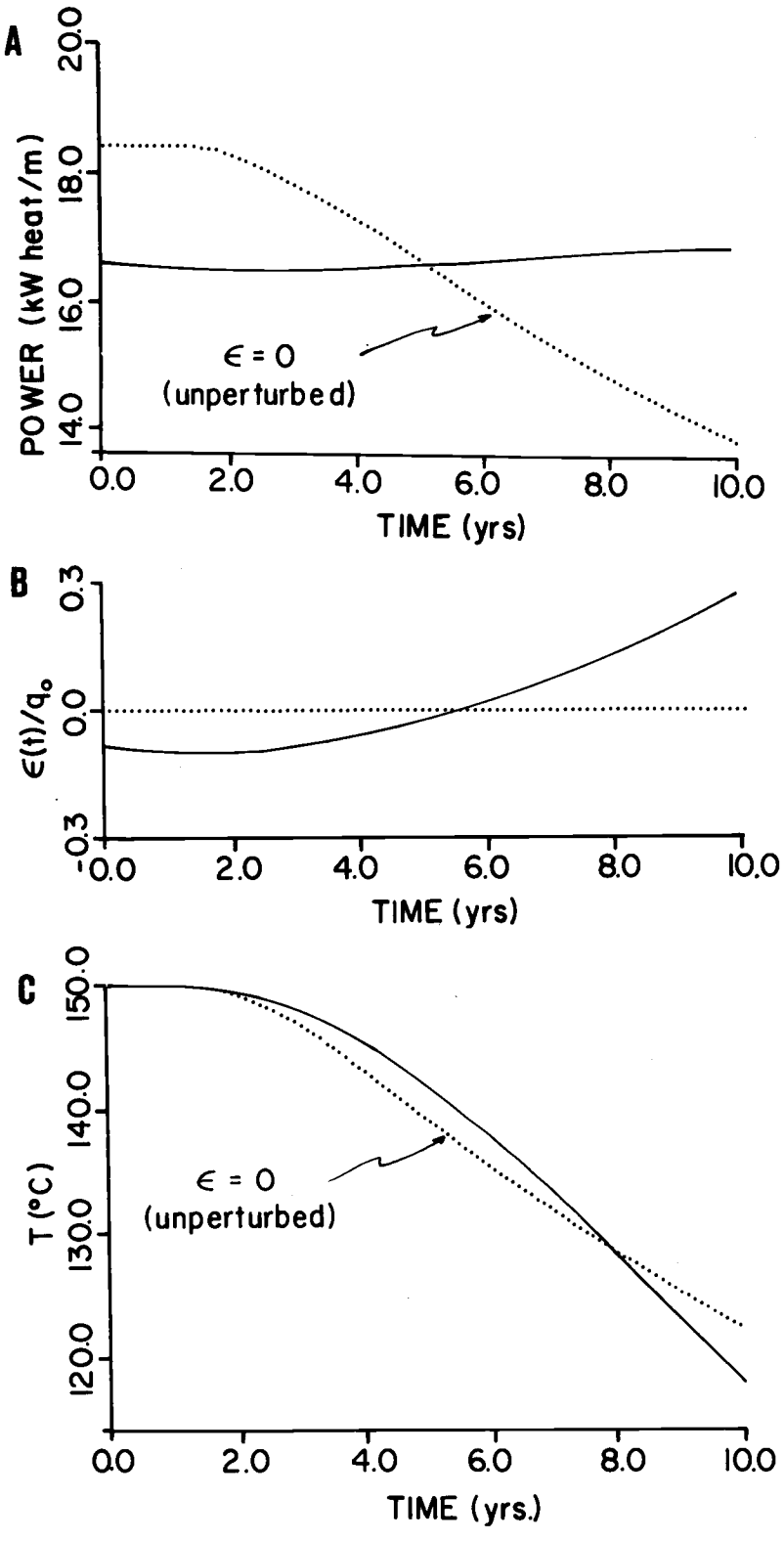

Figure 13. Variation of flow rate to meet constant power demand based on a perturbation method.

a flow variation. The unperturbed system corresponds to a constant flow rate of 0.05 kg/(m. sec). By a trial and error procedure, it was found that a flow perturbation of the form

$$\epsilon(t) = -4.8 \times 10^{-3} - 2.0 \times 10^{-4} t + 2.0 \times 10^{-4} t^2 \quad \text{kg/(m.sec)}$$

was sufficient to maintain a relatively constant effective power output over the 10 year system lifetime. In the above expression for the flow perturbation, the time t is given in years.

Seasonally Varying Power Demand

The validity of the perturbation theory will break down for the case of a varying power demand with large peak loads. A numerical "marching" approach is developed to address the question of the ability of a forced recovery system to meet a seasonally varying power demand. Equation (5.13) can be rewritten as

$$\hat{T}_1(x, y, s) = \{s^2 \hat{T}_1(x, y, s)\big|_{y \downarrow 0}\} \frac{\exp(-\sqrt{\frac{s}{a_r}}\, y)}{s^2} \qquad (5.18)$$

Inverse Laplace transforming $\hat{T}_1(x, y, s)$, one obtains

$$T_1(x, y, t) = 2 \int_0^t \partial_\tau^2 T_1(x, y, \tau)\big|_{y \downarrow 0} (t-\tau) i^2 \operatorname{erfc} \frac{y}{\sqrt{a_r (t-\tau)}}\, d\tau \qquad (5.19)$$

where the convolution theorem for the product of two Laplace transforms has been used (Abramowitz and Stegun, 1964). Thus, the heat flow at a given time and position within the conductor can be expressed in terms of the temperature history of the fluid.

$$\partial_y T_1(x, y, t)\big|_{y\downarrow 0} = -\frac{2}{\sqrt{a_r \pi}} \int_0^t \partial_\tau^2 T_1(x, y, \tau)\big|_{y\downarrow 0} \sqrt{t-\tau}\, d\tau \qquad (5.20)$$

Using the above expression, the heat transfer boundary condition (5.2) can be written as

$$\frac{4k_r}{\sqrt{a_r \pi}} \int_0^t \partial_\tau^2 T_1(x, y, \tau)\big|_{y\downarrow 0} \sqrt{t-\tau}\, d\tau + \sigma_f q(t)\{\partial_x T_1(x, y, t)\big|_{y\downarrow 0} + f'(x)\} = 0 \qquad (5.21)$$

Equation (5.21) is Laplace transformed <u>with respect to x</u> to obtain

$$\frac{4k_r}{\sqrt{a_r \pi}} \int_0^t \partial_\tau^2 \hat{T}_1(r, y, \tau)\big|_{y\downarrow 0} \sqrt{t-\tau}\, d\tau + \sigma_f q(t)\{r\hat{T}_1(r, y, t)\big|_{y\downarrow 0} + c_1 + \frac{c_2}{r} - T_i\} = 0 \qquad (5.22)$$

where r is the transform variable corresponding to x. We have again assumed an initial formation temperature of the form $f(x) = c_1 + c_2 x$, where c_1 and c_2 are constants. The above expression is recast in a finite difference approximation given by

$$\frac{4k_r}{\sqrt{a_r \pi}} \sum_{j=0}^{n-1} \frac{\{\hat{T}_{j-1}(r)-\hat{T}_j(r)+\hat{T}_{j+1}(r)\}}{(\Delta t)^2} \sqrt{n\Delta t - j\Delta t}\, \Delta t$$

$$+ \sigma_f q(n\Delta t)\{r\hat{T}_n(r)+c_1+\frac{c_2}{r}-T_i\} = 0, \quad n = 1, 2, \ldots \tag{5.23}$$

where

$$\hat{T}_n(r) = \hat{T}_1(r, y, n\Delta t)\Big|_{y\downarrow 0}$$

and

$$\hat{T}_1(r) = 0$$

$$\hat{T}_0(r) = 0$$

Solving for $\hat{T}_n(r)$, we obtain

$$\hat{T}_n(r) = -\frac{A_n(r)}{B_n(r)} \tag{5.24}$$

where

$$A_n(r) = \sum_{j=0}^{n-2} \{\hat{T}_{j-1}(r)-2\hat{T}_j(r)+\hat{T}_{j+1}(r)\} \frac{\sqrt{n-j}}{\Delta t}$$

$$+ \frac{(\hat{T}_{n-2}(r)-2\hat{T}_{n-1}(r))}{\Delta t} + \sqrt{\frac{a_r \pi}{\Delta t}} \frac{\sigma_f q(n\Delta t)}{4k_r} (c_1+\frac{c_2}{r}-T_i)$$

and

$$B_n(r) = \frac{1}{\Delta t} + r\sqrt{\frac{a_r \pi}{\Delta t}}\,\frac{\sigma_f q(n\Delta t)}{4k_r}$$

The marching scheme described above can easily be generalized to allow for a time varying injection temperature. The temperature of the fluid within the conductor at time $n\Delta t$ is given by

$$T_f(x, n\Delta t) = \mathbb{L}_r^{-1}[\hat{T}_n(r)] + f(x)$$

where the indicated Laplace inverse transform is done numerically by a procedure described in Appendix A.

The thermal power output of the heat recovery system is

$$P(x, n\Delta t) = \eta\sigma_f q(n\Delta t)\{T_f(x, n\Delta t) - T_d\}$$

where η is the overall heating system efficiency and T_d is the disposal temperature of the water. Assuming that the power demand is a prescribed function of time, the required flow rate at time $(n+1)\Delta t$ can be estimated in a recursive manner from the power demand at time $(n+1)\Delta t$ and the production temperature at time $n\Delta t$. In schematic form, the recursive marching scheme is given by

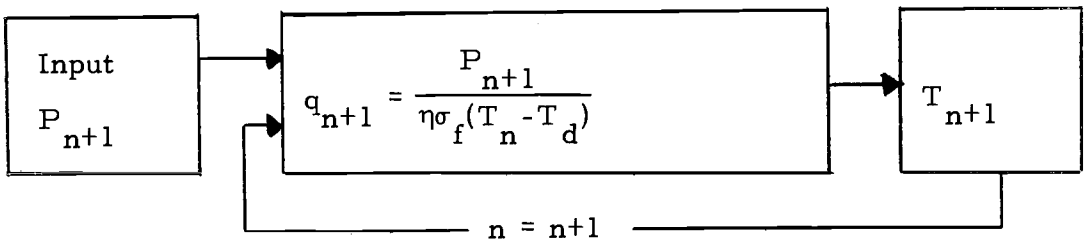

The numerical stability of the recursive marching scheme will be difficult to determine and is beyond the scope of the present work. However, results of the method compare favorably with the perturbation method discussed in the previous section and this observation is taken as an indicator of the stability of the method.

Figure 14 shows an example of a seasonally varying large amplitude flow variation based on the recursive marching scheme discussed above. As in the example given for the perturbation method, the initial rock formation temperature is 150°C and the injection temperature is 30°C. The thermal water is recovered at a distance of 1.5 km from the injection port. The power output is computed assuming that the enthalpy is useable down to 40°C with an overall efficiency of 80%.

It is seen from this example that the production temperature for a seasonally varying power demand is not degraded a significant amount over the production temperature for a constant power demand having the same time-averaged mean value (dotted line).

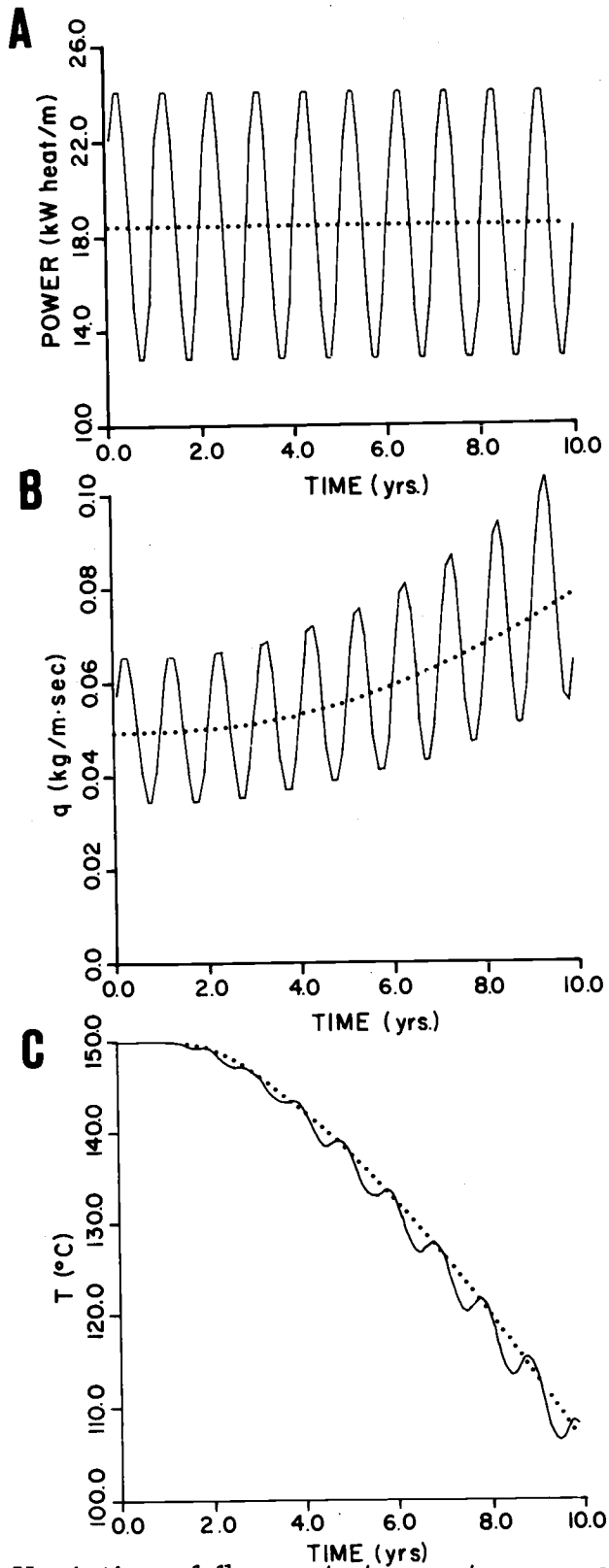

Figure 14. Variation of flow rate to meet seasonally varying power demand based on a numerical recursive marching method.

VI. THERMOELASTIC EFFECTS

The fluid conductance of narrow open spaces such as fractures or other type cracks is very sensitive to changes in their width. Commercial exploitation of geoheat in significant amounts reduces the temperature of large volumes of rock resulting in a substantial volume strain due to thermal contraction. The resulting displacement of the fracture walls due to the volume strain of the adjacent rock will influence the subsurface flow pattern of the thermal fluid and may be of great importance for the time development of a forced recovery system.

The interaction between the thermal and hydrological phenomena in geothermal systems is quite complex. Regional tectonic and lithostatic (overburden) stresses in the rock mass will play a significant role in the behavior of the flow system. The problem is further complicated if the flow system is composed of an interconnected net of fractures. Since the states of flow connectivity and rock stress are likely to be uncertain and difficult to measure, the problem is not amenable to a meaningful theoretical analysis unless very complete observational data are available.

In the present chapter the emphasis is of a general and qualitative nature. The situation is simplified by considering a single flat fracture in the (x, z) plane embedded in a homogeneous isotropic

entire space with Lame's constants λ and μ, Poisson's ratio $\nu = \lambda/(2\lambda+2\mu)$ and coefficient of linear thermal expansion α_T. Starting with an initially unstressed state, let the temperature field in the rock be changed by an amount $\Delta T(P)$, where $P = (x, y, z)$ is a general field point. The temperature change is assumed to be moderate so that no nonlinear or inelastic effects are induced and that uncoupled thermoelastic theory can be applied.

The temperature decrease results in a contraction of the cooled region which is described by the displacement vector field $\vec{u}$. In a homogeneous linear elastic (Hookean) solid, this vector is governed by the differential equation (Parkus, 1968)

$$\nabla^2\vec{u} + \frac{1}{1-2\nu}\,\nabla\nabla\cdot\vec{u} = 2\alpha_T\left(\frac{1+\nu}{1-\nu}\right)\nabla\Delta T \qquad (6.1)$$

Goodier (1937) has shown that the computation of the thermal strain due to an arbitrarily prescribed temperature distribution in an entire space reduces to the determination of the Newtonian potential for a mass distribution whose density coincides with the given temperature field. That is,

$$\vec{u} = -\nabla\varphi \qquad (6.2)$$

where the thermoelastic potential φ is given by

$$\varphi(P,t) = \frac{\alpha_T}{4\pi}\left(\frac{1+\nu}{1-\nu}\right)\int_V \frac{\Delta T(Q,t)dV_Q}{R(P,Q)} \tag{6.3}$$

and satisfies the Poisson equation

$$\nabla^2\varphi + \alpha_T\left(\frac{1+\nu}{1-\nu}\right)\Delta T = 0 \tag{6.4}$$

The difference kernel in expression (6.3) is given by

$$R^{-1}(P,Q) = \{(x-x')^2+(y-y')^2+(z-z')^2\}^{-1/2}$$

where $P = (x, y, z)$ is a general field point and $Q = (x', y', z')$ is a general source point.

For domains other than the entire space, Goodier's approach merely supplies a particular solution of the thermoelastic equations given by equation (6.1) and still necessitates the solution of an ordinary boundary value problem in the theory of elasticity.

Mindlin and Cheng (1950) have extended Goodier's method to the problem of the half-space V_1 in $y > 0$ with a stress-free boundary at $y = 0$. For a temperature change distribution in the region V_1, the displacement is given by

$$\vec{u} = -\nabla\varphi_1 - \nabla_2\varphi_2 \tag{6.5}$$

where

$$\nabla_2 = (3-4\nu)\nabla + 2\nabla y\partial_y - 4(1-\nu)\hat{y}\nabla^2 y \tag{6.6}$$

and

$$\varphi_1(P,t) = \frac{\alpha_T}{4\pi}\left(\frac{1+\nu}{1-\nu}\right)\int_{V_1}\frac{\Delta T(Q,t)dV_Q}{R(P,Q)}$$

$$\varphi_2(P,t) = \frac{\alpha_T}{4\pi}\left(\frac{1+\nu}{1-\nu}\right)\int_{V_2}\frac{\Delta T(Q,t)dV_Q}{R(P,Q)} \tag{6.7}$$

V_2 is the image volume of V_1 in the plane $y = 0$.

In the present case, we are mainly interested in the displacement of the fracture wall in the direction normal to the fracture plane. It is easily shown that the above expression, for this case, yields

$$\begin{aligned}\Delta w(S,t) = \hat{y}\cdot\vec{u}\big|_{y\downarrow 0} &= 4(1-\nu)\partial_y\varphi_1\big|_{y\downarrow 0} \\ &= -\frac{\alpha_T(1+\nu)}{\pi}\int_{V_1}\frac{y'\Delta T(Q,t)dV_Q}{R(S,Q)^3}\end{aligned} \tag{6.8}$$

where

$$R(S,Q) = R(P,Q)\big|_{y\downarrow 0}$$

and $S = (x, z)$ is a general point on the fracture plane. Bodvarsson (1975) has also obtained this result using a slightly different approach.

We will limit the present discussion to the plane thermal strain case in which the temperature field is independent of the z coordinate. Thus, the thermoelastic potential φ_1, given by equation (6.7),

reduces to

$$\varphi_1(x, y, t) = -\frac{\alpha_T}{2\pi}\left(\frac{1+\nu}{1-\nu}\right)\int_A \Delta T(x', y', t)\ln(r')dA' \qquad (6.9)$$

where

$$r' = \{(x-x')^2+(y-y')^2\}^{1/2}$$

and

$$dA' = dx'dy'$$

The above logrithmic potential differs from expression (6.3) by an infinite (ignorable) constant. The normal displacement of the fracture wall for plane thermal strain and with a stress free boundary is thus given by

$$\Delta w(x,t) = -\frac{2\alpha_T(1+\nu)}{\pi}\int_A \frac{y'\Delta T(x', y', t)}{(x-x')^2+y'^2}\,dx'dy' \qquad (6.10)$$

Since Δw represents the displacement of one fracture wall, the total change in fracture width is $2\Delta w$.

We now take advantage of the convolution nature of the above expression to recast the problem as a single integral in Fourier transform space. To this end, we require that the temperature change ΔT is absolutely integrable on the interval $-\infty < x < \infty$ and is piecewise smooth on every finite subinterval. The Laplace transform of Δw (with respect to t) followed by the exponential

Fourier transform (with respect to x) can therefore be written as

$$\hat{\hat{\Delta w}}(\omega, s) = -2\alpha_T(1+\nu)\int_0^\infty e^{-|\omega|y'}\hat{\hat{\Delta T}}(\omega, y', s)dy' \qquad (6.11)$$

where the "$\hat{\hat{\ }}$" denotes the Laplace transform followed by the Fourier transform.

In the present analysis for fracture flow, we assume that water of constant temperature T_i is injected into the fluid conductor at a line source located at $x = 0$. The flow is uniform, stationary and parallel to the x axis with the form

$$\vec{q} = \begin{cases} q\hat{x}, & x > 0 \\ -q\hat{x}, & x < 0 \end{cases}$$

The rock formation is assumed to have an initial uniform temperature $T(x, y, 0) = c_1$. With these requirements, the Laplace transform (with respect to t) of the rock temperature field in $y > 0$ is given by (see Chapter III)

$$\hat{T}(x, y, s) = \frac{(T_i - c_1)}{s}\exp\left[-\sqrt{\frac{s}{a_r}}(\alpha|x|+y)\right] + \frac{c_1}{s} \qquad (6.12)$$

where the dimensionless constant α is given by

$$\alpha = \frac{2k_r}{\sigma_f q}$$

The zero fracture width approximation has been made in the above expression. This approximation has been previously shown to have little effect on the rock temperature field and the error incurred damps out rapidly with time. The change in temperature within the rock due to cooling is given by

$$\Delta\hat{T}(x, y, s) = \frac{(T_i - c_1)}{s} \exp\left[-\sqrt{\frac{s}{a_r}}(\alpha|x| + y)\right] \tag{6.13}$$

and, upon applying the Fourier transform, one obtains

$$\Delta\hat{\hat{T}}(\omega, y, s) = \sqrt{\frac{2}{\pi}} \frac{(T_i - c_1)}{s} \frac{\alpha\sqrt{\frac{s}{a_r}}}{(\alpha^2 \frac{s}{a_r} + \omega^2)} \exp\left(-\sqrt{\frac{s}{a_r}}\, y\right) \tag{6.14}$$

Therefore, the evaluation of the integral (6.11) is elementary, and

$$\Delta\hat{\hat{w}}(\omega, s) = -2\sqrt{\frac{2}{\pi}}\alpha_T\alpha \frac{(T_i - c_1)}{s} \sqrt{\frac{s}{a_r}} \frac{1}{(\omega^2 + \alpha^2 \frac{s}{a_r})(|\omega| + \sqrt{\frac{s}{a_r}})} \tag{6.15}$$

The inverse Fourier transform of the above equation is given by

$$\Delta\hat{w}(x,s) = -\frac{2}{\pi}\sqrt{\frac{s}{a_r}}\,\alpha_T\alpha(1+\nu)\frac{(T_i-c_1)}{s} \times \int_{-\infty}^{\infty}\frac{\exp(-i\omega x)d\omega}{(\omega^2+\alpha^2\frac{s}{a_r})(|\omega|+\sqrt{\frac{s}{a_r}})} \tag{6.16}$$

The integral in the above equation can be evaluated most easily by a contour integration in the complex ζ-plane. The integrand has simple poles at $\pm i\omega\sqrt{\frac{s}{a_r}}$. Thus, upon calculating the residues associated with these poles, the integration is immediate. Figure 15 shows the appropriate contour Γ in the upper half-plane that yields the solution for the half-line $x < 0$. A similar contour in the lower half-plane generates the solution for $x > 0$. The resulting solution defined on $-\infty < x < \infty$ is given by

$$\Delta\hat{w}(x,s) = \frac{2\alpha_T(1+\nu)(T_i-c_1)}{s\sqrt{\frac{s}{a_r}}(1+\alpha)}\exp(-\alpha\sqrt{\frac{s}{a_r}}|x|) \tag{6.17}$$

The evaluation of the inverse Laplace transform of Δw is straight forward, and the final solution for the change in fracture half-width is given by

$$\Delta w(x,t) = 2\alpha_T(\frac{1+\nu}{1+\alpha})(T_i-c_1)\left[2\sqrt{\frac{a_r t}{\pi}}\exp(\frac{-\alpha^2x^2}{4a_r t})-\alpha|x|\operatorname{erfc}(\frac{\alpha|x|}{2\sqrt{a_r t}})\right] \tag{6.18}$$

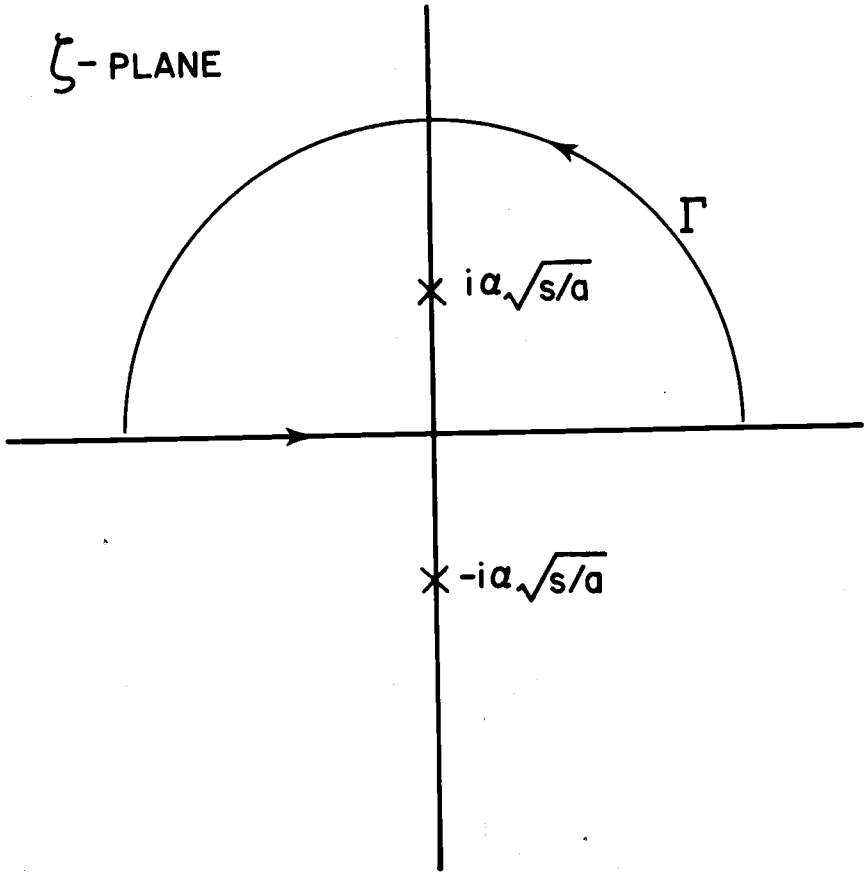

Figure 15. Contour in the complex ζ-plane used in evaluation of the thermoelastic fracture wall response due to cooling of the rock mass.

An example of the change in fracture half-width Δw as a function of time and distance from the injection port is given in Figure 16. The example assumes that water at a temperature of 30°C is injected into the conductor at a constant flow rate $q = 0.05$ kg/(m.sec). The initial formation temperature is 150°C. Figure 16 shows only the $x > 0$ part of the conductor. Since the flow is symmetric about $x = 0$, the change in fracture half-width for $x < 0$ is just a reflection about the plane $x = 0$.

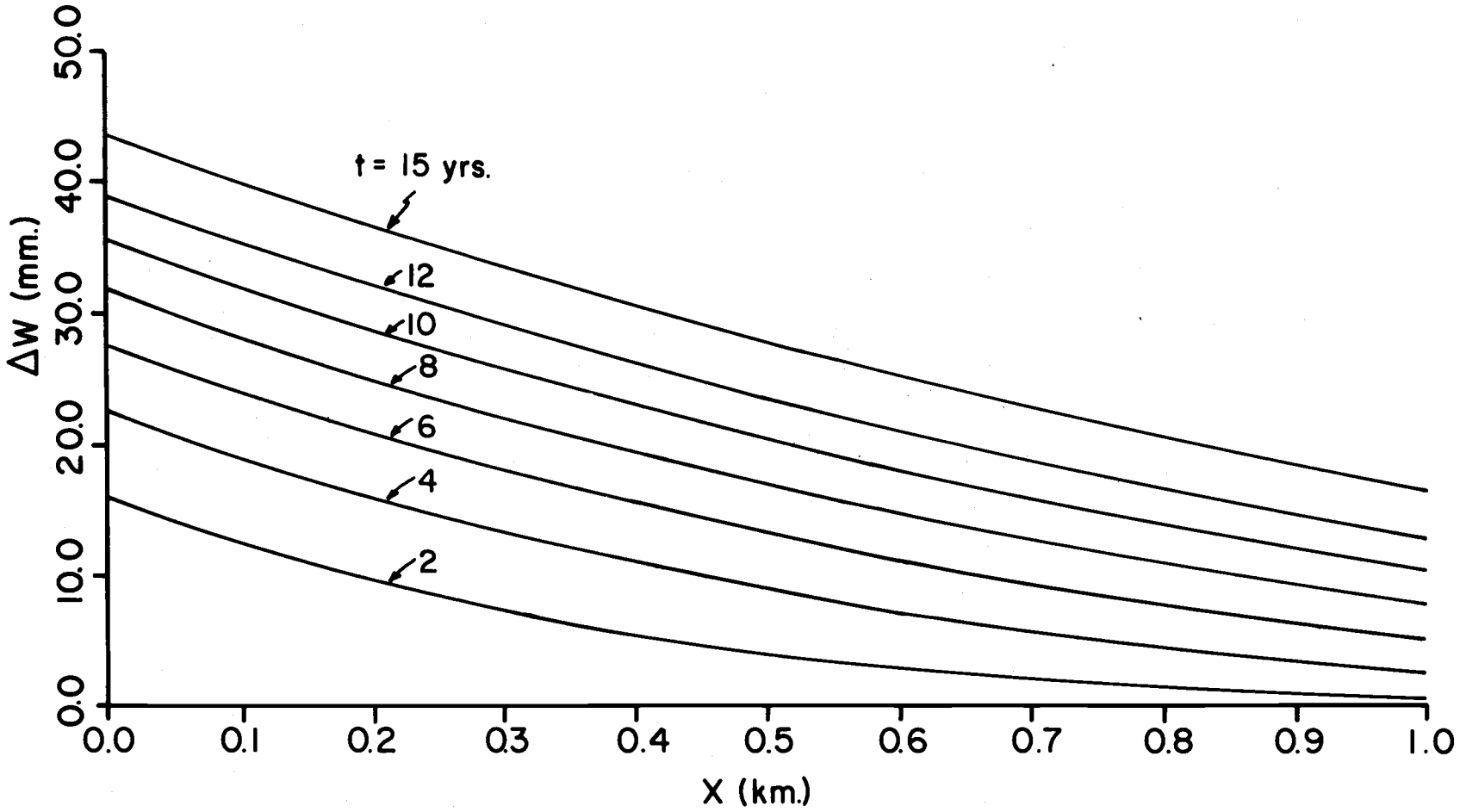

Figure 16. Fracture wall thermoelastic response assuming zero-stress boundary condition. Spatial distribution of the change in half-width Δw as a function of time.

Assuming laminar flow within the conductor, the mass flow q per unit length of conductor is given by (Lamb, 1932)

$$q = -\frac{w^3}{12\nu_f}\frac{dp}{dx}$$

where w is the total fracture width, ν_f is the kinematic viscosity of the fluid, and dp/dx is the pressure gradient in the direction of flow. Therefore, the fluid conductivity per unit length of the fracture is

$$C = \frac{w^3}{12\nu_f}$$

The third power of w indicates the large sensitivity of C to changes in the fracture width. Assuming that the kinematic viscosity of the fluid is constant and that the initial fracture width is 1 millimeter, the above simple examples indicate that over a 10 to 15 year system lifetime, the fluid conductance of the conductor can increase by a factor of 10^4-10^5 due to just thermal effects.

The Reynold's number for fracture flow is given by

$$Re = \frac{q}{\rho_f \nu_f}$$

Since the fracture walls are no doubt quite rough, the onset of

turbulent flow within the fracture spaces will likely occur for $q \gtrsim 600\ \rho_f \nu_f$. Taking the kinematic viscosity of water to be $0.3 \times 10^{-6}\ m^2/sec$ (at 100°C), the critical fracture flow rate for turbulence is 0.18 kg/(m. sec). Assuming that this flow rate is exceeded within the system, the dependence of flow on fracture width is given by the approximate relation (Lamb, 1932)

$$q \propto w\left\{\frac{dp}{dx}\right\}^{1/2}$$

Figure 17 shows the dependence of the fracture half-width Δw on the flow rate q under the same physical situation as in the previous figure. Flow rates between 0.001 kg/(m. sec) and ∞ are considered, the latter corresponding to an isothermal fracture wall temperature of 30°C.

At this juncture, it is of some interest to compare the solution given by equation (6.17) for a fracture wall free of stress with the solution obtained based solely on the entire space thermoelastic potential given by equation (6.3). The latter makes no reference to wall boundary conditions, an assumption that has been made in numerical modeling of convection within a flat fracture because of its computational ease (for example, Blair et al., 1976).

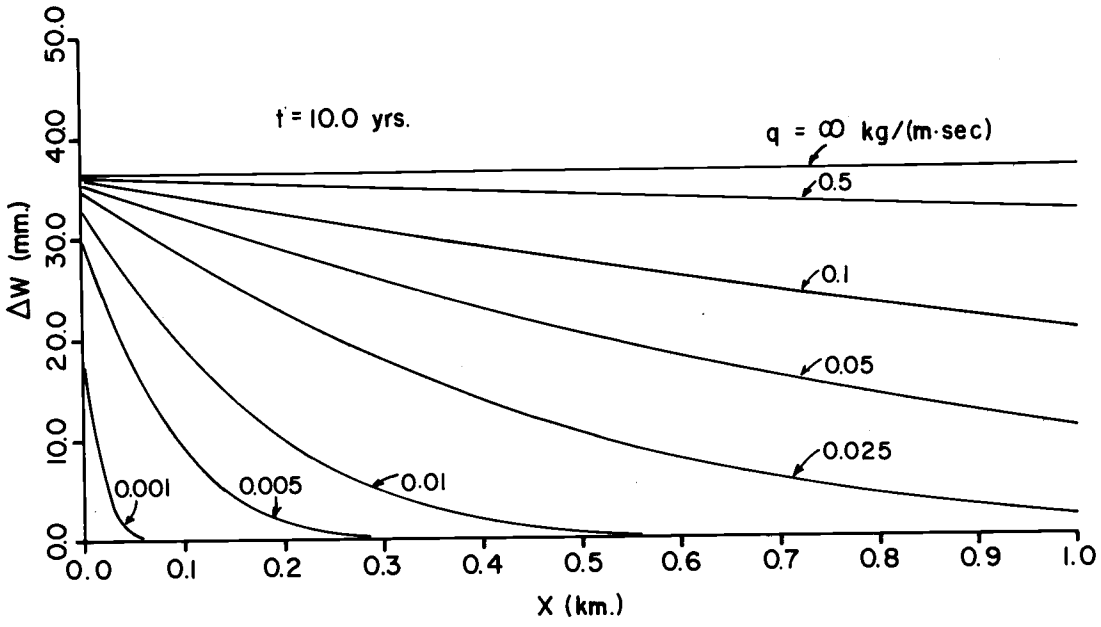

Figure 17. Fracture wall thermoelastic response assuming zero-stress boundary condition. Spatial distribution of the change in half-width Δw as a function of fracture flow rate q.

If the temperature distribution of the rock satisfies the Fourier heat conduction equation, namely

$$\frac{1}{a_r} \partial_t T - \nabla^2 T = 0$$

then the particular solution of the thermoelastic equations may be obtained with a simple integration (as opposed to the multiple integration indicated in 6.3) (Goodier, 1973; Boley and Weiner, 1960). To accomplish this, we note that

$$\nabla^2 \partial_t \varphi + \alpha_T \left(\frac{1+\nu}{1-\nu}\right) \partial_t T = 0$$

or

$$\nabla^2 \{\partial_t \varphi + \alpha_T \left(\frac{1+\nu}{1-\nu}\right) a_r T\} = 0$$

A particular solution of this equation may therefore be obtained by setting

$$\partial_t \varphi + \alpha_T \left(\frac{1+\nu}{1-\nu}\right) a_r T = 0$$

Therefore, the general solution is given by

$$\varphi(P,t) = -\alpha_T a_r \left(\frac{1+\nu}{1-\nu}\right) \int_0^t T(P,\tau) d\tau + \psi(P) \qquad (6.19)$$

where

$$\nabla^2 \psi(P) = -\alpha_T \left(\frac{1+\nu}{1-\nu}\right) T(P,0) \qquad (6.20)$$

For the case under consideration, the initial temperature configuration of the rock mass is uniform and can be taken to be zero (Boley and Weiner, 1960). Thus, a solution of expression (6.20) is $\psi(P) = 0$. Hence, the Laplace transform of the change in fracture half-width based on the entire space thermoelastic potential can be written as

$$\Delta \hat{w}^*(S,s) = -\alpha_T a_r \left(\frac{1+\nu}{1-\nu}\right) \frac{1}{s} \partial_y \hat{T}(P,s)\Big|_{y \downarrow 0} \qquad (6.21)$$

where the "*" indicates that the boundary conditions at the fracture

wall have been ignored in the solution. Using the temperature model (6.12), the above equation can be written as

$$\hat{\Delta w}^*(x, s) = \alpha_T a_r \left(\frac{1+\nu}{1-\nu}\right) \frac{(T_i - c_1)}{s^2} \sqrt{\frac{s}{a_r}} \exp\left(-\alpha \sqrt{\frac{s}{a_r}} |x|\right) \qquad (6.22)$$

Comparing equation (6.22) with equation (6.17), we find that

$$\Delta w(x,t) = \frac{2(1-\nu)}{(1+\alpha)} \Delta w^*(x,t) \qquad (6.23)$$

The difference between the two solutions Δw and Δw^* can be explained as follows. As the rock cools and contracts, tensile and shear stresses are set up at the plane in the entire space coincident with the plane of the fracture. By applying a "virtual" compressive and shear stress to the wall that have an opposite sense, the stresses are removed from the boundary to obtain the stress-free condition. For large flow rates, for which $\alpha \ll 1$, the shear stress set up in the plane is much smaller than the compressive stress. This is most evident for the case of $q = \infty$, in which the fracture wall is isothermal and therefore there are no shear stresses within the rock mass due to thermal causes. Thus, for large flow rates, the applied virtual stress required to eliminate the stress at the boundary is primarily compressive and therefore $\Delta w > \Delta w^*$ as indicated by equation (6.23). On the other hand, for very small flow rates, for

which $\alpha \gg 1$, the shear stress in the plane of the fracture dominates the tensile stress. This is a result of the fact that the temperature field (6.13) does not account for conductive transport in the direction of flow and consequently, large temperature gradients are set up in the x coordinate by this model for small flow rates. The applied virtual stress required to eliminate stress at the boundary is for this case primarily a shear stress which will tend to decrease the fracture width relative to the entire space solution. Thus, as indicated by equation (6.23), $\Delta w < \Delta w^*$.

By including conductive transport in the x coordinate in the temperature model for the thermoelastic response, the relationship between Δw and Δw^*, analogous to equation (6.23), is given by

$$\Delta w(x,t) = 2(1+\alpha^2)^{1/2} \frac{(1-\nu)}{1+\alpha} \Delta w^*(x,t) \tag{6.24}$$

where we have used the results obtained in Appendix B for the temperature field in the rock mass. For this situation, $\Delta w > \Delta w^*$ for all values of $q > 0$.

Fracture flow rates typical of a forced recovery system are on the order of $q > 0.05$ kg/(m.sec) or $\alpha < 0.02$. Thus, to good approximation,

$$\Delta w(x,t) = \frac{3}{2} \Delta w^*(x,t)$$

where we have let $\nu = 0.25$. Therefore, there is roughly a 30% error incurred in estimating the change in fracture width by ignoring the fracture wall boundary for the first-order heat extraction model relative to the entire space solution.

The change in fracture half-width under a non-uniform flow condition within the conductor has been calculated using the Fourier-Galerkin method discussed in Chapter IV. The analysis ignores the stress boundary condition at the fracture wall and consequently, based on the previous discussion, will underestimate the wall response to cooling. The computation is based on equation (6.21) and is contained in program CHFLO given in Appendix E.

Figure 18 shows a particular example of the time development of the change in fracture half-width under a severely non-uniform flow condition. The stationary flow configuration corresponds to curve (a) in Figure 8, where $L = 10$ m. The profiles are plotted at 100 m intervals from the injection port ($x = 0$). The initial rock formation temperature is 150°C and the injection temperature is 30°C. Therefore, Figure 18 corresponds to the temperature history of the fluid given in Figure 10. As in the case of Figures 9 and 10, the curves on the right hand side correspond to the condition where conductive transport in the z coordinate is ignored ("uncoupled model"); i.e., equation (6.15) with q replaced with $q(z)$.

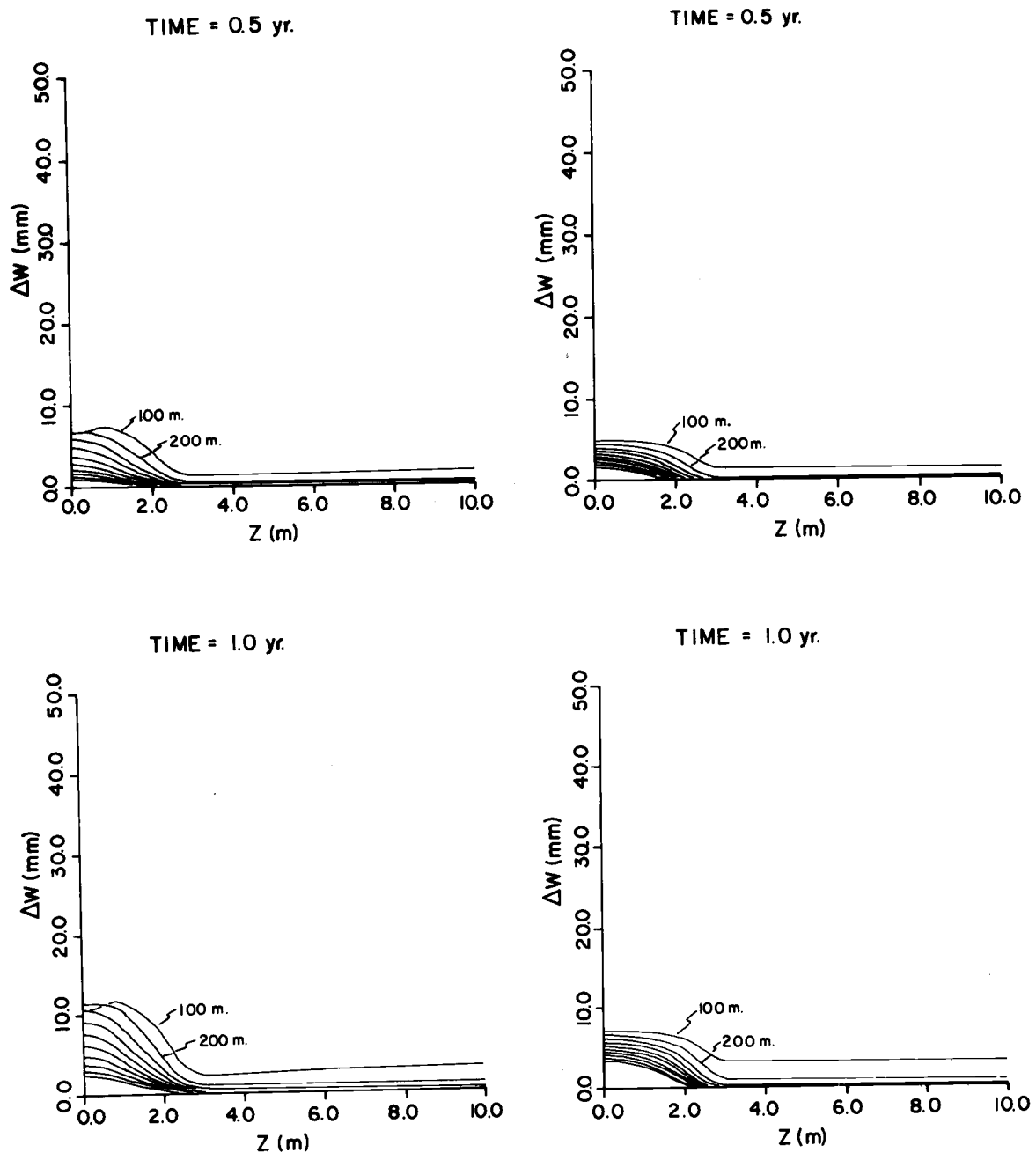

Figure 18. Fracture wall thermoelastic response under severely non-uniform flow conditions. Δw is change in fracture half-width.

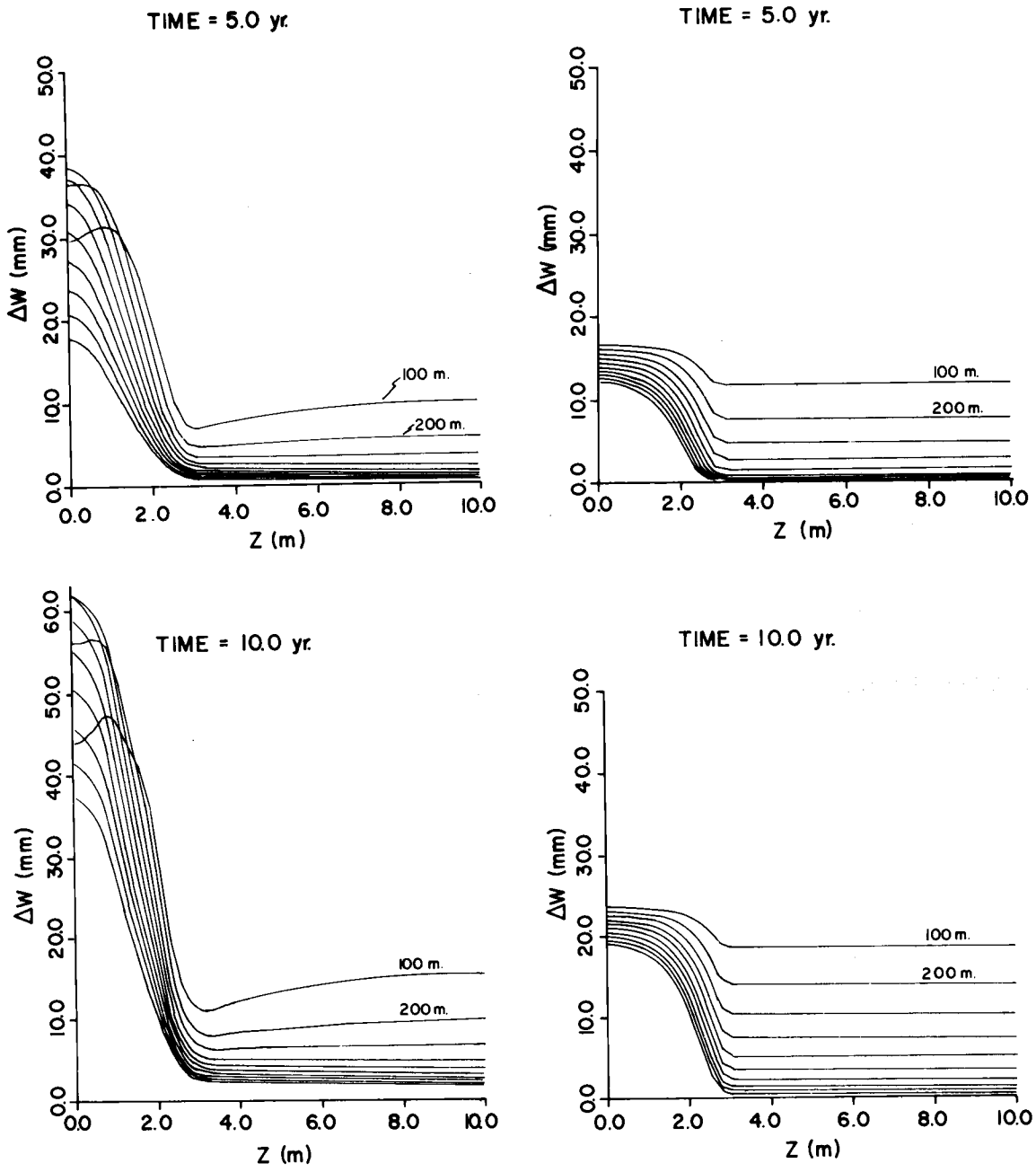

Figure 18. Continued.

It is evident from Figure 18 that, by ignoring the transverse conductive heat transport in the rock, the change in fracture width under the condition of non-uniform flow is substantially altered. The change in fracture width is enhanced in the vicinity of the flow channels over the case where transverse conduction is ignored, reflecting the condition that conduction in two dimensions (y and z) is much more efficient for heat extraction than conductive transport only in the y coordinate. The differences between the two models presented here suggest that, when modeling convective processes of sheet-like flow where non-uniform flow will be expected, some attention must be given to the conductive transport model used for the rock mass adjacent to the flow.

It should be noted here that the relative minima in Δw at $z = 0$ for $x = 100$ m and 200 m are computational artifacts generated by using too few terms in the Fourier expansion of T. In this particular example, 10 terms were retained. The relative minima disappear, with no observable change elsewhere, when 15 terms are kept in the expansion. The maxima in Δw at $z = 0$ and at $x \sim 300$ m for $t = 5$ years and 10 years are real, corresponding to the maximum transverse temperature gradient (and consequently the maximum transverse heat flow) which occurs at this location within the conductor (see discussion in Chapter IV). Since we can no longer use the plane strain symmetry under conditions of

non-uniform flow, an estimate of the change in fracture width under a zero wall stress boundary condition is considerably more difficult. The analysis for the thermoelastic strain in this case is beyond the scope of the present work and will not be considered.

The discussion given above of some thermoelastic effects on fracture width has been limited to very simple flow configurations and rather ideal wall stress boundary conditions. Furthermore, the effect of overburden and tectonic stress on fracture width has been ignored. We have assumed in this analysis that the rock mass is initially free of stress. It is expected that, for the deeper regions of the heat recovery system (for quasi-vertical structures) where the lithostatic stress is greater, substantially more cooling of the rock mass will be required for the negative thermal normal stress at the fracture wall to exceed the normal lithostatic stress and therefore open the fracture. This condition will tend to confine the convective regime to a fixed region within the conductor. Furthermore, it is of interest to note that for a recovery system in the upflow configuration, water flowing from the deeper and hotter regions of the fluid conductor transfers heat to the surrounding rock in the shallower and cooler regions of the formation. Thus, rather than cooling, the rock in this region increases in temperature. This effect is shown in Figure 5A. This may result in a decrease in permeability of the conductor due to the thermoelastic expansion of the material within the conductor and

the adjacent rock mass. In order to maintain the required flow rate in the system, increased pumping pressure may be necessary to overcome this closure effect. Stearns and Friedman (1972) have pointed out however that because fracture surfaces are rarely perfectly planar, a shear displacement of one wall relative to the other can cause a "poorer" fit between adjacent sides of the fracture and thus maintain or even increase the permeability by propping the openings. This phenomenon may counteract the effect of closure due to the thermoelastic response. In addition, if there is also fragmentation into chip-sized material along the fracture openings, these chips may also prop the opening.

VII. SYSTEM DESIGN AND ECONOMICS BASED ON THE FIRST-ORDER MODEL

The economic feasibility of a forced geoheat recovery system is determined by the requirement that total system revenues balance capital and operational costs over a given system lifetime. The present chapter considers fundamental system design and cost criteria to estimate the minimum fluid-rock contact area required for an economically viable forced recovery system under current and projected economic conditions and various geotemperature environments. The analysis is based on the first-order heat recovery model defined in Chapter III.

Design Criteria and Load Characteristics

In the remainder of the present discussion, emphasis will be on the use of quasi-vertical conductors such as fault zones and basaltic dikes. Two basic flow options within the conductors, namely the upflow and downflow configurations, can be considered. Assuming a linear increase of geotemperature with depth, which is the usual situation, the downflow system is more efficient with respect to production temperature than the upflow system. This is easily shown by considering the two initial rock formation temperature distributions

$$f_u(x) = c_1 + c_2(\frac{x_p}{2} - x)$$

$$f_d(x) = c_1 + c_2(x - \frac{x_p}{2})$$

where x_p is the distance from the injection port to the production port within the conductor. In the above expressions $c_2 > 0$ and $0 \leq x \leq x_p$. Both cases have the same initial formation enthalpy in the domain $(0 \leq x \leq x_p) \times (0 < y < \infty)$. $f_u(x)$ is associated with an upflow system and $f_d(x)$ is associated with a downflow system.

Using expression (3.27) for the production temperature model, it is easily shown that

$$T_d(x_p, t) - T_u(x_p, t) = c_2 x_p \operatorname{erf}(\frac{\alpha x_p}{2\sqrt{a_r t}}) + \frac{4c_2}{\alpha}\sqrt{\frac{a_r t}{\pi}}[1 - \exp(-\frac{\alpha^2 x_p^2}{4a_r t})] \geq 0$$

where $T_d(x_p, t)$ and $T_u(x_p, t)$ are the production temperatures associated with the downflow and upflow systems respectively. Thus, the downflow system will have a higher production temperature than the upflow system, given the same initial average formation temperature. In the case of the downflow system, however, fluid is injected at the top, and the flow pattern within the conductor will be more likely to develop a "short-circuit" channelling between injection and

production ports due to convective and thermoelastic effects. The upflow system, where the cold fluid enters from below, will likely be more stable with regard to both short-circuiting and convective mixing. Therefore, it is expected that the upflow system will exhibit a greater flow uniformity than the downflow system. The present economic model assumes that the system is in the upflow configuration. Figure 19 shows a suggested multihole upflow system configuration. In this figure. $A = BL$ is the required contact area and $S = 2B$ is the borehole spacing.

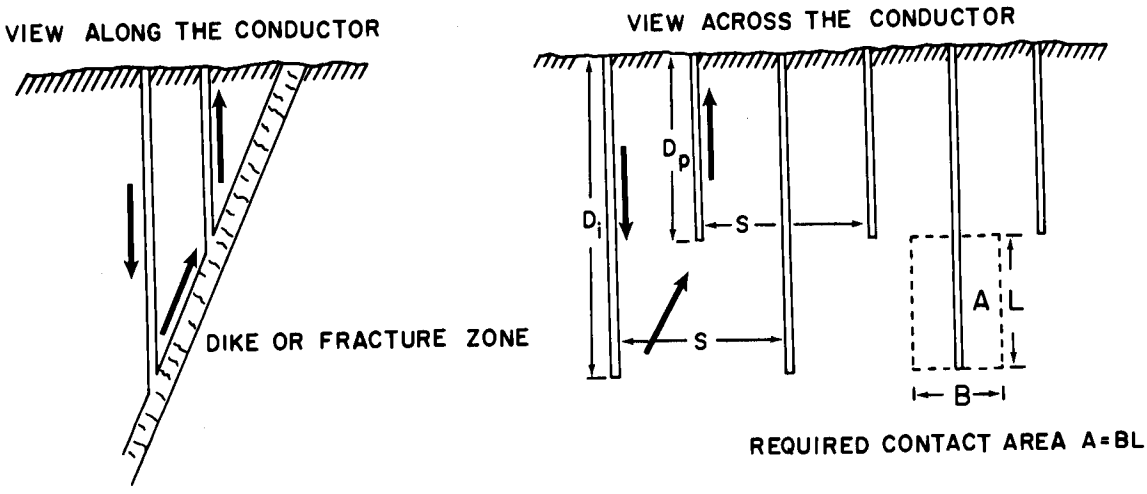

Figure 19. Multihole forced recovery system in the upflow configuration.

A consumer heating system may have highly varying power demand characteristics. For example, domestic heating will typically have a seasonal demand. Such load variations must be

considered in the economic evaluation of a heating system. The flexibility of a forced recovery system to meet a constant or varying power demand has been discussed in Chapter V.

At this juncture, we simplify the picture by basing the economic model on the time-averaged load characteristics of the system rather than on peak load.

Cost Factors

The total construction cost per production unit, which is defined here as a single injection/production borehole pair, consists of two components: (1) the cost of boreholes and (2) the cost of surface equipment such as pumps, pipelines and so on. For the present purpose, we can assume that the cost of drilling per unit depth is a linearly increasing function of depth. The surface equipment constitutes a fixed cost per production unit. Thus, we will assume that the total construction cost per production unit has the form

$$C(D_i, D_p) = c_0 + c_1(D_i+D_p) + c_2(D_i^2+D_p^2)$$

where D_i and D_p are the injection and production depths respectively.

It is well known that borehole drilling costs vary greatly depending on depth, region, and geology. Dagum and Heiss (1968)

give a very comprehensive survey of drilling costs of oil and gas wells in various regions of the United States. The data are given as cost per unit depth as a function of depth, diameter and rock drillability or hardness. Since the Cenozoic volcanics of the Pacific Northwest are quite hard compared with most oil or gas field formations, cost data obtained for drilling to depths of the order of 3 km in formations which are referred to as being very hard are selected. Assuming routine drilling operation and allowing for cost increases since 1968 including additional costs of greater depths and casing, Bodvarsson and Reistad (1975) have arrived at the following estimates for the cost parameters for a single production unit, where the borehole diameters are from 250 to 300 millimeters.

$$c_0 = \$400,000$$

$$c_1 = \$60,000/\text{km}$$

$$c_2 = \$50,000/\text{km}^2$$

An independent investigation of drilling costs based on existing oil and gas well data has been done by Milora and Tester (1976). The cost projection model assumes that the functional relationship of cost with depth will be the same for geothermal wells as it is for oil and gas wells. Again, the cost data are inflated to 1976 dollars to provide a consistent basis for comparison. Figure 20 shows the drilling cost

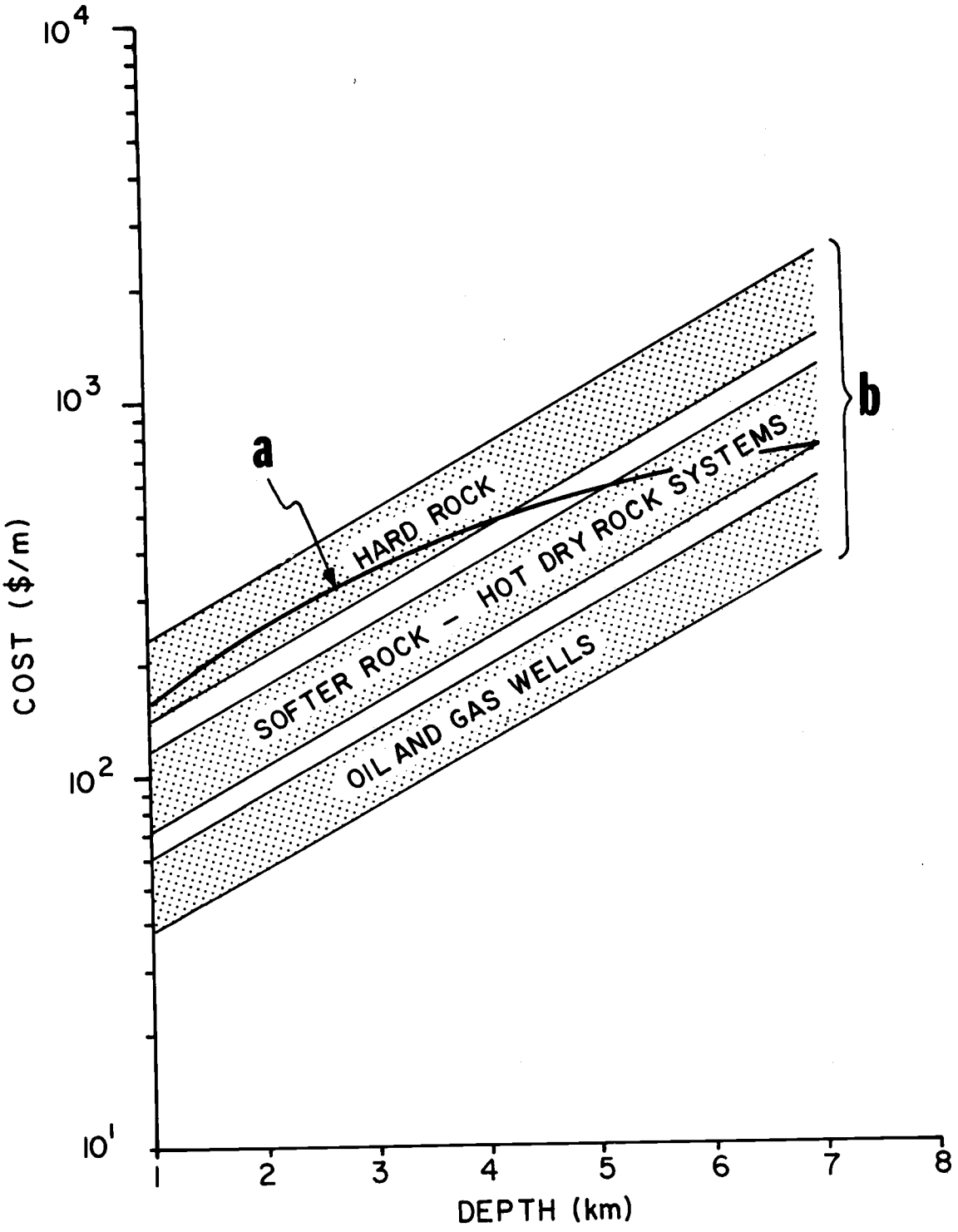

Figure 20. Borehole drilling costs based on existing oil and gas well data. Shaded region (b) from Milora and Tester (1976); solid line (a) from Bodvarsson and Reistad (1975).

per unit depth as a function of depth for the results of Bodvarsson and Reistad (solid curve) and Milora and Tester (shaded region). The data are for a single hole. The economic model presented here assumes drilling costs conform to the estimate by Bodvarsson and Reistad.

Interest on capital is assumed to amount to 8% and is compounded annually. Moreover, the total annual operational costs and expenditures exclusive of electrical energy for pumping are estimated at 5% of the invested capital. Total pumping pressure is assumed to vary from 50 bar for systems with injection at 2 km to 100 bar for injection at 4 km. The resulting pumping energy is 2 to 4 kWhr/metric ton of water. At an energy cost of 3¢/kWhr, the total pumping energy cost will vary as $3\ D_i$ ¢/metric ton, where D_i is the injection depth in kilometers.

In an ideal forced recovery system, no water will be lost from the system and the injected mass flow of fluid can be met simply by reinjection of the produced fluid. In a non-ideal system, where fluid loss due to leakage may occur, additional water for reinjection to replace that lost must be obtained. The cost of the reinjected fluid is assumed to be 1¢/metric ton.

Thermal Water Value and Network Distribution Costs

An estimate of distribution costs fo a district heating system in the Pacific Northwest, based on a yearly average load density of the assumed market of 6 MW/km^2, has been obtained by Bodvarsson and Reistad (1975). The cost is estimated at \$1.7/GJ (one GJ = 10^9 J) and is based on an assumed 100°C effective temperature drop. In the present analysis, a conservative value of \$2/GJ has been used.

It is interesting to note that the production and distribution costs in the Reykjavik Municiple District Heating System are now approximately \$1.50/GJ (Zoega, 1974). The low production costs of the Reykjavik system reflect the extremely favorable source conditions in the low-temperature areas of southwestern Iceland.

Thermal water value is estimated on the basis of the value of effective heat in the domestic, industrial and agricultural heating market using fuel oil with an equivalent price of \$0.39/gal of oil and assuming an overall system (combustion-distribution) efficiency of 70%. This leads to a price of \$4/GJ effective heat.

Evaluation of Required Contact Area

The system production temperature is assumed to have the analytic form $T(D_i, D_p, g, t, q)$, where D_i and D_p are injection and production depths respectively, g is regional geothermal

gradient, t is time after flow start-up, and q is the flow rate. The production temperature is constrained to have a minimum value T_m over the given system lifetime SL and the value of T_m at $t = 0$. Assuming an upflow system, this constraint fixes the production borehole depth and flow rate to specific values, referred to as D_p^* and q^*, for a given injection depth D_i and gradient g. That is,

$$D_p^* = \frac{T_m - T_s}{g} \tag{7.1}$$

and

$$T(D_i, D_p^*, g, SL, q^*) - T_m = 0 \tag{7.2}$$

where T_s is the average ambient surface temperature. The flow rate q^* is calculated numerically using an interative technique applied to the functional (7.2). With this constraint, the production temperature is reduced to dependence only on injection borehole depth, time and gradient. The consequences of relaxing the constraint (7.1) are discussed in a later section. Total revenues of the system are based on the average of the production temperature over the system lifetime. Thus, the fluid-rock contact area required to amortize the capital investment can be considered as a function of the two "physical system" variables, D_i and g, and the set of "economic model" variables discussed earlier.

The minimum required fluid-rock contact area, for a given system lifetime, economic condition, and geologic environment, is determined by the requirement that

$$\frac{\partial A}{\partial D_i}(D_i, g, \alpha_1, \alpha_2, \ldots) = 0$$

and

$$\frac{\partial^2 A}{\partial D_i^2}(D_i, g, \alpha_1, \alpha_2, \ldots) > 0$$

where A is the required fluid rock contact area and the α's are the various economic variables. For the present purpose, we will refer to the system configuration that meets the above requirements as the "optimal" system.

A computer program, ECON, has been developed to evaluate the minimum required fluid-rock contact area based on the above procedure, and is presented in Appendix E.

An example of the dependence of the required contact area on injection depth and geothermal gradient for a forced recovery system based on the production temperature model given by expression (3.27) is presented in Figure 21. The minimum production temperature is constrained to 100°C and the ambient surface temperature is assumed to be 10°C. The injection temperature is 30°C and the thermal power is calculated relative to a 40°C disposal temperature. The system is assumed to have an overall heating system efficiency of 80%--

that is, the water enthalpy down to a temperature of 40°C can be utilized with an overall efficiency of 80%. It is noted that the utilization efficiency for district heating in the Namafjall area of Iceland is about 80% (Ragnars et al., 1970). Furthermore, the fluid is assumed to remain in the liquid phase. These parameter values will be used in later discussions as well. The results displayed in Figure 21 assume a system lifetime of 10 years.

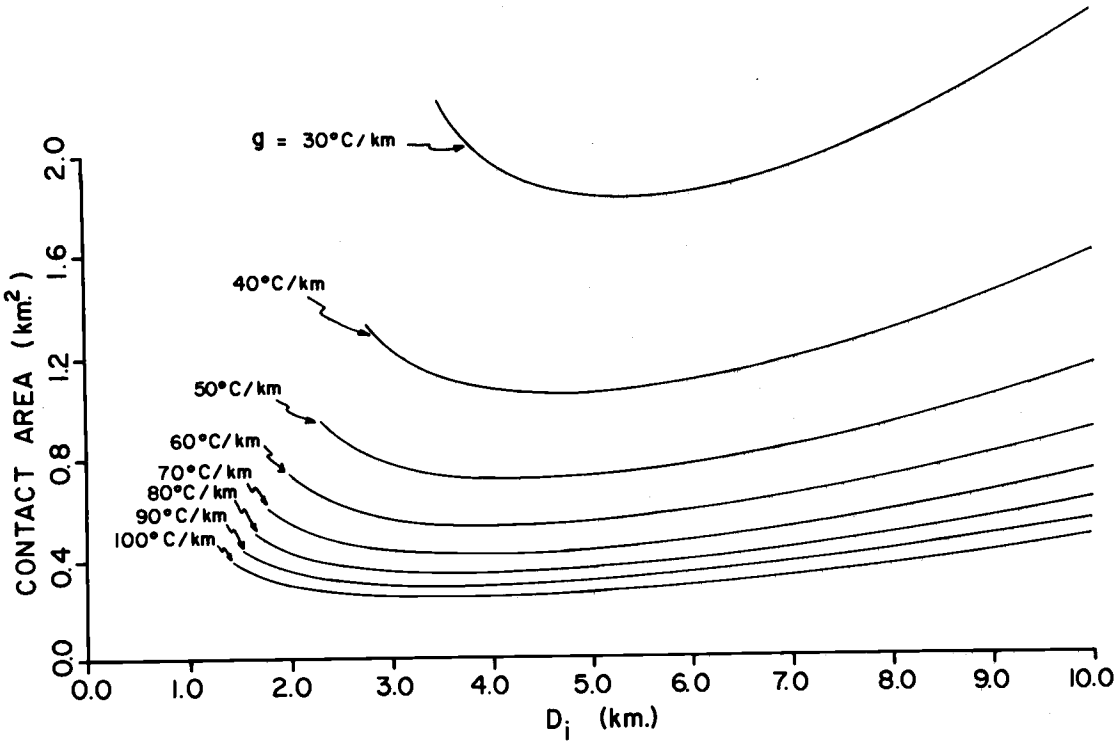

Figure 21. Dependence of required fluid-rock contact area per production unit on injection borehole depth and geothermal gradient. Based on a 10 year system lifetime and direct-contact heating application.

As expected, there exist definite optimum injection borehole depths that minimize the required fluid-rock contact area. For

injection depths greater than the optimum, increased drilling and pumping costs increase the required contact area. Furthermore, as the geothermal gradient increases, the required contact area decreases. This simply reflects the fact that, for higher geothermal gradients, shallower holes are required to meet the constraint of a minimum production temperature. Thus, a smaller fluid rock contact area is needed to amortize the initial capital investment, which is dominated by the drilling costs of the system. A final observation to be made from Figure 21 concerns the nature of the minima. The size of the initial capital investment may serve as a deterrent for the development of geothermal energy by private industry because of the inherent risk associated with exploitation of this resource. The minima of the required contact area curves are quite flat, suggesting that the injection depth may be decreased somewhat from the economic optimum without increasing the required fluid-rock contact area significantly. Since drilling costs are a rapidly increasing function of depth, the capital costs of the system may be reduced from the costs associated with the absolute minima without increasing production costs substantially. On the other hand, in cases where relatively high temperatures are required and adequate fluid conductance is available, the flat minima indicate deep drilling may be feasible. This observation has also been made by Bodvarsson and Reistad (1975).

Tables 1 and 2 present data that correspond to minimum required fluid-rock contact areas for systems with 10 and 20 year lifetimes respectively, based on the production temperature model (3.27). Price levels are expected to increase in the future due to depletion of high grade energy resources. We have therefore investigated the result of increasing the effective energy value on the minimum required contact area. Effective energy values of \$4/GJ \$6/GJ, \$8/GJ, and \$10/GJ are considered in the analysis. It is expected that, along with effective energy costs, distribution costs will also increase. This will be primarily the result of inflationary trends associated with increasing energy costs. Therefore, we have included in the computations an inflated distribution cost scale of \$2/GJ, \$2.33/GJ, \$2.67/GJ, and \$3/GJ corresponding respectively to the effective energy values listed above.

Under current economic conditions, corresponding roughly to the \$4/GJ effective energy value figure, data in Tables 1 and 2 indicate that the minimum contact areas for regional geotemperature gradients of 50°C/km or more are of the order of 1 km^2 or less, depending on system lifetime. A gradient of 50°C/km has been observed in fairly extensive regions of moderately high crustal heat flow and is therefore not an uncommon situation. A comparison of Tables 1 and 2 indicates that an economically viable 20 year system requires a slightly greater fluid-rock contact area than for a 10 year system.

Legend for Tables 1 Through 9

g	geothermal gradient (°C/km)
D_p	production well depth (km)
D_i	injection well depth (km)
A	minimum required contact area (km^2) per production unit
B	"strip width" (km)
T_{av}	time averaged production temperature (°C)
q	flow rate per unit length of conductor (kg/m. sec)
P	time averaged minimum effective power (MW heat*) per production unit
E	time averaged minimum total energy (MW-years) per production unit
F	required minimum production well flow (kg/sec)
C	total initial capital costs (drilling and surface equipment) in M$ per production unit

* = MW(e) for the case of Table 4

Table 1. Optimal system parameters for a single production unit, based on a 10 year system lifetime (direct-contact heating).

g	D_p	D_i	A	B	T_{av}	q	P	E	F	C
$4/GJ										
30	3.00	5.28	1.83	0.80	111.8	0.09	17.2	172.4	71.8	2.74
40	2.25	4.53	1.05	0.46	115.1	0.10	12.1	120.5	47.9	2.09
50	1.80	4.23	0.72	0.29	119.2	0.13	10.1	100.9	38.1	1.82
60	1.50	3.93	0.53	0.22	122.0	0.15	8.7	86.6	31.5	1.61
70	1.29	3.72	0.42	0.17	124.5	0.16	7.7	77.4	27.4	1.48
80	1.13	3.56	0.34	0.14	126.8	0.17	7.1	71.1	24.5	1.38
90	1.00	3.43	0.29	0.12	128.9	0.19	6.7	66.6	22.4	1.31
100	0.90	3.33	0.25	0.10	130.8	0.20	6.3	63.1	20.8	1.25
$6/GJ										
30	3.00	5.88	0.80	0.28	114.5	0.13	8.9	88.6	35.5	3.11
40	2.25	5.13	0.49	0.17	118.3	0.15	6.6	66.0	25.1	2.41
50	1.80	4.68	0.34	0.12	121.8	0.17	5.5	54.6	20.0	2.05
60	1.50	4.38	0.26	0.09	124.8	0.19	4.8	48.0	16.9	1.83
70	1.29	4.17	0.20	0.07	127.4	0.21	4.4	43.6	14.9	1.68
80	1.13	3.89	0.17	0.06	129.0	0.21	3.9	39.1	13.1	1.52
90	1.00	3.76	0.14	0.05	131.2	0.23	3.7	36.9	12.1	1.44
100	0.90	3.66	0.12	0.05	133.1	0.25	3.5	35.2	11.3	1.38

Table 1. Continued.

g	D_p	D_i	A	B	T_{av}	q	P	E	F	C
$8/GJ										
30	3.00	6.13	0.52	0.16	115.5	0.14	6.0	60.0	23.7	3.28
40	2.25	5.34	0.32	0.10	119.4	0.17	4.5	45.2	17.0	2.53
50	1.80	4.74	0.22	0.08	122.1	0.18	3.6	36.4	13.3	2.08
60	1.50	4.44	0.17	0.06	125.1	0.20	3.2	32.2	11.3	1.86
70	1.29	4.23	0.14	0.05	127.8	0.22	2.9	29.4	10.0	1.71
80	1.13	4.07	0.11	0.04	130.2	0.24	2.7	27.4	9.1	1.60
90	1.00	3.94	0.10	0.03	132.3	0.26	2.6	26.0	8.4	1.52
100	0.90	3.84	0.08	0.03	134.2	0.28	2.5	24.9	7.9	1.46
$10/GJ										
30	3.00	6.36	0.38	0.11	116.4	0.16	4.6	46.3	18.1	3.43
40	2.25	5.46	0.23	0.07	120.0	0.18	3.4	34.4	12.8	2.60
50	1.80	4.92	0.17	0.05	123.0	0.19	2.8	28.3	10.2	2.17
60	1.50	4.44	0.13	0.04	125.1	0.20	2.4	23.9	8.4	1.85
70	1.29	4.22	0.10	0.03	127.8	0.22	2.2	21.9	7.4	1.71
80	1.13	4.06	0.08	0.03	130.2	0.24	2.0	20.5	6.8	1.60
90	1.00	3.94	0.07	0.02	132.3	0.26	1.9	19.4	6.3	1.52
100	0.90	3.84	0.06	0.02	134.2	0.28	1.9	18.6	5.9	1.46

Table 2. Optimal system parameters for a single production unit, based on a 20 year system lifetime (direct-contact heating).

g	D_p	D_i	A	B	T_{av}	q	P	E	F	C
$4/GJ										
30	3.00	5.38	2.75	1.16	112.2	0.07	18.8	377.0	77.9	2.80
40	2.25	4.63	1.59	0.67	115.7	0.08	13.2	264.1	52.1	2.14
50	1.80	4.18	1.08	0.45	118.8	0.09	10.6	211.1	40.0	1.79
60	1.50	4.00	0.80	0.32	122.4	0.11	9.4	188.4	34.1	1.64
70	1.29	3.79	0.63	0.25	125.0	0.12	8.4	168.6	29.6	1.50
80	1.13	3.63	0.52	0.21	127.3	0.13	7.8	155.0	26.5	1.41
90	1.00	3.50	0.44	0.17	129.4	0.14	7.3	145.1	24.2	1.33
100	0.90	3.40	0.38	0.15	131.3	0.15	6.9	137.5	22.5	1.28
$6/GJ										
30	3.00	5.90	1.21	0.42	114.6	0.09	9.5	189.6	38.0	3.13
40	2.25	5.15	0.73	0.25	118.5	0.11	7.1	141.3	26.9	2.43
50	1.80	4.70	0.51	0.18	121.9	0.12	5.9	117.1	21.4	2.06
60	1.50	4.40	0.39	0.13	124.9	0.14	5.1	102.9	18.1	1.84
70	1.29	4.06	0.31	0.11	126.8	0.14	4.5	90.0	15.5	1.63
80	1.13	3.90	0.25	0.09	129.1	0.15	4.2	83.6	14.0	1.53
90	1.00	3.78	0.22	0.08	131.3	0.17	3.9	78.9	12.9	1.45
100	0.90	3.68	0.19	0.07	133.2	0.18	3.8	75.3	12.1	1.39

Table 2. Continued.

g	D_p	D_i	A	B	T_{av}	q	P	E	F	C
$8/GJ										
30	3.00	6.27	0.78	0.24	116.1	0.11	6.6	131.9	25.9	3.37
40	2.25	5.30	0.48	0.16	119.2	0.12	4.8	95.2	18.0	2.51
50	1.80	4.85	0.33	0.11	122.7	0.13	4.0	79.8	14.4	2.14
60	1.50	4.55	0.25	0.08	125.7	0.15	3.5	70.6	12.3	1.91
70	1.29	4.18	0.20	0.07	127.5	0.15	3.1	61.7	10.5	1.68
80	1.13	4.02	0.17	0.06	129.9	0.16	2.9	57.5	9.6	1.58
90	1.00	3.90	0.14	0.05	132.0	0.18	2.7	54.5	8.8	1.50
100	0.90	3.80	0.13	0.04	133.9	0.19	2.6	52.1	8.3	1.44
$10/GJ										
30	3.00	6.50	0.57	0.16	117.0	0.12	5.1	101.5	19.7	3.53
40	2.25	5.49	0.35	0.11	120.1	0.13	3.7	73.7	13.7	2.62
50	1.80	4.86	0.25	0.08	122.7	0.13	3.0	59.3	10.7	2.14
60	1.50	4.56	0.19	0.06	125.8	0.15	2.6	52.6	9.2	1.91
70	1.29	4.34	0.15	0.05	128.5	0.16	2.4	48.2	8.1	1.76
80	1.13	4.18	0.13	0.04	130.9	0.18	2.3	45.1	7.4	1.66
90	1.00	4.06	0.11	0.04	133.0	0.20	2.1	42.8	6.9	1.58
100	0.90	3.82	0.09	0.03	135.1	0.20	2.0	39.3	6.2	1.45

The minimum required borehole flow rates, however, are roughly the same for the two system lifetimes.

The tabulated injection borehole depths in Tables 1 and 2 are those that minimize the required fluid-rock contact area. It is emphasized that the required contact area is quite insensitive to injection borehole depth in the vicinity of the "optimal" system configuration, as indicated in Figure 21. It is therefore expected that, in practice, the injection depths can be significantly shallower than those indicated by the optimum depth without increasing production costs significantly. Table 3 illustrates the consequences of constraining the injection borehole depth to be 1 km deeper than the production borehole depth. The data are calculated based on a 10 year system lifetime and a $4/GJ effective heat value. A comparison of Table 3 with Table 1 shows that the required contact area for these cases is not significantly elevated above the absolute minimum. Furthermore, there is a substantial reduction of initial capital cost reflecting the decreased drilling costs for these systems.

At this juncture, it is of some interest to compare the required fluid-rock contact areas for systems based on electrical power production application with the above results for direct-contact heating application. Since thermal energy is only partially convertible to useful mechanical energy, enthalpy is not a convenient measure of the mechanical work which can be derived from the heat content of a

Table 3. System parameters for a single production unit, based on a 10 year system lifetime with a constrained suboptimal injection borehole depth (direct-contact heating).

g	D_p	D_i	A	B	T_{av}	q	P	E	F	C
$4/GJ										
30	3.00	4.00	1.97	1.97	105.3	0.03	12.1	120.7	55.2	2.07
40	2.25	3.25	1.17	1.17	107.0	0.03	8.1	81.4	36.3	1.51
50	1.80	2.80	0.81	0.81	108.8	0.03	6.3	63.3	27.5	1.23
60	1.50	2.50	0.61	0.61	110.4	0.04	5.3	53.3	22.6	1.07
70	1.29	2.29	0.49	0.49	112.0	0.04	4.7	47.3	19.6	0.96
80	1.13	2.13	0.41	0.41	113.5	0.04	4.2	42.3	17.2	0.88
90	1.00	2.00	0.35	0.35	115.0	0.05	4.0	39.7	15.8	0.85
100	0.90	1.90	0.31	0.31	116.4	0.05	3.8	38.1	14.9	0.79

substance at a given initial and end temperature. The exergy, or specific availability, of thermal water is the maximum amount of mechanical work which can be derived from the enthalpy by cooling it, at a constant pressure, from some initial temperature to a final temperature. For a production temperature in the range $100°C < T < 300°C$, Bodvarsson and Eggers (1972) have shown that the exergy $e(T)$ of thermal water can be represented to good approximation by a second order polynomial

$$e(T) = a_0 + a_1 T + a_2 T^2$$

where a_0, a_1, and a_2 are constants that depend on the disposal temperature. For electrical power production, we have calculated system revenues on the basis of total exergy produced and have assumed that the overall mechanical to electrical conversion efficiency is 65%. Revenues are computed on the basis of the time averaged exergy produced over the system lifetime.

Table 4 presents the data that correspond to minimum required contact areas for power production. A 10 year system lifetime has been assumed in the model. Injection temperature, disposal temperature, ambient surface temperature, and the constraint on minimum production temperature are the same as those used for the heating situation in Tables 1 and 2. Current buss-bar power costs fall

Table 4. Optimal system parameters for a single production unit, based on a 10 year system lifetime (electrical power production).

g	D_p	D_i	A	B	T_{av}	q	P	E	F	C
3¢/kWhr										
30	3.00	*	*	*	*	*	*	*	*	*
40	2.25	3.86	8.38	5.22	111.1	0.06	6.2	62.2	319.5	1.76
50	1.80	4.16	3.90	1.65	118.7	0.12	4.9	48.6	204.1	1.79
60	1.50	4.13	2.33	0.89	123.2	0.16	3.9	38.8	145.2	1.70
70	1.29	4.17	1.59	0.55	127.4	0.21	3.4	34.3	115.7	1.68
80	1.13	4.18	1.17	0.38	130.9	0.26	3.1	31.4	97.3	1.66
90	1.00	4.18	0.91	0.29	133.7	0.30	2.9	29.2	84.5	1.63
100	0.90	4.08	0.73	0.23	135.6	0.32	2.7	26.7	73.6	1.57
4¢/kWhr										
30	3.00	4.88	9.45	5.04	109.8	0.07	6.4	63.8	339.6	2.51
40	2.25	5.13	3.63	1.26	118.3	0.15	4.4	44.3	187.5	2.41
50	1.80	5.01	2.00	0.62	123.5	0.20	3.4	33.9	126.0	2.23
60	1.50	4.88	1.30	0.39	127.5	0.25	2.8	28.4	95.5	2.08
70	1.29	4.78	0.94	0.27	130.9	0.29	2.5	25.1	77.9	2.00
80	1.13	4.62	0.71	0.20	133.3	0.32	2.2	22.4	65.3	1.88
90	1.00	4.49	0.57	0.16	135.4	0.35	2.0	20.5	56.7	1.79
100	0.90	4.52	0.47	0.13	138.0	0.40	2.0	19.9	51.7	1.79

*Required contact area greater than 10 km^2.

within the range of 3¢/kWhr to 4¢/kWhr. It is evident from this data that the minimum required contact areas are elevated considerably over the heating case, reflecting the inherent inefficiency of electrical power production. This is a direct consequence of the low Carnot efficiency associated with the relatively small temperature difference between the thermal reservoir and the disposal temperature. It should also be pointed out that the required minimum production well flow rates are increased by a factor of three to four over the case for heating application. The conductor must exhibit a significantly higher permeability to meet these required flow rates. Figure 22 displays graphically selected data from Tables 1 and 4 for direct-contact heating systems and electrical power production systems.

We now consider the effect on the economic model of relaxing the constraint (7.1) on the production well depth. Table 5 presents data for a heat recovery system based on a 10 year system lifetime with an effective energy value of $4/GJ. The data corespond to a geothermal gradient of 50°C/km and production well depths greater than or equal to D_p^*. It is seen from this data that as D_p increases, the injection well depth that minimizes the required contact area decreases. This simply reflects the fact that, by relaxing the constraints on both the production and injection borehole depths, the economic model will search for the configuration that minimizes the sum of the drilling costs for both boreholes in the production unit

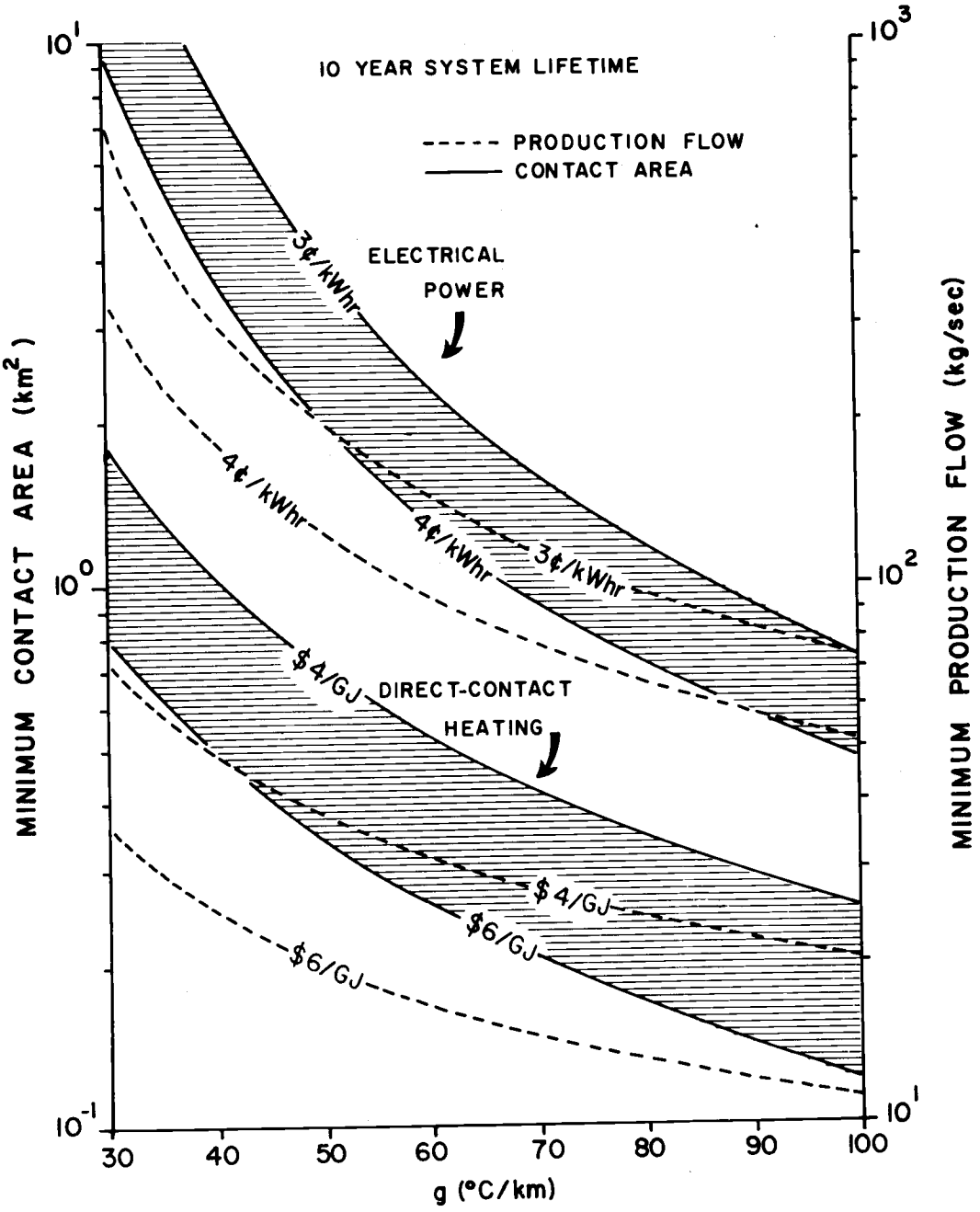

Figure 22. Minimum required fluid-rock contact area and production flow rate for electrical power production and direct-contact heating. Based on a 10 year system lifetime. Buss-bar costs are given for the electrical power case and effective heat costs are given for the direct-contact heating case.

while still meeting the constraint that the production temperature be $\geq T_m$ over the given system lifetime. The approach to this configuration is seen in Table 5, where the "strip-width" B increases by a factor of three. At this point, it is convenient to define a geometric "aspect ratio" as the ratio B/L, where L is the distance between the injection and production ports of the system. The aspect ratio for the given example ranges between 0.12 and 1.6. An evaluation of a realistic value for the aspect ratio is governed by the characteristics of the convective processes within the fluid conductor and the borehole location and spacing. Such an evaluation will require considerably more field data on the permeability conditions of the conductor and the regional stresses at the system site than is presently available. Furthermore, such an evaluation will require that the point source/sink nature of the system ports be accounted for in the convection model. The simple first-order heat extraction model used in this work is not applicable to this problem. The estimation of suitable or optimum aspect ratios is therefore beyond the scope of the present analysis. We will take those values computed on the basis of constraint (7.1) as a conservative estimate of the minimum required fluid-rock contact area. These values can be interpreted as a "greatest" lower bound on the contact area.

Table 5. Optimal system parameters for a single production unit, based on a 10 year system lifetime with unconstrained production borehole depth (direct-contact heating).

	D_p	D_i	A	B	T_{av}	q	P	E	F	C
$4/GJ, g = 50°C/km										
	1.80	4.23	0.72	0.29	119.2	0.13	10.1	101.0	38.1	1.82
	2.00	3.95	0.67	0.35	119.8	0.10	9.4	94.0	35.2	1.74
	2.20	3.67	0.63	0.43	120.5	0.08	8.8	88.2	32.7	1.67
	2.40	3.42	0.60	0.59	121.5	0.05	8.4	84.1	30.8	1.62
	2.60	3.20	0.57	0.95	122.6	0.03	8.2	81.6	29.5	1.60

Adverse Flow Effects

Flow Channelling

The effect of non-uniform flow within the fluid conductor on heat recovery efficiency is investigated on the basis of the theoretical development of Chapter IV. The thermal power output (averaged over the interval $0 \leq z \leq L$, where $2L$ is the channel period) is calculated as a function of time:

$$P(x,t) = \frac{\sigma_f}{L} \int_0^L q(z)\{T(x,z,t) - T_d\}dz$$

where the fluid temperature $T(x,z,t)$ is computed on the basis of the Fourier-Galerkin solution given by expressions (4.31) and (4.36) and where T_d is the disposal temperature. The integration indicated above is calculated numerically using an algorithm based on Simpson's Rule.

As an example of the effect of non-uniform flow in a forced recovery system, Figures 23 and 24 present the thermal power output history of a system with a flow channel half-period L of 10 m and 50 m respectively. The top set of curves (set "a") in both figures corresponds to an initial formation temperature of 150°C. The lower set of curves (set "b") in both figures corresponds to an upflow system where the regional geothermal gradient is 50°C/km. The

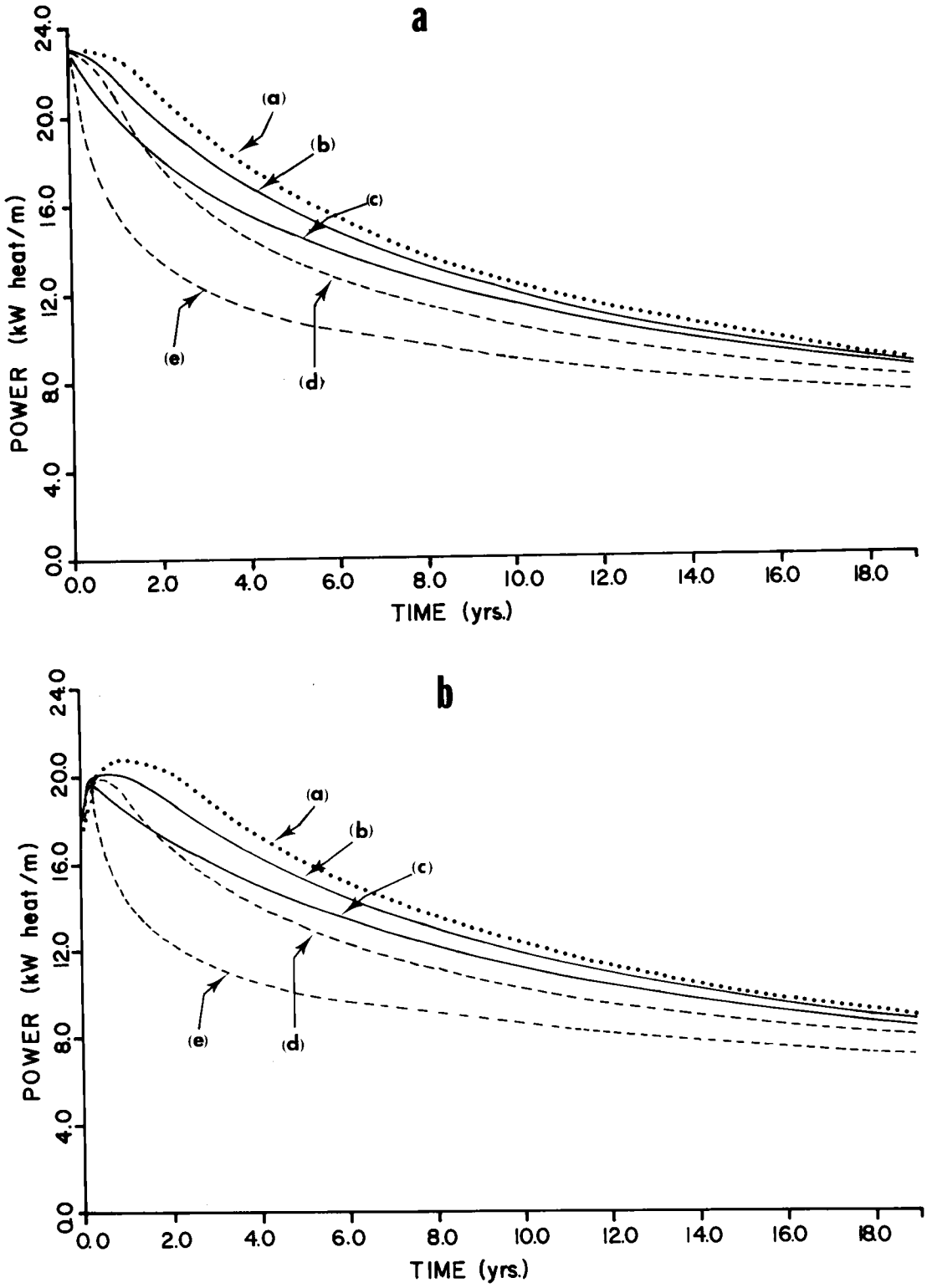

Figure 23. System power output under non-uniform flow conditions. Channel periodicity 2L = 20 m.

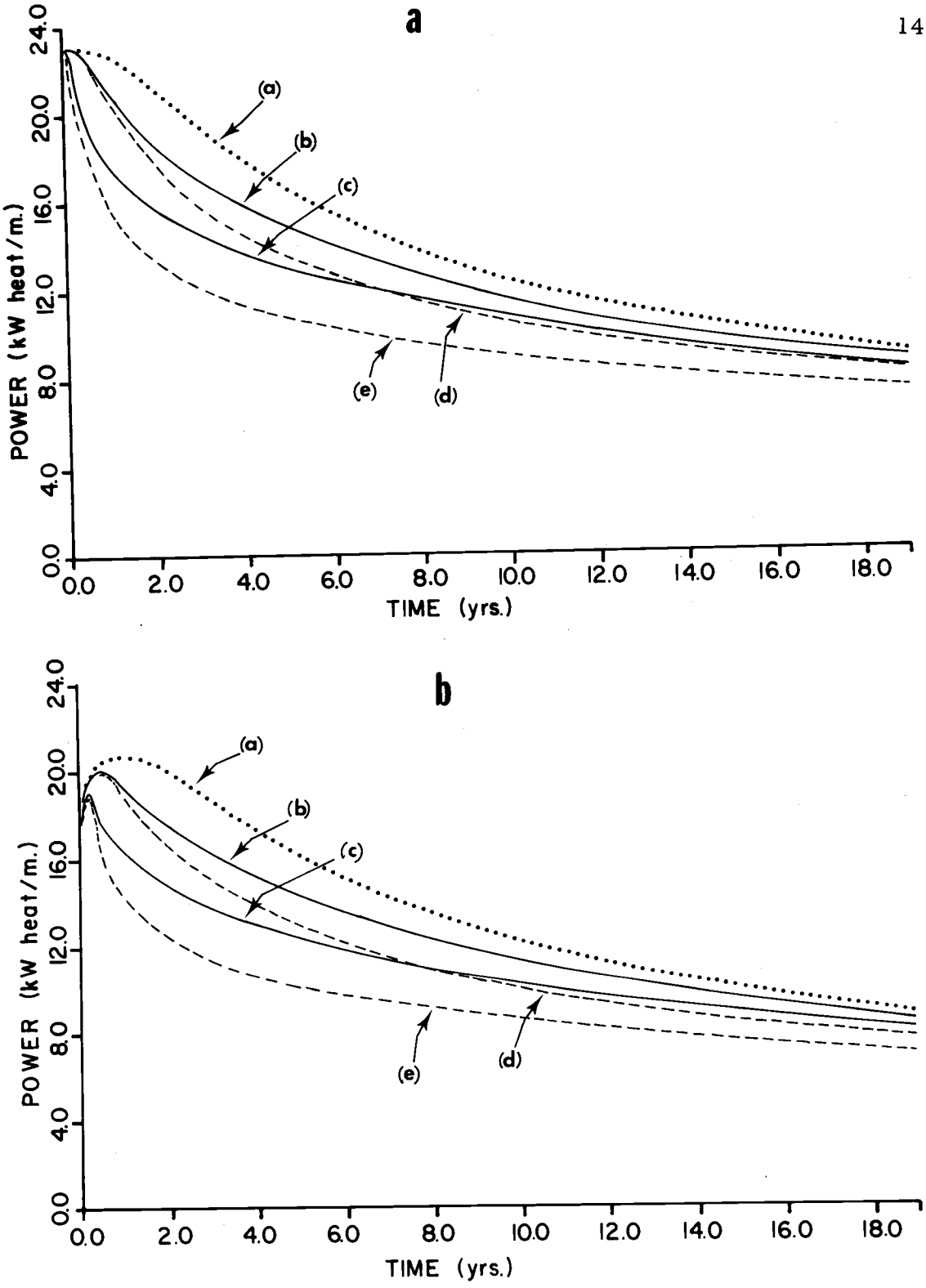

Figure 24. System power output under non-uniform flow conditions. Channel periodicity 2L = 100 m.

computations for the latter case are based on the initial formation temperature $f(x)$ given by equation (3.29). In all cases the production port is 1 km from the injection port. The set of individual curves, labeled (a), (b), (c), (d) and (e) correspond to the following situations:

(a) "uncoupled" model (equation 3.27) using flow configuration (c) in Figure 8

(b) Fourier-Galerkin solution ("coupled" model) using flow configuration (b) in Figure 8

(c) Fourier-Galerkin solution ("coupled" model) using flow configuration (a) in Figure 8

(d) "uncoupled" model (equation 3.27) using flow configuration (b) in Figure 8

(e) "uncoupled" model (equation 3.27) using flow configuration (a) in Figure 8.

It is evident from these specific examples that the heat extraction efficiency is not degraded a significant amount from the uniform situation by a severely non-uniform flow within the conductor with channel spacing on the order of tens of meters. This is a consequence of the large thermal communication between channels for this magnitude of channel spacing (see Chapter IV). A substantially greater degradation of power output will occur, however, for spacing on the order of a hundred or so meters. The latter is of the same magnitude as the expected borehole spacing for the system under consideration

as indicated by Tables 1 and 2. With proper borehole placement, the flow non-uniformity on this scale may possibly be reduced.

Fluid Losses

The minimum fluid-rock contact area required for an economically viable forced recovery system with fluid losses is calculated according to the procedure discussed previously using expression (4. 54) as the production temperature model.

Tables 6 and 7 present data based on a 10 year system lifetime assuming a 25% and 50% fluid loss from the system respectively. Tables 8 and 9 are based on a 20 year system lifetime with 25% and 50% fluid loss respectively. The economic and physical variables used in the calculation of these data are the same as those used in the calculations of Tables 1 and 2.

The reduction in heat recovery efficiency due to fluid loss is evident in these data. The effect is particularly noticeable for the lower values of the regional geothermal gradient. The required fluid-rock contact area is increased by over a factor of two for the case of a 20 year system lifetime and a 30°C/km gradient under current economic conditions and a 50% fluid loss. This is an extreme example, however, and it is noted that an increase in effective energy value from $4/GJ to $6/GJ brings the required contact area down to less than 1 km^2 for gradients equal to or greater than 50°C/km

assuming the rather severe fluid loss of 50%.

Discussion and Conclusion

The previous analysis establishes a lower bound on the required fluid-rock contact area necessary for an economically viable forced recovery system based on a sheet-like flow for low-temperature non-electrical application. The ability to approach these minimal requirements will depend strongly on the permeability characteristics of the fluid conductor. Unfortunately, little work has been devoted to the study of the natural fluid conductors which have been considered in this work. Hence, considerably more field data than that presently available will be necessary to satisfactorily account for the interaction of the elastic, thermoelastic, and chemical effects within these types of conductors.

The values of the required fluid-rock contact area and production well flow rates do not, however, appear unreasonable for the case of direct-contact heating under the condition of a moderately high crustal heat flow ($g \geq 50°C/km$). Furthermore, the analysis indicates that, as the effective heat value increases, as will no doubt occur under current economic trends, the required contact area will decrease substantially. It is evident that under these conditions, the relative feasibility of the system will increase and the associated risk involved in exploitation will correspondingly decrease.

In view of the present trends in the national energy economy, the results derived in this work appear sufficiently favorable to warrant further investigation into this type of forced recovery geoheat recovery system.

Table 6. Optimal system parameters for a single production unit, based on a 10 year system lifetime with 25% distributed fluid loss (direct-contact heating).

g	D_p	D_i	A	B	T_{av}	q	P	E	F	C
$4/GJ										
30	3.00	4.64	2.64	1.61	108.0	0.05	17.2	171.9	75.5	2.39
40	2.25	4.12	1.47	0.78	111.9	0.06	12.2	122.1	50.7	1.89
50	1.80	3.85	0.98	0.47	115.8	0.08	10.1	100.6	39.7	1.65
60	1.50	3.68	0.72	0.33	119.2	0.10	8.8	88.4	33.3	1.50
70	1.29	3.47	0.56	0.26	121.6	0.11	7.8	78.0	28.5	1.37
80	1.13	3.41	0.46	0.20	124.6	0.13	7.4	73.9	26.1	1.32
90	1.00	3.29	0.38	0.17	126.7	0.14	6.9	68.7	23.7	1.25
100	0.90	3.19	0.33	0.14	128.5	0.15	6.5	64.7	21.8	1.20
$6/GJ										
30	3.00	5.66	1.06	0.40	112.7	0.09	9.2	92.0	37.8	2.97
40	2.25	4.91	0.63	0.24	116.3	0.11	6.7	66.9	26.2	2.29
50	1.80	4.46	0.44	0.16	119.5	0.13	5.5	54.6	20.5	1.93
60	1.50	4.16	0.33	0.12	122.3	0.14	4.7	47.5	17.2	1.72
70	1.29	3.95	0.26	0.10	124.9	0.15	4.3	42.8	15.1	1.58
80	1.13	3.79	0.22	0.08	127.2	0.17	4.0	39.6	13.6	1.48
90	1.00	3.66	0.18	0.07	129.3	0.18	3.7	37.3	12.5	1.40
100	0.90	3.56	0.16	0.06	131.2	0.20	3.5	35.5	11.6	1.34

Table 6. Continued.

g	D_p	D_i	A	B	T_{av}	q	P	E	F	C
$8/GJ										
30	3.00	5.89	0.66	0.23	113.6	0.11	6.0	60.2	24.4	3.12
40	2.25	5.14	0.40	0.14	117.4	0.13	4.5	45.0	17.4	2.42
50	1.80	4.69	0.28	0.10	120.7	0.14	3.7	37.4	13.8	2.05
60	1.50	4.28	0.21	0.08	123.1	0.15	3.2	31.9	11.5	1.78
70	1.29	4.07	0.17	0.06	125.7	0.17	2.9	29.0	10.1	1.63
80	1.13	3.91	0.14	0.05	128.0	0.18	2.7	26.9	9.1	1.53
90	1.00	3.78	0.12	0.04	130.1	0.20	2.5	25.4	8.4	1.45
100	0.90	3.68	0.10	0.04	132.0	0.21	2.4	24.3	7.9	1.39
$10/GJ										
30	3.00	6.12	0.48	0.15	114.5	0.12	4.6	45.9	18.4	3.27
40	2.25	5.24	0.29	0.10	117.9	0.13	3.4	33.8	12.9	2.48
50	1.80	4.79	0.21	0.07	121.3	0.15	2.8	28.3	10.4	2.11
60	1.50	4.39	0.16	0.05	123.7	0.16	2.4	24.2	8.6	1.83
70	1.29	4.12	0.13	0.04	126.3	0.18	2.2	22.1	7.6	1.68
80	1.13	4.01	0.10	0.04	128.7	0.19	2.1	20.6	6.9	1.58
90	1.00	3.89	0.09	0.03	130.8	0.21	2.0	19.5	6.4	1.50
100	0.90	3.79	0.08	0.03	132.7	0.23	1.9	18.7	6.0	1.44

Table 7. Optimal system parameters for a single production unit, based on a 10 year system lifetime with 50% distributed fluid loss (direct-contact heating).

g	D_p	D_i	A	B	T_{av}	q	P	E	F	C
$4/GJ										
30	3.00	3.78	5.23	6.74	103.3	0.01	18.8	188.0	88.7	1.97
40	2.25	3.42	2.64	2.25	106.8	0.03	12.8	128.3	57.3	1.58
50	1.80	3.19	1.68	1.21	110.0	0.04	10.1	101.1	43.1	1.37
60	1.50	3.10	1.20	0.75	113.5	0.05	8.9	88.7	36.0	1.27
70	1.29	3.02	0.92	0.53	116.6	0.06	8.0	80.3	31.3	1.20
80	1.13	2.86	0.74	0.43	118.5	0.06	7.1	71.4	27.2	1.11
90	1.00	2.91	0.61	0.32	121.9	0.08	7.0	70.3	25.7	1.11
100	0.90	2.81	0.52	0.27	123.6	0.09	6.5	65.4	23.4	1.06
$6/GJ										
30	3.00	4.85	1.69	0.91	108.1	0.04	9.0	89.6	39.3	2.50
40	2.25	4.28	0.97	0.48	111.6	0.06	6.5	64.6	26.9	1.96
50	1.80	3.95	0.66	0.31	115.0	0.07	5.3	53.0	21.1	1.69
60	1.50	3.77	0.49	0.22	118.2	0.08	4.7	46.8	17.9	1.54
70	1.29	3.55	0.39	0.17	120.6	0.09	4.2	41.6	15.4	1.40
80	1.13	3.39	0.32	0.14	122.8	0.10	3.8	38.1	13.7	1.31
90	1.00	3.39	0.27	0.11	125.7	0.12	3.7	37.1	12.9	1.29
100	0.90	3.29	0.23	0.10	127.5	0.13	3.5	35.1	12.0	1.23

Table 7. Continued.

g	D_p	D_i	A	B	T_{av}	q	P	E	F	C
$8/GJ										
30	3.00	5.32	0.98	0.42	110.1	0.06	5.9	59.4	25.3	2.77
40	2.25	4.57	0.59	0.25	113.2	0.07	4.3	42.6	17.4	2.11
50	1.80	4.27	0.41	0.16	116.9	0.09	3.6	36.1	14.0	1.84
60	1.50	3.97	0.31	0.12	119.5	0.10	3.1	31.2	11.7	1.63
70	1.29	3.56	0.24	0.10	122.0	0.10	2.8	28.1	10.2	1.49
80	1.13	3.71	0.20	0.08	124.0	0.12	2.7	26.9	9.5	1.44
90	1.00	3.58	0.17	0.07	127.0	0.13	2.5	25.3	8.7	1.37
100	0.90	3.48	0.15	0.06	128.9	0.14	2.4	24.0	8.1	1.31
$10/GJ										
30	3.00	5.61	0.69	0.26	111.3	0.07	4.5	44.7	18.7	2.94
40	2.25	4.86	0.42	0.16	114.6	0.08	3.3	32.9	13.2	2.26
50	1.80	4.41	0.29	0.11	117.7	0.08	2.7	27.1	10.4	1.91
60	1.50	4.11	0.22	0.08	120.4	0.10	2.4	23.6	8.8	1.70
70	1.29	3.90	0.18	0.07	122.9	0.11	2.1	21.4	7.7	1.55
80	1.13	3.74	0.15	0.06	125.2	0.13	2.0	19.8	7.0	1.45
90	1.00	3.61	0.12	0.05	127.2	0.14	1.9	18.7	6.4	1.28
100	0.90	3.61	0.11	0.04	129.8	0.16	1.8	18.4	6.1	1.37

Table 8. Optimal system parameters for a single production unit, based on a 20 year system lifetime with 25% distributed fluid loss (direct-contact heating).

g	D_p	D_i	A	B	T_{av}	q	P	E	F	C
$4/GJ										
30	3.00	4.60	3.98	2.49	107.8	0.03	18.0	360.7	79.4	2.36
40	2.25	4.15	2.21	1.17	112.1	0.05	13.1	262.0	54.3	1.90
50	1.80	3.87	1.47	0.71	115.9	0.06	10.8	215.0	42.3	1.65
60	1.50	3.68	1.08	0.50	119.2	0.07	9.4	187.7	35.4	1.50
70	1.29	3.46	0.84	0.39	121.5	0.08	8.3	165.6	30.3	1.37
80	1.13	3.40	0.69	0.30	124.5	0.09	7.8	156.4	27.6	1.31
90	1.00	3.28	0.58	0.25	126.5	0.10	7.3	145.3	25.1	1.24
100	0.90	3.18	0.50	0.22	128.4	0.11	6.8	137.0	23.1	1.19
$6/GJ										
30	3.00	5.57	1.60	0.62	112.3	0.06	9.6	191.4	39.5	2.92
40	2.25	4.82	0.95	0.37	115.8	0.07	6.9	138.8	27.3	2.24
50	1.80	4.37	0.66	0.26	118.9	0.08	5.7	113.1	21.4	1.89
60	1.50	4.07	0.49	0.19	121.8	0.09	4.9	98.2	17.8	1.68
70	1.29	3.86	0.39	0.15	124.3	0.10	4.4	88.6	15.7	1.54
80	1.13	3.70	0.32	0.13	126.6	0.11	4.1	81.9	14.1	1.44
90	1.00	3.67	0.27	0.10	129.4	0.13	4.0	79.6	13.3	1.41
100	0.90	3.57	0.24	0.09	131.3	0.14	3.8	75.8	12.4	1.35

Table 8. Continued.

g	D_p	D_i	A	B	T_{av}	q	P	E	F	C
$8/GJ										
30	3.00	5.85	0.99	0.35	113.4	0.07	6.4	127.0	25.8	3.09
40	2.25	5.10	0.60	0.21	117.2	0.09	4.7	94.8	18.3	2.39
50	1.80	4.65	0.42	0.15	120.5	0.10	3.9	78.6	14.6	2.03
60	1.50	4.35	0.32	0.11	123.4	0.11	3.5	69.1	12.4	1.81
70	1.29	4.13	0.26	0.09	126.0	0.12	3.1	62.8	10.9	1.66
80	1.13	3.97	0.21	0.07	128.4	0.13	2.9	58.5	9.9	1.56
90	1.00	3.85	0.18	0.06	130.5	0.14	2.8	55.2	9.1	1.48
100	0.90	3.75	0.16	0.06	132.4	0.16	2.6	52.7	8.5	1.42
$10/GJ										
30	3.00	6.09	0.72	0.23	114.4	0.08	4.9	97.0	19.5	3.25
40	2.25	5.22	0.44	0.15	117.0	0.09	3.6	71.5	13.7	2.46
50	1.80	4.77	0.31	0.10	121.2	0.11	3.0	59.8	11.0	2.09
60	1.50	4.47	0.24	0.08	124.1	0.12	2.6	52.8	9.4	1.87
70	1.29	4.26	0.19	0.06	126.8	0.13	2.4	48.2	8.3	1.72
80	1.13	4.10	0.16	0.05	129.2	0.14	2.3	45.0	7.5	1.61
90	1.00	3.83	0.13	0.05	130.4	0.14	2.0	40.8	6.7	1.47
100	0.90	3.73	0.12	0.04	132.4	0.15	2.0	39.0	6.3	1.41

Table 9. Optimal system parameters for a single production unit, based on a 20 year system lifetime with 50% distributed fluid loss (direct-contact heating).

g	D_p	D_i	A	B	T_{av}	q	P	E	F	C
$4/GJ										
30	3.00	3.74	7.88	10.70	103.1	0.01	19.7	393.1	93.0	1.95
40	2.25	3.42	3.97	3.40	106.8	0.02	13.6	272.4	61.0	1.58
50	1.80	3.19	2.52	1.82	110.0	0.03	10.8	215.4	45.9	1.37
60	1.50	3.08	1.80	1.14	113.4	0.03	9.4	187.7	38.2	1.26
70	1.29	3.01	1.38	0.80	116.6	0.04	8.5	170.7	33.3	1.19
80	1.13	2.95	1.11	0.61	119.3	0.05	7.9	158.6	29.8	1.14
90	1.00	2.83	0.92	0.50	121.2	0.05	7.2	144.8	26.6	1.08
100	0.90	2.86	0.78	0.40	124.1	0.06	7.1	142.5	25.3	1.08
$6/GJ										
30	3.00	4.84	2.54	1.38	108.0	0.03	9.5	190.4	41.8	2.49
40	2.25	4.28	1.46	0.72	111.6	0.04	6.9	137.4	28.6	1.96
50	1.80	3.96	0.99	0.46	115.1	0.05	5.7	113.2	22.5	1.69
60	1.50	3.66	0.74	0.34	117.6	0.05	4.8	96.2	18.5	1.49
70	1.29	3.59	0.58	0.25	120.9	0.07	4.5	89.9	16.6	1.42
80	1.13	3.43	0.48	0.21	123.1	0.07	4.1	82.2	14.8	1.33
90	1.00	3.31	0.40	0.17	125.0	0.08	3.8	76.7	13.5	1.26
100	0.90	3.33	0.35	0.14	127.8	0.09	3.8	75.8	12.9	1.25

Table 9. Continued.

g	D_p	D_i	A	B	T_{av}	q	P	E	F	C
8$/GJ										
30	3.00	5.28	1.48	0.65	109.9	0.04	6.2	124.9	26.7	2.74
40	2.25	4.66	0.88	0.37	113.6	0.05	4.7	93.1	18.9	2.15
50	1.80	4.21	0.61	0.25	116.5	0.06	3.8	75.5	14.7	1.81
60	1.50	4.03	0.46	0.18	119.9	0.07	3.4	67.7	12.6	1.66
70	1.29	3.81	0.37	0.14	122.3	0.08	3.0	60.9	11.0	1.52
80	1.13	3.65	0.30	0.12	124.6	0.08	2.8	56.2	9.9	1.42
90	1.00	3.53	0.26	0.10	126.6	0.09	2.6	52.8	9.1	1.34
100	0.90	3.43	0.22	0.09	128.5	0.10	2.5	50.2	8.5	1.29
$10/GJ										
30	3.00	5.62	1.03	0.40	111.3	0.05	4.8	95.3	20.0	2.95
40	2.25	4.87	0.63	0.24	114.6	0.06	3.5	70.2	14.0	2.27
50	1.80	4.42	0.44	0.17	117.7	0.07	2.9	57.7	11.1	1.91
60	1.50	4.12	0.33	0.13	120.4	0.07	2.5	50.4	9.4	1.70
70	1.29	3.90	0.27	0.10	122.9	0.08	2.3	45.6	8.2	1.56
80	1.13	3.83	0.22	0.08	125.7	0.09	2.2	43.4	7.6	1.49
90	1.00	3.70	0.19	0.07	127.8	0.10	2.0	40.9	7.0	1.42
100	0.90	3.60	0.16	0.06	129.7	0.11	2.0	39.0	6.5	1.36

BIBLIOGRAPHY

Abramowitz, M., and I. A. Stegun, ed., Handbook of Mathematical Functions, Applied Mathematics Series 55, National Bureau of Standards, Washington, D.C., 1964

Armstead, H. C. H., Geothermal economics, in Geothermal Energy: Review of Research and Development, edited by H. C. H. Armstead, Unesco Press, Paris, 1973

Blair, A. G., J. W. Tester, and J. J. Mortensen, LASL Hot Dry Rock Geothermal Project; July 1, 1975-June 30, 1976, progress report LA-6525-PR, U. S. Energy Research and Development Administration, 1976

Bodvarsson, G., Physical characteristics of natural heat resources in Iceland, in Proceedings of the U. N. Conference on New Sources of Energy, Rome, 1961

_____, On the temperature of water flowing through fractures, J. Geophys. Res., 74, 1987-1992, 1969

_____, Thermoelastic phenomena in geothermal systems, in Proceedings of the Second U. N. Symposium on the Development and use of Geothermal Resources, San Francisco, 1975

_____, A Secondary Recovery Method for the Extraction of Geothermal Energy; July 1, 1975-June 30, 1976, progress report RLO-2227-T21-1, U. S. Energy Research and Development Administration, 1976

_____, and D. Eggers, The exergy of thermal water, Geothermics, 1, 93-95, 1972

_____, and J. M. Hanson, Forced geoheat extraction from sheet-like fluid conductors, in Proceedings of the Second Workshop on Geothermal Reservoir Engineering, Stanford University, 1976

_____, and J. M. Hanson, Forced geoheat extraction, in Proceedings of the Second NATO-CCMS Information Meeting on Dry Hot Rock Geothermal Energy, Los Alamos Scientific Laboratory, 1977 (in press)

_____, and G.M. Reistad, Econometric analysis of forced geoheat recovery for low temperature uses in the Pacific Northwest, in Proceedings of the Second U.N. Symposium on the Development and Use of Geothermal Resources, San Francisco, 1975

Boley, B.A., and J.H. Weiner, Theory of Thermal Stress, 586 pp., John Wiley and Sons, Inc., New York, 1960

Carslaw, H.S., and J.C. Jaeger, Conduction of Heat in Solids, 510 pp., Oxford, London, 1959

Coulbois, P., and J.P. Herault, Les conditions de compétitivité de la géothermie dans le chauffage des habitations, in Proceedings of the Second U.N. Symposium on the Development and Use of Geothermal Resources, San Francisco, 1975

Dagum, E.M., and K. Heiss, An Econometric Study of Small and Intermediate Size Diameter Drilling Costs for the United States, PNE-3012 (vol. 1 and 2), prepared for the U.S. Atomic Energy Commission by Mathematica, Princeton, New Jersey, 1968

Delegation Generale à la Recherche Scientifique et Technique, Report, Paris, 1976

Galerkin, B.G., Rods and Plates, Vestnik Inshenerov (Engineering Bulletin), 19, 897-908, 1915

Goodier, J.N., Integration of thermoelastic equations, Phil. Mag., 23, 1017-1032, 1937

Hammond, P.E., S.A. Pederson, K.D. Hopkins, D. Aiken, D.S. Harle, Z.F. Daneš, D.L. Konicek, and C.R. Stricklin, Geology and gravimetry of the Quaternary basaltic volcanic field, southern Cascade Range, Washington, in Proceedings of the Second U.N. Symposium on the Development and Use of Geothermal Energy Resources, San Francisco, 1975

Harlow, F.H., and W.E. Pract, A theoretical study of geothermal energy extraction, J. Geophys. Res., 77, 7038-7048, 1972

Hose, R.K., and B.K. Taylor, Geothermal Systems of Northern Nevada, U.S. Geological Survey open file report No. 74-271, 1974

Hull, D. A., R. G. Bowen, D. D. Blackwell, and N. V. Peterson, Preliminary heat-flow map and evaluation of Oregon's geothermal energy potential, The Ore Bin, 39, 109-123, Oregon State Dept. of Geological and Mineral Industries, 1977

Isaacson, E., and H. B. Keller, Analysis of Numerical Methods, 541 pp., John Wiley and Sons, Inc., New York, 1966

Karkheck, J., J. Powell, and E. Beardsworth, Prospects for district heating in the United States, Science, 195, 948-955, 1977

Kato, T., On the convergence of the perturbation method, Journal of Faculty of Science, University of Tokyo, Sect. I, 6, 145-226, 1951

_____, Perturbation Theory for Linear Operators, 592 pp., Springer-Verlag, New York, 1966

Kruger, P., and H. J. Ramey, Jr., eds., Proceedings of Workshop on Geothermal Reservoir Engineering, Stanford University, 1975

Lamb, Sir Horace, Hydrodynamics, 738 pp., Dover Publications, New York, 1932

Lee, W. H. K., On the global variations of terrestrial heat flow, Phys. Earth Plan. Int., 2, 332-341, 1970

Leighton, W., Ordinary Differential Equations, 246 pp., Wadsworth Publishing Co., Belmont, Calif., 1966

Lienau, P. J., and J. W. Lund, eds., Multipurpose Use of Geothermal Energy, Proceedings of the International Conference on Geothermal Energy for Industrial, Agricultural and Commercial-Residential Uses, Oregon Institute of Technology, 1974

Magnus, W., and F. Oberhettinger, Formulas and Theorems for the Special Functions of Mathematical Physics, 508 pp., Springer-Verlag, New York, 1966

Mikhlin, S. G., and K. L. Smolitskiy, Approximate Methods for Solution of Differential and Integral Equations, 308 pp., American Elsevier Publishing Co., Inc., New York, 1967

Milora, S. L., and J. W. Tester, Geothermal Energy as a Source of Electric Power, 186 pp., MIT Press, Cambridge, 1976

Mindlin, R. D., and D. H. Cheng, Thermoelastic stress in the semi-infinite solid, J. App. Phys., 21, 931-933, 1950

Parkus, H., Thermoelasticity, 112 pp., Blaisdell Publishing Co., Waltham, Mass., 1968

Proffett, J. M., Jr., Cenozoic geology of the Yerington district, Nevada, and implications for the nature and origin of Basin and Range faulting, Geol. Soc. Am. Bull., 88, 247-266, 1977

Ragnars, K., K. Saemundsson, S. Benediktsson, and S. S. Einarsson, Development of the Namafjall area, northern Iceland, in Proceedings of the U. N. Symposium on the Development and Utilization of Geothermal Resources, Pisa, 1970

Rayleigh, Lord, The Theory of Sound, Vol. I, 480 pp., Macmillan and Co., Ltd., London, 1926

Reistad, G. M., Industrial applications of geothermal energy, in Present Status and Future Prospects for Nonelectrical Uses of Geothermal Resources, Lawrence Livermore Laboratory, NATO-CCMS Report No. 40, edited by J. H. Howard, 1975a

_____, Potential for nonelectrical applications of geothermal energy and their place in the National economy, in Proceedings of the Second U. N. Symposium on the Development and Use of Geothermal Energy, San Francisco, 1975b

Sass, J. H., A. H. Lachenbruch, R. J. Munroe, G. W. Greene, and T. H. Moses, Jr., Heat flow in the western United States, J. Geophys. Res., 76, 6376-6413, 1971

Schrodinger, E., Collected Papers on Wave Mechanics. (English translation), 146 pp., Blackie and Son Limited, London and Glasgow, 1928

Snow, D. T., Rock fracture spacings, openings, and porosities, J. Soil Mech. and Found. Div., Proceedings of the ASCE, 94, 73-91, 1968

Stanford Research Institute, Patterns of Energy Consumption in the United States, prepared for the Office of Science and Technology, Executive Office of the President, Washington, D.C., 1972

Stearns, D.W., and M. Friedman, Reservoirs in fractured rock, in Stratigraphic Oil and Gas Fields, AAPG Mem. 16 (SEG Special Pub. 10), edited by R.E. King, 1972

Taubeneck, W.H., Dikes of Columbia River basalt in northeastern Oregon, western Idaho, and southeastern Washington, in Proceedings of the Second Columbia River Basalt Symposium, Eastern Washington State College, 1969

Titchmarsh, E.C., Some theorems on perturbation theory, Proceedings of Royal Society of London, ser. A, 200, 34-36, 1949

_____, Some theorems on perturbation theory II, Proceedings of Royal Society of London, ser. A, 201, 473-479, 1950

Tolman, C.F., Groundwater, 593 pp., McGraw-Hill Book Co., Inc., New York, 1937

Varga, R.S., Matrix Iterative Analysis, 322 pp., Prentice-Hall, Inc., Englewood Cliffs, New Jersey, 1962

Warner, M.M., Special aspects of Cenozoic history of southern Idaho and their geothermal implications, in Proceedings of the Second U.N. Symposium on the Development and Use of Geothermal Energy, San Francisco, 1975

White, D.E., and D.C. Williams, eds., Assessment of Geothermal Resources of the United States - 1975, U.S. Geological Survey, Circular 726, 1975

Williams, P.L., D.R. Mabey, A.A.R. Zohdy, H. Ackermann, D.B. Hoover, K.L. Pierce, and S.S. Oriel, Geology and geophysics of the southern Raft River valley geothermal area, Idaho, USA, in Proceedings of the Second U.N. Symposium on the Development and Use of Geothermal Energy, San Francisco, 1975

Zoega, J., The Reykajavik Municipal District Heating System, in Multipurpose Use of Geothermal Energy, Proceedings of the International Conference on Geothermal Energy for Industrial, Agricultural, and Commercial-Residential Uses, Oregon Institute of Technology, edited by P. J. Lienau and J. W. Lund, 1974

APPENDICES

APPENDIX A

The Numerical Laplace Inverse Transform Method

Considerable use of the numerical Laplace transform inversion has been made in this work. Since the numerical method used is based on a substantially different approach than the more "classical" numerical inversion techniques, a brief description of the method is presented here with some examples of its application.

The Laplace transform of a function $F(t)$ is given by the integral

$$\hat{F}(s) = \int_0^\infty e^{-st} F(t)dt \qquad (A.1)$$

In determining a function $F(t)$ from its Laplace transform $\hat{F}(s)$, one applies an integration along some contour in the complex s-plane, given by

$$F(t) = \frac{1}{2\pi i} \int_{c-i\infty}^{c+i\infty} e^{st} \hat{F}(s)ds \qquad (A.2)$$

One thus obtains $F(t)$ in terms of the poles and residues and/or the values of $\hat{F}(s)$ on a contour of the s-plane. Several numerical approximation methods have been proposed for inverting equation (A.2) based on the expansion of $F(t)$ in a finite series of given

functions $\varphi_k(t)$. That is,

$$F(t) = \sum_{k=0}^{N} C_k \varphi_k(t) \qquad (A.3)$$

The functions φ_k can be exponential, trigonometric, Legendre or Laguerre functions where the expansion coefficients C_k are calculated based on the value of $\hat{F}(s)$ at discrete values of s (Lanczos, 1956; Papoulis, 1957; Bellman et al., 1966; Piessens, 1969).

The method of numerical Laplace transform inversion used in this work differs from the aforementioned procedure in that no presumption as to the form of $F(t)$, such as is given by expression (A.3), is made. The calculation method originates from Gaver (1966), who considers the integral of $F(t)$ with respect to a given weighting function. The procedure is illustrated by the problem of evaluating the integral

$$R_n(a) = \int_0^{\infty} F(t) f_n(a, t) dt \qquad (A.4)$$

where $R_n(a)$ can be considered the "expectation" of $F(t)$ under the weighting function $f_n(a, t)$. The particular weighting function considered by Gaver is

$$f_n(a, t) = \frac{a(2n)!}{n!(n-1)!} (1-e^{-at})^n e^{-nat}, \quad a > 0 \qquad (A.5)$$

Upon inserting expression (A. 5) into equation (A. 4), it is easily shown that

$$R_n(a) = \frac{a(2n)!}{n!(n-1)!} \sum_{i=0}^{n} \binom{n}{i}(-1)^i \hat{F}([n+i]a) \qquad (A.6)$$

where the binomial expansion (Jolley, 1961)

$$(1+x)^n = \sum_{j=0}^{n} \binom{n}{j} x^j$$

has been used in the calculation. Gaver has shown that, as $n \to \infty$, the asymptotic expansion of $R_n(a)$ is given by

$$R_n(a) \sim F(\frac{\ln 2}{a}) + \frac{\alpha_1}{n} + \frac{\alpha_2}{n^2} + \ldots$$

Thus, by retaining a sufficient number of terms in the series (A. 6), $R_n(\ln 2/t)$ will be a good approximation to the function $F(t)$. This approximation is given by

$$F(t) \approx \frac{\ln 2}{t} \frac{(2n)!}{n!(n-1)!} \sum_{i=0}^{n} \binom{n}{i}(-1)^i \hat{F}([n+i] \frac{\ln 2}{t}) \qquad (A.7)$$

The above scheme requires $n+1$ discrete values of $\hat{F}$ for the evaluation of $F(t)$ at a specific value of t. Stehfest (1969) has found that, for a given $n+1$ values of $\hat{F}$, a much better

approximation to $F(t)$ than that given by expression (A. 7) is attainable. This is done by using a linear combination of the $n+1$ values $R_j(\ln 2/t)$, $j = 0, 1, \ldots, n$. Stehfest's result is given by

$$F(t) \approx \frac{\ln 2}{t} \sum_{i=1}^{n} V_i \hat{F}\left(\frac{\ln 2}{t} i\right) \tag{A.8}$$

where

$$V_i = (-1)^{\frac{n}{2}+i} \sum_{k=(\frac{i+1}{2})}^{\min(i,\frac{n}{2})} \frac{k^{\frac{n}{2}}(2k)!}{(\frac{n}{2}-k)!k!(k-1)!(i-k)!(2k-i)!}$$

In comparing the inverses of 50 test functions using both the above method as well as the inversion technique of Bellman et al. (1966), where $\varphi_k(t) = e^{-kt}$, Stehfest concludes that the above method "generally produces better results". It is the generalization of Stehfest given by expression (A. 8) that is used in this work.

The computer subprogram LINV, given in Appendix E, evaluates the numerical inverse of the Laplace transform according to the above scheme. Several examples of the application of this method are given below. The function $F(t)$ being considered along with its Laplace transform $\hat{F}(s)$ are given at the top of each table. The exact value of $F(t)$ is also given for comparison. All computations were done using 18 significant figure (double precision) arithmetic and rounded to 6 significant figures.

References Cited

Bellman, R., R. Kalaba, and J. Lockett, Numerical Inversion of the Laplace Transform, 249 pp., Elsevier, New York, 1966

Gaver, D.P., Observing stochastic processes, and approximate transform inversion, Oper. Res., 14, 444-459, 1966

Lanczos, C., Applied Analysis, 539 pp., Prentice-Hall, Englewood Cliffs, New Jersey, 1956

Papoulis, A., A new method of inversion of the Laplace transform, Quart. App. Math., 14, 405-414, 1957

Piessens, R., Numerical inversion of the Laplace transform, IEEE Transactions on Automatic Control, Correspondence, June, 1969, vol. AC-14, 299-301, 1969

Stehfest, H., Algorithm 368, Collected Algorithms from CACM, 1969

Table 10. Examples of the numerical Laplace transform inversion method.

t	F(t) (exact)	F(t) (LINV) N = 5	N = 7	N = 10
$F(t) = \mathrm{erfc}(1/2\sqrt{t})$; $\hat{F}(s) = (1/s)\exp(-\sqrt{s})$				
1.0	0.479500	0.486963	0.479012	0.479500
2.0	0.617075	0.621102	0.616621	0.617093
3.0	0.683091	0.686021	0.682761	0.683104
4.0	0.723674	0.726073	0.723423	0.723612
5.0	0.751830	0.753913	0.751630	0.751835
6.0	0.772830	0.774701	0.772664	0.772834
7.0	0.789268	0.790984	0.789126	0.789271
8.0	0.802587	0.804183	0.802463	0.802589
9.0	0.813664	0.815164	0.813553	0.813665
10.0	0.823063	0.824484	0.822963	0.823064
		N = 7	N = 10	N = 15
$F(t) = \exp(-t)$; $\hat{F}(s) = 1/(s+1)$				
1.0	0.367879	0.362884	0.367784	0.367875
2.0	0.135335	0.138335	0.135613	0.135343
3.0	0.497879×10^{-1}	0.566080×10^{-1}	0.502589×10^{-1}	0.498002×10^{-1}
4.0	0.183156×10^{-1}	0.239532×10^{-1}	0.184358×10^{-1}	0.182947×10^{-1}
5.0	0.673795×10^{-2}	0.988510×10^{-2}	0.644480×10^{-2}	0.668800×10^{-2}
6.0	0.247875×10^{-2}	0.351690×10^{-2}	0.197091×10^{-2}	0.243243×10^{-2}
7.0	0.911882×10^{-3}	0.569946×10^{-2}	0.387155×10^{-3}	0.892637×10^{-3}
8.0	0.335463×10^{-3}	-0.776785×10^{-3}	-0.917344×10^{-4}	0.347781×10^{-3}
9.0	0.123410×10^{-3}	-0.134902×10^{-2}	-0.166031×10^{-3}	0.159392×10^{-3}
10.0	0.454000×10^{-4}	-0.154009×10^{-2}	-0.110112×10^{-3}	0.932897×10^{-4}

Table 10. Continued.

t	F(t) (exact)	F(t) (LINV) N = 5	F(t) (LINV) N = 7	F(t) (LINV) N = 10
$F(t) = (1/\sqrt{\pi t})\exp(-1/4t)$; $\hat{F}(s) = (1/\sqrt{s})\exp(-\sqrt{s})$				
1.0	0.439391	0.425791	0.438596	0.439558
2.0	0.352065	0.345335	0.352645	0.352051
3.0	0.299691	0.295406	0.300288	0.299659
4.0	0.265004	0.261848	0.265503	0.264976
5.0	0.240008	0.237475	0.240417	0.239987
6.0	0.220930	0.218782	0.221269	0.220914
7.0	0.205762	0.203875	0.206048	0.205750
8.0	0.193334	0.191634	0.193579	0.193325
9.0	0.182911	0.181351	0.183124	0.182904
10.0	0.174007	0.172557	0.174195	0.174002

APPENDIX B

Justification for Ignoring Conductive Heat Transfer within the Solid in the Coordinate Parallel to the Direction of Fluid Flow

A common approximation made in both analytic and numerical heat extraction models for sheet-like fluid flow within a rock mass is that of ignoring conductive heat transfer in the rock in all directions except that coordinate perpendicular to the fluid sheet (Bodvarsson, 1969; Harlow and Pracht, 1972; Grigarten et al., 1975; Blair et al., 1976). If the fluid flow is quasi-uniform and "sufficiently large" the approximation will be quite good. The error incurred by this approximation when dealing with severely non-uniform flow can be large and is discussed in some detail in Chapter IV. The purpose of this investigation is to obtain a lower bound on the fluid flow rate within the fracture below which this approximation breaks down. That is, we will quantify what is meant by a "sufficiently large" flow rate.

The basic heat extraction model under consideration assumes that a flat fracture of infinitesimal width (see Chapter III for the "zero fracture width" approximation) is embedded in the plane $y = 0$ in an infinite, homogeneous, and isotropic rock mass of thermal conductivity k_r and thermal diffusivity a_r. For $t \leq 0$, the temperature of the fluid in the fracture is equal to the initial rock formation

temperature c_1 where c_1 is a constant. For $t > 0$, a stationary fluid flow per unit length of fracture, q, is injected into the fracture at $x = 0$ with an injection temperature T_i. The fluid flow is in the positive x direction. The fluid has specific heat σ_f.

The temperature field within the solid is governed by the heat conduction equation

$$\frac{1}{a_r} \partial_t T - \partial_{xx} T - \partial_{yy} T = 0, \quad y > 0 \tag{B.1}$$

The heat transfer boundary condition at the fracture wall is given by (see equation 3.10)

$$2k_r \partial_y T = \sigma_f q \partial_x T, \quad y \downarrow 0 \tag{B.2}$$

The additional initial and boundary conditions required to complete the statement of the problem are

$$T(x, y, t)\big|_{t \leq 0} = c_1 \tag{B.3}$$

$$T(0, 0, t)\big|_{t > 0} = T_i \tag{B.4}$$

Equations (B.1) through (B.4), which correspond to equations (3.9) through (3.12), are solved using two significantly different methods.

Method I

The first method requires a transformation of the set of independent variables according to

$$T(x, y, t) \rightarrow T'(x, p, t)$$

where

$$p = 2k_r x + \sigma_f q y$$

This transformation reduces the distributed Neumann boundary equation (B. 2) to a homogeneous Neumann boundary condition. Equations (B. 1) through (B. 4), under the above transformation, take the form

$$\frac{1}{a_r} \partial_t T' - \beta \partial_{pp} T' = 0 \qquad \text{(B. 1)'}$$

$$\partial_x T' = 0 \qquad \text{(B. 2)'}$$

$$T'(x, p, t)\big|_{t \leq 0} = c_1 \qquad \text{(B. 3)'}$$

$$T'(0, 0, t)\big|_{t > 0} = T_i \qquad \text{(B. 4)'}$$

where

$$\beta = 4k_r^2 + \sigma_f^2 q^2$$

Applying the Laplace transform with respect to time to (B. 1)' through (B. 4)' and solving the resulting set of equations, one obtains

$$\hat{T}'(x, p, s) = \frac{(T_i - c_1)}{s} \exp\left(-\sqrt{\frac{s}{a_r'\beta}}\, p\right) + \frac{c_1}{s} \qquad \text{(B. 5)}$$

Inverting the above equations to t-space followed by a transformation from the independent variable set (x, p, t) to (x, y, t), we obtain the solution for the temperature field of the rock.

$$T(x, y, t) = (T_i - c_1)\operatorname{erfc}\left(\frac{\alpha x + y}{2\sqrt{a_r' t}}\right) + c_1 \qquad \text{(B. 6)}$$

where

$$\alpha = \frac{2k_r}{\sigma_f q}$$

and

$$a_r' = (1+\alpha^2)a_r$$

Thus we have the interesting result that including conductive heat transport in the rock in the direction parallel to the fluid flow does not, for the case considered, change the form of the solution (see equation 3. 27) but does introduce a flow-dependent "effective" thermal diffusivity a_r' which is greater than the thermal diffusivity of the rock.

Method II

The second method of solution is presented here primarily because it demonstrates an alternative formulation based on the

diffusion of isothermal surfaces. Such an approach gives considerable insight into this simple problem and may be useful in dealing with other conductive heat transfer problems where the geometry of the isothermal surfaces is known a priori to be simple and/or to be time independent.

We note that the inverse transform (with respect to s) of expression (3.25), in the limit of zero fracture width ($\beta \to 0$) and an initial uniform formation temperature ($c_2 = 0$), reduces to

$$T(x, y, t) = (T_i - c_1)\operatorname{erfc}\left(\frac{\alpha x + y}{2\sqrt{a_r t}}\right) + c_1$$

For a given time $t = t^*$, an isothermal surface within the rock mass is a plane, denoted by $\alpha x + y = \text{const.}$ This observation suggests that we try, as a solution of (B.1), a rock temperature field of the form

$$T(x, y, t) = A \operatorname{erfc}\left\{\frac{h(x, y)}{\sqrt{t}}\right\} + B \qquad \text{(B.7)}$$

where A and B are constants and the functional $h(x, y) - \text{const.} = 0$ defines an isothermal surface within the rock.

Inserting (B.7) into equations (B.1) through (B.4), one obtains

$$(\partial_x h)^2 + (\partial_y h)^2 - \frac{1}{4a_r} = 0 \qquad \text{(B.8)}$$

$$2k_r \partial_y h = \sigma_f q \partial_x h, \quad y \downarrow 0 \tag{B. 9}$$

$$A = T_i - c_1, \quad B = c_1 \tag{B. 10}$$

If the geometry of the isothermal surfaces is allowed to be time dependent, $h(x, y, t)$ must also satisfy a diffusion equation given by

$$\frac{1}{a_r} \partial_t h - \partial_{xx} h - \partial_{yy} h = 0, \quad y > 0$$

Expression (B. 8) is called the Eikonal equation and appears often in the context of wave propagation in solids (Officer, 1974).

It is obvious that the reformulation of the problem in terms of diffusing isothermal surfaces has not simplified the mathematics for the general case of an arbitrary field. However, if the "geometrical structure" of the isotherms is known a priori to be time independent, it may be that a solution of (B. 8) through (B. 10) is more easily attained than (B. 1) through (B. 4). For a case under investigation, we consider a surface of the form

$$h(x, y) = d_1 x + d_2 y$$

where d_1 and d_2 are constants to be determined. Inserting the above expression into equations (B. 8) and (B. 12), one obtains

$$d_1^2 + d_2^2 = \frac{1}{4a_r}$$

$$2k_r d_2 = \sigma_f q d_1$$

Thus, d_1 and d_2 are given by

$$d_1 = \frac{\alpha}{2\sqrt{a_r'}}, \qquad d_2 = \frac{1}{2\sqrt{a_r'}}$$

where

$$a_r' = (1+\alpha^2)a_r$$

and we again obtain the result (B. 6).

Based on typical values of the physical parameters of the system (see Appendix E), the table given below displays the dependence of $(1+\alpha^2)^{1/2}$ on q.

q (kg/m. sec)	α^2	$(1+\alpha^2)^{1/2}$
1×10^{-4}	10^2	10.049876
1×10^{-3}	10^0	1.414213
1×10^{-2}	10^{-2}	1.000500
1×10^{-1}	10^{-4}	1.000050

It is evident from these data that for fracture flow rates greater than 0.01 kg/(m. sec) the error incurred by ignoring heat conduction within the rock in the direction of fluid flow is negligible. That is, the "true" rock diffusivity is very close to the value of the "effective"

rock diffusivity. However, the approximation breaks down for flow rates on the order of 0.001 kg/(m.sec) or less.

References Cited

Blair, A.G., J.W. Tester, and J.J. Mortensen, LASL Hot Dry Rock Geothermal Project; July 1, 1975-June 30, 1976, progress report LA-6525-PR, U.S. Energy Research and Development Administration, 1976

Bodvarsson, G., On the temperature of water flowing through fractures, J. Geophys. Res., 74, 1987-1992, 1969

Gringarten, A.C., P.A. Witherspoon, and Y. Ohnishi, Theory of heat extraction from fractured hot dry rock, J. Geophys. Res., 80, 1120-1124, 1975

Harlow, F.H., and W.E. Pracht, A theoretical study of geothermal energy extraction, J. Geophys. Res., 77, 7038-7048, 1972

Officer, C.B., Introduction to Theoretical Geophysics, 385 pp., Springer-Verlag, New York, 1974

APPENDIX C

Temperature Transients in Borehole Flow

Throughout this work, the temperature of the water injected into the heat extraction system (e. g. fracture zone, sedimentary horizon, etc.) has generally been assumed constant. This approximation ignores the thermal interaction that will occur between the fluid flowing in the borehole and the hot rock formation through which the borehole passes. As a result of this thermal interaction, the injection temperature at the borehole-fluid conductor intersection will vary with time. Numerical finite difference models (Lowell and Bodvarsson, 1975) and analytic models (Bodvarsson et al., 1974) have been constructed to investigate temperature transients of borehole flow under the assumption that the rock formation temperature prior to the initiation of flow is uniform and that the flow is constant. The purpose of this investigation is to extend these models of borehole flow to account for an initially non-uniform formation temperature.

The borehole flow model being considered assumes that a borehole of radius r_0 is drilled vertically down through a homogeneous, isotropic, and impermeable solid. At $t \leq 0$, the temperature of the fluid in the borehole is equal to the temperature of the surrounding rock, given by $f(x)$ where x is the distance from the position of fluid injection into the borehole. A constant mass flow F of a

homogeneous liquid having a density ρ_f, velocity v in the positive x direction, and specific heat σ_f enters the borehole at $x = 0$ for $t > 0$. The injection temperature T_i at $x = 0$ is assumed constant. Moreover, the radius r_0 of the borehole is assumed so small that the temperature of the liquid is independent of r, where r is the coordinate perpendicular to the borehole axis. Conductive heat transfer within the rock mass parallel to the borehole axis is ignored.

The temperature field within the solid is governed by the heat conduction equation which, due to cylindrical symmetry, takes the form

$$\frac{1}{a_r}\partial_t T - \frac{1}{r}\partial_r(r\partial_r T) = 0, \quad r > r_0 \tag{C. 1}$$

The heat transfer boundary condition at the borehole wall is given by

$$\rho_f\sigma_f\{\partial_t T + v\partial_x T\} = \frac{2k_r}{r_0}\partial_r T, \quad r \downarrow r_0 \tag{C. 2}$$

The additional initial and boundary conditions required to complete the statement of the problem are given by the following two expressions.

$$T(x, r, t)\big|_{t \leq 0} = f(x) \tag{C. 3}$$

$$T(0, r_0, t)\big|_{t>0} = T_i \tag{C. 4}$$

Laplace transforming equations (C. 1) and (C. 2) with respect to time,

$$\partial_{rr}\hat{T} + \frac{1}{r}\partial_r\hat{T} - \frac{s}{a_r}\hat{T} = -\frac{f(x)}{a_r} \tag{C. 5}$$

$$\partial_x\hat{T}\big|_{r\downarrow r_0} = \{\beta\partial_r\hat{T} - \gamma s\hat{T}\}_{r\downarrow r_0} + \gamma f(x) \tag{C. 6}$$

where

$$\beta = \frac{2k_r\pi r_0}{\sigma_f F} \quad \text{and} \quad \gamma = \frac{\rho_f\pi r_0^2}{F}$$

The general solution to expression (C. 5) that remains finite as $r \to \infty$ is

$$\hat{T}(x, r, s) = \hat{A}(x, s)K_0\left(\sqrt{\frac{s}{a_r}}\, r\right) + \frac{f(x)}{s}, \quad r \geq r_0 \tag{C. 7}$$

where K_0 is the modified Bessel function defined according to the integral representation (Abramowitz and Stegun, 1964)

$$K_0(\xi) = \int_0^\infty \frac{\cos(\xi t)}{\sqrt{t^2+1}}\, dt, \quad \xi > 0$$

Inserting expression (C. 7) into boundary condition (C. 6), we obtain the following first order differential equation for $\hat{A}(x, s)$.

$$\partial_x \hat{A}(x, s) + \beta\psi(s)\sqrt{\frac{s}{a_r}}\,\hat{A}(x, s) = -\frac{f'(x)}{sK_0\left(\sqrt{\frac{s}{a_r}}\,r_0\right)} \qquad (C.8)$$

$$r \geq r_0$$

where $\psi(s)$ is defined by

$$\psi(s) = \frac{K_1\left(\sqrt{\frac{s}{a_r}}\,r_0\right)}{K_0\left(\sqrt{\frac{s}{a_r}}\,r_0\right)} + \frac{\gamma a_r}{\beta}\sqrt{\frac{s}{a_r}} \qquad (C.9)$$

and K_1 is the modified Bessel function, defined according to the integral representation (Abramowitz and Stegun, 1964)

$$K_1(\xi) = \xi \int_1^\infty e^{-\xi t}\sqrt{t^2 - 1}\, dt$$

The general solution to equation (C. 8) is given by

$$\hat{A}(x, s) = \frac{\hat{B}(s)}{K_0\left(\sqrt{\frac{s}{a_r}}\,r_0\right)} \exp\left(-\beta\psi(s)\sqrt{\frac{s}{a_r}}\,x\right)$$

$$- \frac{1}{sK_0\left(\sqrt{\frac{s}{a_r}}\,r_0\right)} \int_0^x \exp\left\{\beta\psi(s)\sqrt{\frac{s}{a_r}}\,(x - x')\right\} f'(x')\,dx' \qquad (C.10)$$

Using expressions (C. 3) and (C. 4), it is easily shown that the function $\hat{B}(s)$ in the above equation is given by

$$\hat{B}(s) = \frac{T_i - f(0)}{s}$$

Evaluating $\hat{A}(x, s)$ assuming an initial formation temperature of the form $f(x) = c_1 + c_2 x$, where c_1 and c_2 are constants, and substituting the resulting expression into (C. 7), we find that

$$\hat{T}(x, r_0, s) = \frac{(T_i - c_1)}{s} \exp(-\beta\psi(s)\sqrt{\frac{s}{a_r}}\, x) - \frac{c_2}{\beta\psi(s)s\sqrt{\frac{s}{a_r}}}\{1 - \exp(-\beta\psi(s)\sqrt{\frac{s}{a_r}}\, x)\} + \frac{(c_1 + c_2 x)}{s} \tag{C. 11}$$

It is of some interest to note that the form of (C. 11) is identical with (3. 25) for the temperature of fluid flowing through a flat fracture. The product $\beta\psi(s)$ in (C. 11) represents a geometrical "form factor", which takes the value $\alpha = 2k_r/(\sigma_f q)$ for the case of fracture flow. Unlike other analytic models of borehole flow (Bodvarsson et al., 1975), the previous formulation has included the time derivative component of boundary condition (C. 2) and as a result, solution (C. 11) includes the effect of a non-zero borehole radius (see discussion of the zero fracture width approximation in Chapter III). As in the case of fracture flow, this term becomes important for the very early history of the borehole flow and its effect damps out rapidly for increasing time.

An analytic form for the inverse Laplace transform of expression (C. 11) will be very difficult to obtain due to the rather complex nature of $\psi(s)$. An approximate inverse has been calculated using the numerical Laplace transform inversion method discussed in Appendix A. The modified Bessel functions K_0 and K_1 are evaluated using polynomial approximations (Abramowitz and Stegun, 1964) and are presented in function subprogram form, BESK0 and BESK1, in Appendix E.

Assuming a borehole radius of $r_0 = 0.1$ m and physical parameters given in Appendix E, some numerical results are displayed in the figures below. Figure 25 represents the case for an initial uniform $(c_2 = 0)$ rock formation temperature of 150°C and a constant fluid injection temperature T_i of 30°C. The temperature of the fluid 1 km from the injection point is plotted as a function of time for several borehole flow rates ranging from 1 kg/sec to 50 kg/sec. The results indicate, for this particular case, a very short relaxation time for borehole flows greater than 10 kg/sec and much longer relaxation times for borehole flows less than 2 or 3 kg/sec. Relaxation time, in the present context, is a measure of the characteristic time required for the temperature of the fluid in the borehole to fall to within a close margin of the asymptote T_i.

Figure 26 shows the effect of a non-uniform initial rock formation temperature on the fluid temperature within a flowing borehole.

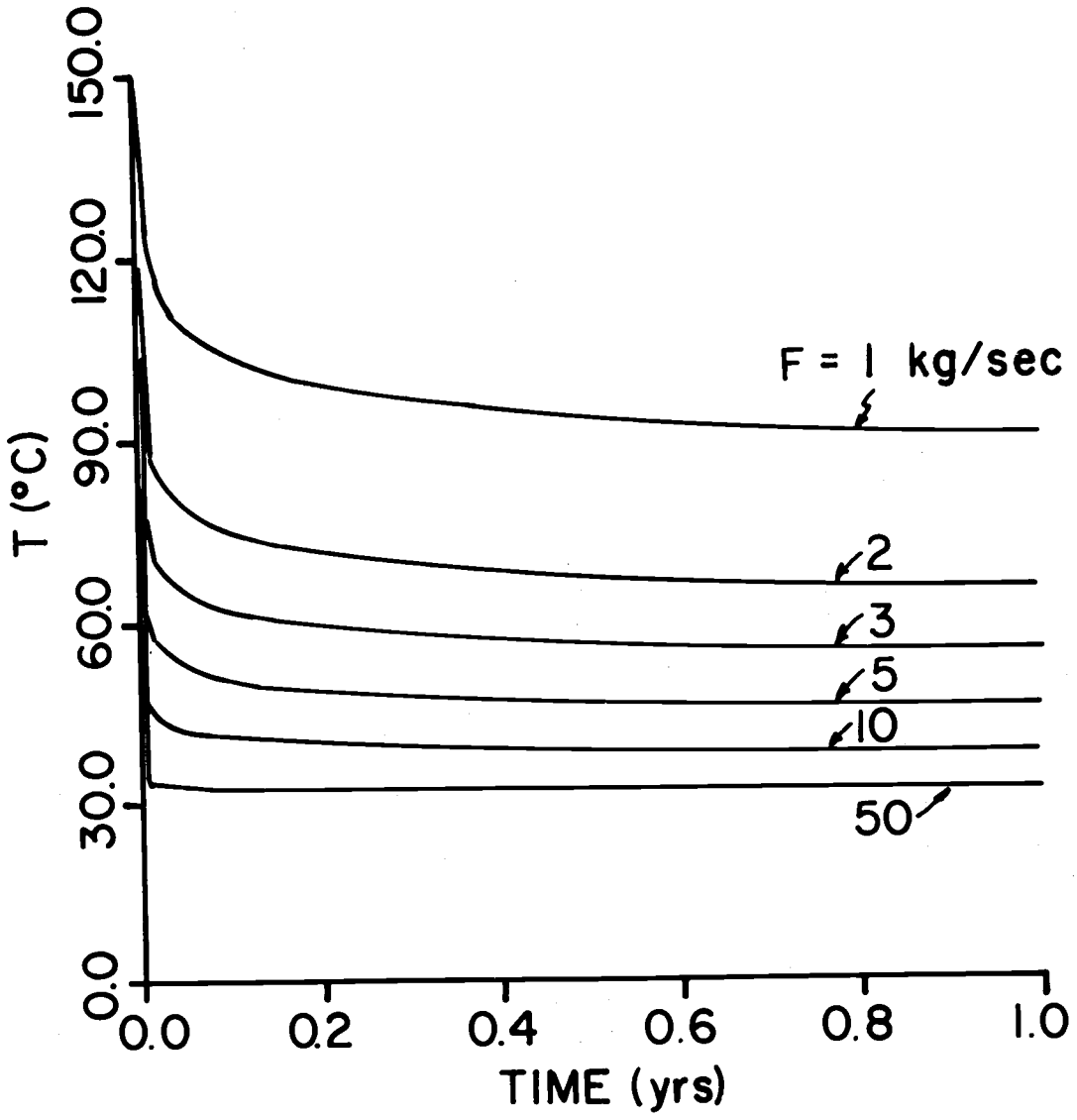

Figure 25. Temperature transients in borehole flow for various flow rates F. Assumes an initial uniform formation temperature with outlet temperature T measured at 1 km from injection port.

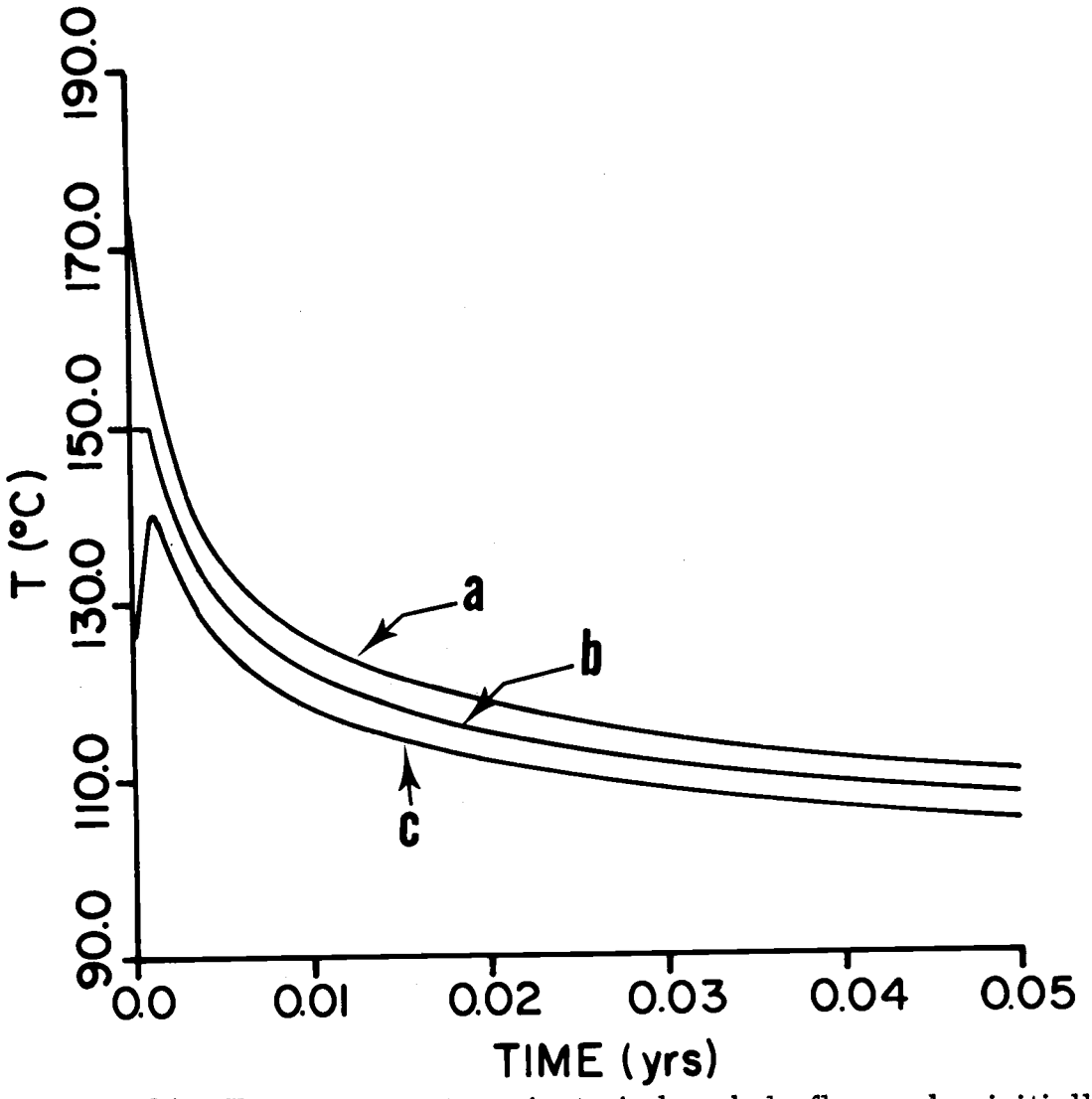

Figure 26. Temperature transients in borehole flow under initially non-uniform formation temperature conditions. Examples given for a downflow (a), uniform (b), and upflow (c) configuration.

In this example, the injection temperature is assumed to be 30°C and the borehole flow is 1 kg/sec. The temperature of the fluid 1 km from the injection point is plotted as a function of time for upflow (c) and downflow (a) configurations as well as the case of an initial uniform rock formation temperature (b) (see Chapter III for terminology). A geothermal gradient of 50°C/km, representative of a moderately high crustal heat flow, is assumed for both the upflow and downflow configurations. The initial rock formation temperature distributions are summarized as follows:

$$f(x) = \begin{cases} 125 + 50x\,^{\circ}C & \text{(Case a)} \\ 150\,^{\circ}C & \text{(Case b)} \\ 175 - 50x\,^{\circ}C & \text{(Case c)} \end{cases}$$

where x is in kilometers.

It is evident from this example that the borehole temperature transients associated with a non-uniform rock formation temperature have, as in the case of fracture flow, characteristic signatures dependent on the geothermal gradient. However, because of the geometry of the heat extraction surface, in this case the borehole wall, the temperature transients are much shorter lived than for the case of fracture flow. Curves (a) and (c) trend asymptotically to curve (b) for increasing time, reflecting the fact that the three cases under consideration have the same initial average formation

temperatures. The short (10^{-3} yr) constant temperature section at the beginning of curve (b) corresponds to the length of time for water entering the borehole at the injection point to travel 1 km through the borehole. The rather sharp break in this curve at 10^{-3} years shows the ability of the numerical Laplace inversion method to represent a step-like function quite well.

Temperature logging in boreholes is usually performed by lowering a temperature sensitive device, such as a thermistor, into the hole and taking either discrete or continuous readings. At temperatures less than 200°C, temperature measurements using a thermistor device can attain a precision of 10^{-2}°C. However, there frequently are difficulties associated with installing down-hole devices due to the elevated temperature and pressure of the downhole environment. Monitoring temperature of a flowing borehole at the top of the borehole is usually much more convenient.

The numerical results presented in Figure 26 suggest that, for small borehole flows, monitoring wellhead fluid temperature as a function of time shortly after (within days or weeks) the initiation of flow will yield a measure of the initial down-hole rock formation temperature distribution. An additional observation is that, assuming the initial rock formation temperature is already known from well logging, a measure of the down-hole in situ thermal conductivity of the rock formation may be obtained using a curve matching procedure. A

method similar to this has recently been used with good results to determine the in situ thermal conductivity of granite at depth in a high crustal heat flow area west of the Valles Caldera in northern New Mexico (Blair et al., 1976).

References Cited

Abramowitz, M., and I. A. Stegun, eds., Handbook of Mathematical Functions, Applied Mathematics Series 55, National Bureau of Standards, Washington, D.C., 1964

Blair, A. G., J. W. Tester, and J. J. Mortensen, LASL Hot Dry Rock Geothermal Project; July 1, 1975-June 30, 1976, progress report LA-6525-PR, U. S. Energy Research and Development Administration, 1976

Bodvarsoson, G., S. Lu, and R. P. Lowell, Temperature transients in flowing boreholes, Geothermics, 3, 21-24, 1974

Lowell, R. P., and G. Bodvarsson, Finite difference models for flowing boreholes, in Proceedings of the Second U. N. Symposium for the Development and Use of Geothermal Resources, San Francisco, 1975

APPENDIX D

Thermal Relaxation Time of Fluid in a Fracture

The length of time for a mass of fluid within a fracture to equilibrate with the surrounding rock can be estimated by the following simple example. Consider a flat slab of fluid of thickness w and initial uniform temperature T_0. At $t = 0$, the temperature of the slab faces is instantaneously increased to the constant temperature T_r. A measure of the thermal relaxation time of the fluid slab is that length of time for the fluid temperature, averaged across the fracture width, to increase to a factor 0.5 of the face temperature T_r. Referring to the diagram below, the problem can be stated as

$$\begin{aligned} &\frac{1}{a_f}\,\partial_t T - \partial_{yy} T = 0, \quad 0 < y < w \\ &T(y,t) = T_0, \qquad t \leq 0 \\ &T(0,t) = T(w,t) = T_r, \quad t > 0 \end{aligned} \tag{D. 1}$$

where a_f is the thermal diffusivity of the fluid and $T(y,t)$ is the temperature of the fluid.

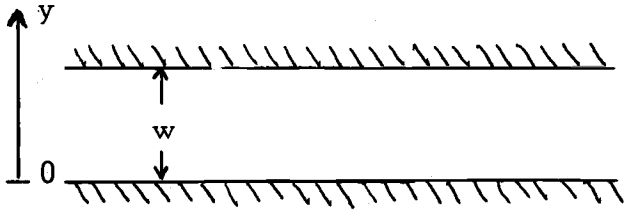

The solution for T is easily obtained using standard classical techniques (Carslaw and Jaeger, 1959) and can be shown to be

$$T(y,t) = \frac{4(T_0-T_r)}{\pi} \sum_{n=0}^{\infty} \frac{1}{(2n+1)} \exp\{-\frac{a_f(2n+1)^2\pi^2 t}{w^2}\}$$

$$\times \sin[\frac{(2n+1)\pi v}{w}] + T_r$$

Averaging the above expression across the slab width, one obtains

$$<T(t)> = \frac{8(T_0-T_r)}{\pi^2} \sum_{n=0}^{\infty} \frac{1}{(2n+1)^2} \exp\{-\frac{a_f(2n+1)^2\pi^2 t}{w^2}\} + T_r \qquad (D.2)$$

Since considerable use of the numerical Laplace transform inversion (see Appendix A) is made in this work, it is of some practical interest to recast the above simple problem so that the numerical inversion can be applied and the results compared with expression (D. 2) as an additional check on the precision of the inversion procedure. To this end, we Laplace transform equations (D. 1) with respect to time and solve the resulting equations for the transform of the fluid temperature, which is easily shown to be

$$\hat{T}(y,s) = \frac{(T_r-T_0)}{s \sinh(\sqrt{\frac{s}{a_f}}\, w)} \{\sinh[\sqrt{\frac{s}{a_f}}\,(w-y)] + \sinh(\sqrt{\frac{s}{a_f}}\, y)\} + \frac{T_0}{s}$$

The average across the fracture width of the above expression is given by

$$\hat{<T(s)>} = \frac{2(T_r - T_0)}{sw \sinh\left(\sqrt{\frac{s}{a_f}}\, w\right)} \sqrt{\frac{a_f}{s}} \left\{\cosh\left(\sqrt{\frac{a_f}{s}}\, w\right) - 1\right\} + \frac{T_0}{s} \qquad (D.3)$$

Figure 27 shows some examples of $<T>/T_r$ plotted as a function of time for several fracture widths ranging from 1 mm to 20 mm, where T_0 is taken to be 0. Values of $<T>/T_r$ computed according to (D.2) are denoted by circles and values computed by applying the numerical inverse Laplace transform to expression (D.3) are denoted by the solid lines. The maximum series truncation error imposed on expansion (D.2) is 10^{-6} and 6 terms were retained in the numerical Laplace transform inversion summation. It is quite evident that the numerical inversion method does an acceptable job of inverting (D.3) for what may be considered a relatively few number of terms retained in the inversion expansion. The numerical results presented here indicate that the relaxation time for fractures of widths of a few millimeters to tens of millimeters varies from a few seconds up to a minute or so, respectively.

References Cited

Carslaw, H. S., and J. C. Jaeger, Conduction of Heat in Solids, 510 pp., John Wiley and Sons, Inc., New York, 1960

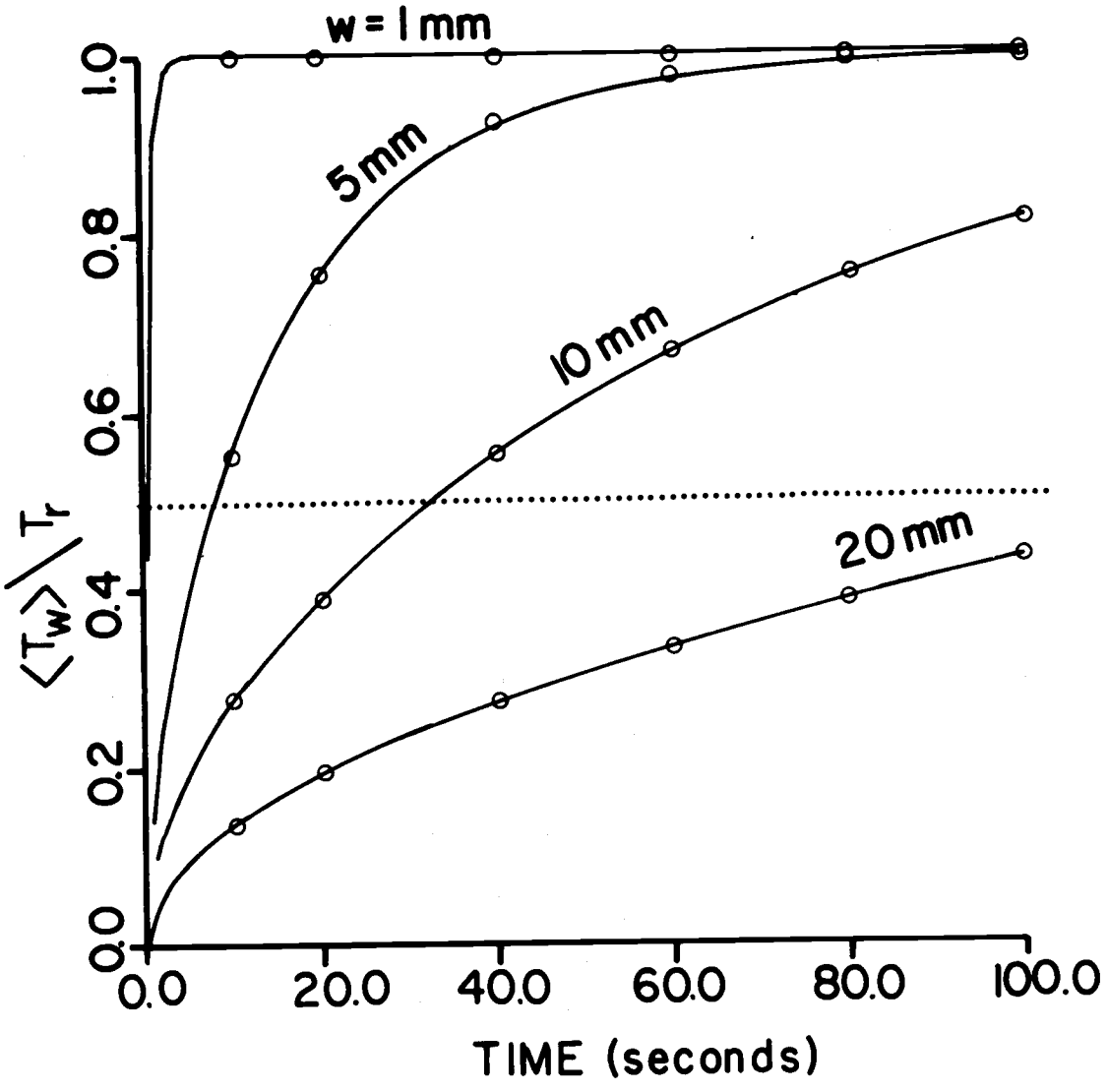

Figure 27. Thermal relaxation of water in a fracture for several values of fracture width. Solid lines correspond to numerical Laplace transform inversion and circles correspond to exact solution.

APPENDIX E

Notes on Numerical Computation and Computer Program Listings

1. All calculations in this work were done on a NOVA 1200 computer with a 32K 16-bit word memory.
2. The following values for the physical parameters were used in the calculations:

$$k_r = 2.1 \text{ watts}/(\text{m.}\,^\circ\text{C})$$

$$a_r = 1.0 \times 10^{-6} \text{ m}^2/\text{sec}$$

$$\rho_r = 2.7 \times 10^{3} \text{ kg}/\text{m}^3$$

$$\sigma_r = 7.8 \times 10^{2} \text{ J}/(\text{kg.}\,^\circ\text{C})$$

$$\alpha_T = 0.6 \times 10^{-5} \,^\circ\text{C}^{-1}$$

$$k_f = 0.63 \text{ watts}/(\text{m.}\,^\circ\text{C})$$

$$a_f = 1.5 \times 10^{-7} \text{ m}^2/\text{sec}$$

$$\rho_f = 1.0 \times 10^{3} \text{ kg}/\text{m}^3$$

$$\sigma_f = 4.2 \times 10^{3} \text{ J}/(\text{kg.}\,^\circ\text{C})$$

3. Unless otherwise stated, all numerical Laplace transform inversions retained 6 terms in the inversion summation (see equation A.8). It was found that an increase in the number of terms

retained resulted in an insignificant change in solution for these cases.

Chapter IV

4. In integrating the Fourier-Galerkin solution (equation 4.36) using the BDA method the integration step size used was $\Delta x = 10$ m. Ten terms were retained in the Fourier expansion of the temperature field given by equation (4.28). Unless otherwise noted in the text, no significant change in solution was observed upon decreasing step size or increasing the number of terms retained in the Fourier expansion.

5. The norm of the Jacobi matrix relevant to the BDA procedure for the solutions based on the Fourier-Galerkin method were found to be (referring to Figure 8):

L = 10 m

$\|M\| \leq 0.46$ (curve a), $0.1 \leq s \leq 10.0$

$\|M\| \leq 0.40$ (curve b), "

$\|M\| = 0.0$ (curve c), "

L = 50 m

$\|M\| \leq 0.24$ (curve a), $0.1 \leq s \leq 10.0$

$\|M\| \leq 0.19$ (curve b), "

$\|M\| = 0.0$ (curve c), "

where s is the transform variable corresponding to t.

6. The specific parameters defining the flow channel configurations in Figure 8 are given by:

curve (a): $z_L = 0.0$

$z_H = 0.3L$

$q_1 = 0.02$ kg/(m. sec)

curve (b): $z_L = 0.3L$

$z_H = 0.6L$

$q_1 = 0.02$ kg/(m. sec)

7. Elements of the matrix inverse indicated in equation (4.41) were computed to a precision of 10^{-6}.

Chapter V

8. Fifteen terms were retained in the numerical Laplace inverse (see equation A. 8) in the inversion of equation (5.24). The time step size was $\Delta t = 0.1$ year.

Chapter VII

9. q* was calculated to a precision of 10^{-6} in the iterative solution of the functional equation given by equation (7.2).

10. Injection depths D_i that minimize the required fluid-rock contact area were calculated to a precision of 0.1 km using Newton's method of root location.

```
      SUBROUTINE BDA(NUM,N,DX,A,F,B)
      DIMENSION F(15),B(15),C(15),A(15,15)
C
C     BDA SOLVES, USING THE IMPLICIT BACKWARD DIFFERENCE APPROX
C     IMATION, THE SET OF COUPLED FIRST ORDER DIFFERENTIAL
C     EQUATIONS WHICH, IN MATRIX FORM, ARE:
C
C                    (D/DX)B + G.B = F
C
C     WHERE: F AND B ARE N-VECTORS
C            G IS AN NXN MATRIX
C
C     IN THE FOLLOWING SCHEME, A IS AN NXN MATRIX WHICH IS EQUAL
C     TO THE INVERSE OF:
C
C                    (I + DX.G)
C
C     WHERE: I IS THE IDENTITY MATRIX
C
C     NUM = X-INDEX AT WHICH SOLUTION VECTOR IS RETURNED
C     DX  = INTEGRATION STEP SIZE
C
C
      KOUNT=1
    5 DO 20 J=1,N
      SUM=0.0
      SUM2=0.0
      DO 10 K=1,N
      SUM=SUM+A(J,K)*B(K)
      SUM2=SUM2+DX*A(J,K)*F(K)
   10 CONTINUE
      C(J)=SUM+SUM2
   20 CONTINUE
      DO 30 J=1,N
      B(J)=C(J)
   30 CONTINUE
      KOUNT=KOUNT+1
      IF(KOUNT.EQ.NUM) GOTO 50
      GOTO 5
   50 RETURN
      END
```

```
      FUNCTION BESK0(X)
      A1=-.57721566
      A2=.42278420
      A3=.23069756
      A4=.03488590
      A5=.00262698
      A6=.00010750
      A7=.00000740
      B1=1.25331414
      B2=-.07832358
      B3=.02189568
      B4=-.01062446
      B5=.00587872
      B6=-.00251540
      B7=.00053208
C
      IF(X.GT.2.0) GOTO 50
      R=(X/2.0)**2
      F=R*(A2+R*(A3+R*(A4+R*(A5+R*(A6+R*A7)))))
      BESK0=-ALOG(X/2.0)*BESI0(X)+A1+F
      RETURN
   50 R=2.0/X
      F=R*(B2+R*(B3+R*(B4+R*(B5+R*(B6+R*B7)))))
      BESK0=EXP(-X)*(B1+F)/SQRT(X)
      RETURN
      END
```

```
      FUNCTION BESI0(X)
      A1=3.5156229
      A2=3.0899424
      A3=1.2067492
      A4=.2659732
      A5=.0360768
      A6=.0045813
      B1=.39894228
      B2=.01328592
      B3=.00225319
      B4=-.00157565
      B5=.00916281
      B6=-.02057706
      B7=.02635537
      B8=-.01647633
      B9=.00392377
C
      T=X/3.75
      IF(X.GT.3.75) GOTO 50
      R=T*T
      F=R*(A1+R*(A2+R*(A3+R*(A4+R*(A5+R*A6)))))
      BESI0=1.0+F
      RETURN
   50 R=1.0/T
      F=R*(B2+R*(B3+R*(B4+R*(B5+R*(B6+R*(B7+R*(B8+R*B9)))))))
      BESI0=EXP(X)*(B1+F)/SQRT(X)
      RETURN
      END
```

```
      FUNCTION BESK1(X)
      A1=.15443144
      A2=-.67278579
      A3=-.18156897
      A4=-.01919402
      A5=-.00110404
      A6=-.00004686
      B1=1.25331414
      B2=.23498619
      B3=-.03655620
      B4=.01504268
      B5=-.00780353
      B6=.00325614
      B7=-.00068245
C
      IF(X.GT.2.0) GOTO 50
      R=(X/2.0)**2
      F=R*(A1+R*(A2+R*(A3+R*(A4+R*(A5+R*A6)))))
      BESK1=(1.0+F+X*ALOG(X/2.0)*BESI1(X))/X
      RETURN
50    R=2.0/X
      F=R*(B2+R*(B3+R*(B4+R*(B5+R*(B6+R*B7)))))
      BESK1=(B1+F)*EXP(-X)/SQRT(X)
      RETURN
      END
```

```
      FUNCTION BESI1(X)
      A1=.87890594
      A2=.51498869
      A3=.15084934
      A4=.02658733
      A5=.00301532
      A6=.00032411
      B1=.39894228
      B2=-.03988024
      B3=-.00362018
      B4=.00163801
      B5=-.01031555
      B6=.02282967
      B7=-.02895312
      B8=.01787654
      B9=-.00420059
C
      T=X/3.75
      IF(X.GT.3.75) GOTO 50
      R=T*T
      F=R*(A1+R*(A2+R*(A3+R*(A4+R*(A5+R*A6)))))
      BESI1=(0.5+F)*X
      RETURN
50    R=1.0/T
      F=R*(B2+R*(B3+R*(B4+R*(B5+R*(B6+R*(B7+R*(B8+R*B9)))))))
      BESI1=EXP(X)*(B1+F)/SQRT(X)
      RETURN
      END
```

```
      FUNCTION CHAN(Q0,Q1,ZL,ZH,Z)
C
C     CHAN GENERATES A FLOW CHANNEL CONFIGURATION OF THE
C     FORM:
C
C     Q(Z) = Q0 , 0<Z<ZL
C          = Q1 , Z>ZH
C          = (A COSINE TAPER) , ZL<Z<ZH
C
C     WHERE THE TAPER WIDTH IS DEFINED AS:
C
C          W = ZH-ZL
C
      PI=3.14159
      W=ZH-ZL
      IF(Z.GE.ZL) GOTO 20
      CHAN=Q0
      RETURN
   20 IF(Z.LT.ZH) GOTO 30
      CHAN=Q1
      RETURN
   30 CHAN=(Q0-Q1)*(1.0-COS((ZH-Z)*PI/W))/2.0+Q1
      RETURN
      END
```

```
 1;C      PROGRAM CHFLO
 2;       COMMON P(2,9)
 3;       DIMENSION X(10,15),S(15),V(15),D(15),B(15)
 4;       DIMENSION G(40),F(15),ZZ(40),TEMP(40),WIDTH(40),B2(15)
 5;       DIMENSION Q(40),A2(15,15),X2(10,15),A(15,15),AINV(15,15)
 6;       CALL INITIAL(6,100,11.0,11.0)
 7;C
 8;C      CHFLO CALCULATES THE TEMPERATURE DISTRIBUTION OF A
 9;C      CHANNELLED FLOW WITHIN A QUASI-FLAT FRACTURE IN AN
10;C      INITIALLY HOT FORMATION. THE FLUID FLOW IS ASSUMED UNI-
11;C      DIRECTIONAL AND THE FLOW CHANNEL CONFIGURATION IS ASSUMED
12;C      PERIODIC IN THE DIRECTION TRANSVERSE TO THE DIRECTION OF
13;C      FLOW. CONDUCTIVE HEAT TRANSFER IN THE ROCK IS ASSUMED TO
14;C      OCCUR IN THE COORDINATE PERPENDICULAR TO THE FRACTURE
15;C      PLANE AS WELL AS IN THE COORDINATE TRANSVERSE TO THE DIR-
16;C      ECTION OF FLOW. IN ADDITION, CHANGE IN FRACTURE WIDTH
17;C      DUE TO THERMAL EXPANSION/CONTRACTION OF THE ROCK MASS
18;C      IS CALCULATED. THIS IS BASED ONLY ON THE THERMOELASTIC
19;C      POTENTIAL WITHOUT REGARD TO STRESS BOUNDARY CONDITIONS
20;C      AT THE FRACTURE WALLS. THE FOURIER-GALERKIN METHOD IS USED
21;C      IN ALL CALCULATIONS. INITIAL FORMATION TEMPERATURE IS
22;C      ASSUMED LINEAR IN THE DIRECTION OF FLOW...I.E. T0=R1+R2*X.
23;C
24;       PI=3.14159
25;C      INPUT ROCK AND FLUID PARAMETERS
26;       ACCEPT "ROCK CONDUCTIVITY...W/M.DEG ",COND
27;       ACCEPT "ROCK DIFFUSIVITY...M**2/SEC ",DIFF
28;       ACCEPT "SPECIFIC HEAT OF FLUID...J/KG.DEG ",SIGMA
29;       ACCEPT "INJECTION TEMP. ",TINJ
30;       ACCEPT "DISPOSAL TEMP. ",TD
31;       ACCEPT "R1 = ",R1
32;       ACCEPT "R2 = ",R2
33;       ACCEPT "CHANNEL DOMAIN LENGTH (M) ",XL
34;       DIFF=31.536E06*DIFF
35;       ACCEPT "NO. Z-POINTS TO BE PLOTTED/INTEGRATED ",NUM
36;C
37;     5 ACCEPT "NO. TERMS IN FOURIER EXPANSION ",N
38;C
39;C      SET UP FOURIER COEFFS. FOR FLOW CHANNEL CONFIGURATION
40;       CALL FOURIER(N,NUM,XL,SIGMA,COND,Q0,Q1,ZL,ZH,G,Q,ZZ
41;      &,WIDTH)
42;C
43;       ACCEPT "PLOT CHANNEL CONFIGURATION? (YES=1)",IFLAG
44;       IF(IFLAG.EQ.1) CALL XPLOT(NUM,ZZ,Q,0,1,-2)
45;       IF(IFLAG.EQ.1) CALL XPLOT(NUM,ZZ,WIDTH,1,1,0)
46;C
47;       ACCEPT "SATISFACTORY CHANNEL? (YES=1) ",IFLAG
48;       IF(IFLAG.NE.1) GOTO 5
49;C
50;       ACCEPT "N-FACTOR FOR LAPLACE INVERSE ",NLAP
51;C
52;       ACCEPT "DO THERMOELASTIC COMPS.?(Y=1,N=0) ",ITHERM
53;       IF(ITHERM.NE.1) GOTO 6
54;       ACCEPT "POISSONS RATIO ",PR
55;       ACCEPT "LINEAR EXPANSION COEF.(E-05) ",EXPC
56;       ACCEPT "INITIAL FRACTURE HALF-WIDTH (MM) ",W0
57;       WFAC=-1.0E-02*EXPC*DIFF*(1.0+PR)/(1.0-PR)
58;C
```

```
      6 ACCEPT "DO ANY PLOTTING?(YES=1) ",JKPL
        ACCEPT "CONVERGENCE PARAMETER FOR MAT INV ",EPS
        DZ=XL/FLOAT(NUM-1)
C
C       CALCULATE V-ARRAY USED IN THE LAPLACE INVERSION
        CALL LINV(NLAP,V)
C
        IFLAG=0
C
        DDX=0.0
        DDT=0.0
C
        ACCEPT "STEP ALONG TIME? (YES=1) ",NTYPE
        IF(NTYPE-1)7,8,7
      7 ACCEPT "X-STEP SIZE (M) ",DDX
        ACCEPT "MAX. X (M) ",XSTOP
        ACCEPT "NO. X GRID POINTS PER STEP ",NX
        ACCEPT "TIME (YRS) ",T
        XMAX=DDX
        NNX=NX
        GOTO 10
      8 ACCEPT "TIME-STEP SIZE (YRS) ",DDT
        ACCEPT "MAX. TIME(YRS) ",TSTOP
        ACCEPT "DISCHARGE POSITION (M) ",XMAX
        ACCEPT "BEGIN TIME (YRS) ",T
        ACCEPT "NO. X GRID POINTS ",NX
C
     10 DX=XMAX/FLOAT(NX-1)
        FX=R1+R2*XMAX/1000.
C
        CO=0.69314/T
        DO 20 J=1,NLAP
        S(J)=FLOAT(J)*CO
     20 CONTINUE
C
        DO 120 KK=1,NLAP
C
C       SET UP COUPLING MATRIX
        DO 30 J=1,N
        BB=FLOAT(J-1)*PI/XL
        D(J)=SQRT(BB*BB+S(KK)/DIFF)
     30 CONTINUE
C
        DO 50 J=1,N
        IF(J.EQ.1) BB=2.0
        IF(J.NE.1) BB=1.0
        DO 40 K=1,N
        I1=J+K-1
        I2=IABS(J-K)+1
        A2(J,K)=D(K)*(G(I1)+G(I2))/(2.0*BB)
        A(J,K)=DX*A2(J,K)
        IF(J.EQ.K) A(J,K)=A(J,K)+1.0
     40 CONTINUE
     50 CONTINUE
C
C
C       CALCULATE INVERSE OF COUPLING MATRIX
        CALL PJINV(EPS,N,A,AINV,ITER,IER)
```

```
C
      DO 60 J=1,N
      F(J)=0.0
   60 CONTINUE
      F(1)=-R2/(S(KK)*(R1-TINJ)*1000.0)
C
C     INITIALIZE SCALED SOLUTION VECTOR
      B(1)=-1.0/S(KK)
      DO 100 J=2,N
      B(J)=0.0
  100 CONTINUE
C
C     INTEGRATE COUPLED D.E.'S VIA PADE BACKWARD DIFFERENCE
C     APPROXIMATION
      CALL BDA(NX,N,DX,AINV,F,B)
C
C     STORE SOLUTION VECTOR IN MASTER ARRAYS
C     X( , )... TEMPERATURE
C     X2( , )... FRACTURE WIDTH
      DO 110 J=1,N
      SUM=0.0
      DO 105 L=1,N
      SUM=SUM+A2(J,L)*B(L)
  105 CONTINUE
      SUM=SUM/S(KK)
      X2(KK,J)=SUM
      X(KK,J)=B(J)
  110 CONTINUE
  120 CONTINUE
C
C
C     MAP MASTER ARRAYS TO THE TIME DOMAIN
      DO 150 J=1,N
      SUM=0.0
      SUM2=0.0
      DO 140 K=1,NLAP
      SUM=SUM+V(K)*X(K,J)
      SUM2=SUM2+V(K)*X2(K,J)
  140 CONTINUE
      B(J)=SUM*0.69314/T
      B2(J)=SUM2*0.69314/T
  150 CONTINUE
C
C
C     CALCULATE TEMPERATURE/FRACTURE WIDTH DISTRIBUTION
C     ALONG Z
      DO 180 J=1,NUM
      ALPHA=SIGMA*Q(J)/(2.0*COND)
      SUM=0.0
      SUM2=0.0
      DO 170 K=1,N
      CO=FLOAT(K-1)*PI/XL
      SUM=SUM+B(K)*(R1-TINJ)*COS(CO*ZZ(J))
      SUM2=SUM2+B2(K)*(R1-TINJ)*COS(CO*ZZ(J))
  170 CONTINUE
      TEMP(J)=SUM+FX
      WIDTH(J)=SUM2*WFAC*ALPHA+W0
  180 CONTINUE
```

```
175;C
176;       IF(JKPL.NE.1) GOTO 185
177;C
178;       CALL XPLOT(NUM,ZZ,TEMP,IFLAG,1,0)
179;       CALL PLOT(P(1,9),0.0,-3)
180;       CALL XPLOT(NUM,ZZ,WIDTH,IFLAG,2,0)
181;       CALL PLOT(P(2,9),0.0,-3)
182;C
183;       IFLAG=1
184;C
185;C      CALCULATE POWER ASSUMING CONDUCTION IN Z-DIRECTION
186;  185 DO 190 J=1,NUM
187;       TEMP(J)=Q(J)*(TEMP(J)-TD)
188;  190 CONTINUE
189;       CALL SIMP(DZ,TEMP,SUM,NUM)
190;       SUM=SUM*SIGMA/XL
191;       SUM=SUM/1000.
192;       P1=SUM
193;C      P1 IS POWER (KW/M).
194;C
195;       WRITE(12,500) T,XMAX,P1
196;  500 FORMAT(1H ,3(F8.3,5X))
197;C
198;       IF(NTYPE.NE.1.AND.XMAX.GE.XSTOP) GOTO 600
199;       IF(NTYPE.EQ.1.AND.T.GE.TSTOP) GOTO 600
200;       IF(NTYPE.EQ.1) T=T+DDT
201;       IF(NTYPE.NE.1) XMAX=XMAX+DDX
202;       IF(NTYPE.NE.1) NX=NX+NNX
203;       GOTO 10
204;  600 IF(NTYPE-1) 7,8,7
205;       END
```

```
 1;C      PROGRAM ECON
 2;       COMMON P(2,9)
 3;       COMMON COND,DIFF,SIGMA,TI,C,GRAD
 4;       DIMENSION T(200),X(3),A(3),D(3),FLOW(3),TAVG(3),TCAP(3)
 5;       DIMENSION XR(200),AA(200),EXR(200),E(3)
 6;       CALL INITIAL(6,100,11.0,11.0)
 7;C
 8;C      ECON CALCULATES THE MINIMUM FLUID-ROCK CONTACT AREA
 9;C      REQUIRED FOR AN ECONOMICALLY VIABLE GEOTHERMAL HEATING/
10;C      POWER SYSTEM. THE PHYSICAL SYSTEM IS APPROXIMATED WITH
11;C      A UNI-DIRECTIONAL FRACTURE FLOW WITH AN IMBEDDED LINEAR
12;C      FLUID LOSS BETWEEN INJECTION AND PRODUCTION PORTS. (SEE
13;C      SUBROUTINE TMOD). THE INITIAL ROCK FORMATION TEMPERATURE
14;C      IS ASSUMED LINEAR WITH DEPTH AND THE MINIMUM PRODUCTION
15;C      TEMPERATURE IS CONSTRAINED TO A GIVEN CONSTANT VALUE. THE
16;C      SYSTEM IS IN AN UPFLOW CONFIGURATION...THAT IS, THE
17;C      INJECTION PORT IS AT A DEEPER (AND HOTTER) POSITION
18;C      WITHIN THE QUASI-VERTICAL FRACTURE THAN THE PRODUCTION
19;C      PORT.
20;C
21;C       ********** INPUT PHYSICAL SYSTEM PARAMETERS **********
22;       ACCEPT "ROCK CONDUCTIVITY...W/M.DEG ",COND
23;       ACCEPT "ROCK DIFFUSIVITY...M**2/SEC ",DIFF
24;       DIFF=31.536*DIFF
25;       ACCEPT "SPECIFIC HEAT OF FLUID...J/KG.DEG ",SIGMA
26;       ACCEPT "INJECTION TEMPERATURE ",TI
27;       ACCEPT "SURFACE TEMPERATURE ",ST
28;C
29;C       ********** INPUT ECONOMIC SYSTEM PARAMETERS **********
30;       ACCEPT "SYSTEM LIFETIME (YRS) ",SL
31;       ACCEPT "MIN. ACCEPTABLE PROD. TEMP. ",PTM
32;       TYPE
33;       TYPE "INPUT (DRILLING COSTS/BOREHOLE) PARAMETERS"
34;       ACCEPT "A1 (K$/KM) = ",A1
35;       ACCEPT "A2 (K$/KM**2) = ",A2
36;       TYPE
37;       ACCEPT "SURFACE EQUIP. COSTS (K$)/BOREHOLE ",SEC
38;       SEC=SEC*2.0
39;       ACCEPT "OPERATION COST PARAMETER ",OCP
40;       ACCEPT "INTEREST COST FACTOR ",CF
41;       TYPE
42;       ACCEPT "INJECTION WATER VALUE (CENTS/MT.) ",WVI
43;       TYPE "INPUT PUMPING COST PARAMETERS"
44;       ACCEPT "B0 (CENTS/MT.) ",B0
45;       ACCEPT "B1 (CENTS/MT.KM) ",B1
46;       TYPE
47;       ACCEPT "SYSTEM EFFICIENCY ",EFF
48;       ACCEPT "BUILD. HEAT =1,POWER=0 ",NTYPE
49;C
50;C       ********** INPUT PROGRAM PARAMETERS **********
51;       ACCEPT "NO. TIME POINTS (LT 200) ",NT
52;       ACCEPT "ACCEPTABLE ERROR IN MINIMUM (KM) ",EPS2
53;       ACCEPT "FLOW CONVERGENCE PARAMETER ",EPS1
54;       DX=EPS2/5.0
55;       DXP=0.0
56;C
57;       N2=1
58;       ACCEPT "STEP PRODUCTION DEPTHS? (YES=1) ",NSTEP
```

```
 59;       IF(NSTEP.NE.1) GOTO 10
 60;       ACCEPT "NUMBER OF CASES ",N2
 61;       ACCEPT "DEPTH CHANGE (KM) ",DXP
 62;C
 63;    10 ACCEPT "MIN. GEOTHERMAL GRADIENT (DEG/KM) ",GMIN
 64;       ACCEPT "GRADIENT SPACING (DEG/KM) ",DG
 65;       ACCEPT "NO. SPECIFIC GRADIENT CASES ",NG
 66;C
 67;       ACCEPT "PLOT AREA VS DEPTH (YES=1) ",NPLOT
 68;       ACCEPT "LIST AREA VS DEPTH? (YES=1) ",NLIST
 69;       IF(NPLOT.EQ.1.OR.NLIST.EQ.1) ACCEPT "XMAX (KM) ",XMAX
 70;       IF(NPLOT.EQ.1.OR.NLIST.EQ.1) ACCEPT "NO. X POINTS ",NX
 71;       NTOP1=1
 72;       NTOP2=3
 73;       IF(NPLOT.EQ.1.OR.NLIST.EQ.1) NTOP2=1
 74;       IF(NPLOT.EQ.1.OR.NLIST.EQ.1) NTOP1=NX
 75;C
 76;       IF(NTYPE.EQ.1) GOTO 20
 77;       TYPE "INPUT EXERGY COEFFICIENTS"
 78;       ACCEPT "E1 (KJ/KG) ",E1
 79;       ACCEPT "E2 (KJ/KG.DEG) ",E2
 80;       ACCEPT "E3 (KJ/KG.DEG**2) ",E3
 81;C
 82;    20 ACCEPT "MAX. FLOW (KG/M.SEC) ",QMAX
 83;       ACCEPT "MIN. FLOW (KG/M.SEC) ",QMIN
 84;C
 85;    22 ACCEPT "FLUID LOSS PARAMETER ",FLF
 86;       IF(NTYPE.EQ.0) GOTO 23
 87;       ACCEPT "DISPOSAL TEMPERATURE ",TD
 88;       ACCEPT "THERMAL WATER VALUE ($/GJ) ",WV
 89;       ACCEPT "DISTRIBUTION COSTS ($/GJ) ",TC
 90;       GOTO 24
 91;    23 ACCEPT "BUSS-BAR POWER COST (CENTS/KWHR) ",PC
 92;C
 93;    24 ACCEPT "BEGIN SEARCH DEPTH (KM) ",SSH
 94;       ACCEPT "UPPER LIMIT ON DEPTH SEARCH (KM) ",SMAX
 95;       IFLAG=0
 96;C
 97;C
 98;C      ********** MARCH THROUGH SPECIFIED GRADIENT CASES *****
 99;       DO 1000 KK=1,NG
100;       GR=GMIN+FLOAT(KK-1)*DG
101;       GRAD=-GR
102;C
103;       DO 900 MM=1,N2
104;C      CALCULATE PRODUCTION WELL DEPTH
105;       D1=(PTM-ST)/GR+FLOAT(MM-1)*DXP
106;C
107;       D2=SSH
108;       IF(NPLOT.EQ.1.OR.NLIST.EQ.1) DX=(XMAX-D2)/FLOAT(NX-1)
109;       IF(NPLOT.EQ.1.OR.NLIST.EQ.1) GOTO 27
110;C
111;    26 D(1)=D2-DX
112;       D(2)=D2
113;       D(3)=D2+DX
114;C
115;    27 DO 500 JJ=1,NTOP1
116;       IF(NPLOT.EQ.1.OR.NLIST.EQ.1) D(1)=D2+FLOAT(JJ-1)*DX
```

```
117;        DO 400 J=1,NTOP2
118;        X(J)=D(J)-D1
119;        XX=X(J)
120;C
121;        C=ST+GR*D(J)
122;C
123;C       D1 IS DEPTH OF PRODUCTION WELL (KM)
124;C       D2 IS DEPTH OF INJECTION WELL (KM)
125;C       X  IS DISTANCE OF PROD. PORT FROM INJ. PORT (KM)
126;C
127;C       ITERATE TO FIND FLOW RATE FL THAT YIELDS TEMP. PTM
128;C       AT TIME SL. (AT PRODUCTION PORT)
129;C       (QMIN,QMAX) IS SEARCH DOMAIN FOR FL
130;C
131;        ITER=1
132;        FL=3.0
133;        Q1=QMIN
134;        Q2=QMAX
135;    30  CALL TMOD(SL,XX,Q1,FLF,TEMP)
136;        F1=TEMP-PTM
137;        CALL TMOD(SL,XX,Q2,FLF,TEMP)
138;        F2=TEMP-PTM
139;        IF(F1.EQ.F2) GOTO 50
140;        Q3=(Q1+Q2)/2.0
141;        CALL TMOD(SL,XX,Q3,FLF,TEMP)
142;        F3=TEMP-PTM
143;        RAT=ABS(Q3-FL)/ABS(Q3)
144;        IF(RAT.LE.EPS1) GOTO 50
145;        FL=Q3
146;C
147;C       LOGIC BLOCK
148;        IF(F3.GT.0.0) Q1=Q3
149;        IF(F3.LT.0.0) Q2=Q3
150;        ITER=ITER+1
151;        IF(ITER.GT.200) GOTO 20
152;        GOTO 30
153;C
154;    50  FLOW(J)=FL
155;C
156;C       CHECK ON CONSTRAINT
157;        CALL TMOD(SL,XX,FL,FLF,TEMP)
158;        IF(ABS(TEMP-PTM).GT.1.0) TYPE "FLOW CONV. ERROR"
159;C
160;        FL2=FL/(1.0-FLF)
161;C       FL2 IS FLOW AT INJECTION PORT (KG/M.SEC)
162;        DEL1=ABS(FL-QMAX)/ABS(QMAX)
163;        DEL2=ABS(FL-QMIN)/ABS(QMIN)
164;        IF(DEL1.LT.0.001) GOTO 20
165;        IF(DEL2.LT.0.001) GOTO 20
166;C
167;C       CALCULATE TEMPERATURE HISTORY OF SYSTEM
168;        DT=SL/FLOAT(NT-1)
169;        DO 60 K=1,NT
170;        TIME=FLOAT(K-1)*DT
171;        CALL TMOD(TIME,XX,FL,FLF,TEMP)
172;        T(K)=TEMP
173;    60  CONTINUE
174;C
```

```
C     CALCULATE SPECIFIC PRODUCTION OF SYSTEM (MT./M**2)
      Q=FL*SL*31.536/X(J)
      Q2=FL2*SL*31.536/X(J)
C
C     CALCULATE TOTAL PUMPING COSTS ($/M**2)
      TPC=(B0+B1*D(J))*Q2*1.0E-02
C
C     CALCULATE INJECTION WATER COSTS ($/M**2)
      TIC=WVI*FLF*Q2*1.0E-02
C
C     CALCULATE AVERAGE PRODUCTION TEMPERATURE
      CALL SIMP(DT,T,ANS,NT)
      TAVG(J)=ANS/SL
C
C     CALCULATE TOTAL ENERGY PRODUCED PER SQUARE METER OF
C     FRACTURE OVER SYSTEM LIFETIME (GJ/M**2)
      IF(NTYPE.EQ.0) GOTO 70
      E(J)=SIGMA*(TAVG(J)-TD)*EFF*Q*1.0E-06
      GOTO 150
   70 DO 80 LL=1,NT
      EXR(LL)=E1+T(LL)*(E2+T(LL)*E3)
   80 CONTINUE
      CALL SIMP(DT,EXR,ANS,NT)
      E(J)=ANS*EFF*Q*1.0E-03/SL
C
C     CALCULATE SPECIFIC REVENUE OF SYSTEM ($/M**2)
  150 IF(NTYPE.EQ.1) SPV=(WV-TC)*E(J)
      IF(NTYPE.EQ.0) SPV=PC*E(J)/0.36
C
C     SUBTRACT PUMPING COSTS AND INJECTION WATER COSTS FROM
C     SPECIFIC REVENUE
      SPV=SPV-TPC-TIC
C
C     CALCULATE DRILLING COST FOR SYSTEM (K$)
      DRIL=A1*(D1+D(J))+A2*(D1**2+D(J)**2)
C
C     CALCULATE TOTAL CAPITAL INVESTMENT (MEGA$)
      TCAP(J)=(SEC+DRIL)/1.0E03
C
C     CALCULATE TOTAL OPERATION COSTS (K$)
      OC=OCP*(SEC+DRIL)*SL
C
C     CALCULATE TOTAL EXPENDITURES OVER SYSTEM LIFETIME (K$)
      TOTEX=CF*(SEC+DRIL)+OC
C
C     CALCULATE CONTACT AREA (KM**2)
      IF(SPV.GT.0.0) A(J)=TOTEX*1.0E-03/SPV
      IF(SPV.LE.0.0) A(J)=-1.0
C
      IF(NLIST.EQ.1) WRITE(12,2001) GR,D1,D(1),A(1)
C
  400 CONTINUE
      IF(NPLOT.EQ.1) XR(JJ)=D(1)
      IF(NPLOT.EQ.1) AA(JJ)=A(1)
  500 CONTINUE
C     ************************************************************
C
      IF(NPLOT.EQ.1) CALL XPLOT(NX,XR,AA,IFLAG,1.0)
```

```
      IFLAG=1
      IF(NPLOT.EQ.1.OR.NLIST.EQ.1) GOTO 1000
C
C     CALCULATE FIRST DERIVATIVE OF SYSTEM FUNCTION
      DER1=(A(3)-A(1))/(2.0*DX)
C     CALCULATE SECOND DERIVATIVE OF SYSTEM FUNCTION
      DER2=(A(3)-2.0*A(2)+A(1))/(DX**2)
C
C     UPDATE DISTANCE BETWEEN INJECTION AND PRODUCTION PORTS.
C     NEWTON'S METHOD IS USED TO FIND THE ZERO OF THE
C     SYSTEM FUNCTION FIRST DERIVATIVE
      DD2=D2-DER1/DER2
C
C     CHECK IF UPDATE IS IN SEARCH RANGE
      IF(DD2.LE.D1) GOTO 24
      IF(DD2 GE.SMAX) GOTO 24
C
C     CHECK FOR CONVERGENCE
      IF(ABS(DD2-D2).LT.EPS2) GOTO 600
      D2=DD2
      GOTO 26
C
C     HAVE CONVERGED ON OPTIMUM SYSTEM CONFIGURATION
  600 SW=A(2)/X(2)
      ASP=SW/X(2)
      FLO=FLOW(2)
      Q=FLO*SL*31.536/X(2)
      POW=E(2)*A(2)*31.71/SL
      EN=POW*SL
      FF=FLO*SW*1.0E03
C
C     A(2) = FLUID-ROCK CONTACT AREA (KM**2)
C     SW   = 'STRIP WIDTH' (KM)
C     ASP  ='ASPECT RATIO'
C     FLO  = PRODUCTION FLOW (KG/M.SEC)
C     Q    = SPECIFIC PRODUCTION (MET. TONS/M**2)
C     POW  = POWER PRODUCTION (MWATTS)
C     EN   = ENERGY (MW-YRS)
C     FF   = PRODUCTION WELL FLOW (KG/SEC)
C
      WRITE(12,2000) GR,D1,D(2),Q,FLO,TAVG(2),A(2),SW,ASP,
     CPOW,EN,FF,TCAP(2)
C
C     UPDATE BEGIN SEARCH POINT FOR NEXT CASE
      SSH=D(2)
C
  900 CONTINUE
 1000 CONTINUE
      PAUSE
C
 2000 FORMAT(1H ,13(F7.3,2X))
 2001 FORMAT(1H ,4(F7.3,3X))
      GOTO 22
      END
```

```
1;        FUNCTION ERF(X)
2;C
3;C       ERF COMPUTES THE ERROR FUNCTION ERF(X). FROM ABROMOWITZ
4;C       AND STEGUN, PAGE 299 (7.1.26). ESTIMATED ERROR IN
5;C       RETURNED FUNCTION VALUE IS LESS THAN 1.5E-07.
6;C
7;        P=.3275911
8;        A1=.254829592
9;        A2=-.284496736
10;       A3=1.421413741
11;       A4=-1.453152027
12;       A5=1.061405429
13;       T=1.0/(1.0+P*X)
14;       F1=A1+T*(A2+T*(A3+T*(A4+T*A5)))
15;       F1=T*F1
16;       ERF=1.0-F1*EXP(-X*X)
17;       RETURN
18;       END
```

```
      SUBROUTINE FOURIER(N,NUM,XLEN,SIGMA,COND,Q0,Q1,ZL,ZH,G
     0,F,ZZ,H)
      DIMENSION G(40),F(40),ZZ(40),H(40)
C
      PI=3.14159
      M=2*N-1
C
C     INPUT NUMBER OF Z-POINTS ON WHICH FOURIER COEFFS. ARE TO
C     BE COMPUTED
      ACCEPT "NZ = ",NZ
C
C     SPECIFY MEAN FLOW (AVERAGE ACROSS CHANNELS)
      ACCEPT "QBAR...KG/M.SEC ",QBAR
C
      ACCEPT "ZL (M) ",ZL
      ACCEPT "CHANNEL TAPER WIDTH (M) ",W
C
C     (SEE FUNCTION CHAN FOR DEFINITIONS OF W,ZL,ZH,Q0,Q1)
C
      ZH=ZL+W
C
      ACCEPT "Q1..KG/M.SEC = ",Q1
      F1=W/(2.0*XLEN)
      F2=1.0-(W+ZL)/XLEN
      F3=F1+ZL/XLEN
      Q0=(QBAR-Q1*(F1+F2))/F3
      TYPE "Q0..KG/M.SEC = ",Q0
C
C
      NZM1=NZ-1
      DZ=XLEN/FLOAT(NZM1)
      DO 10 J=1,NZ
      Z=FLOAT(J-1)*DZ
      F(J)=2.0*COND/(SIGMA*CHAN(Q0,Q1,ZL,ZH,Z))
   10 CONTINUE
C
C     ***** DETERMINE FOURIER COEFFS. OF F(Z) *****
C     CALCULATE DC COEFF.
      SUM=0.0
      DO 20 J=2,NZM1
      SUM=SUM+F(J)
   20 CONTINUE
      G(1)=((F(1)+F(NZ))+2.0*SUM)*DZ/XLEN
C
C     CALCULATE HIGHER COEFFS.
      S=-1.0
      DO 40 K=2,M
      XK=FLOAT(K-1)
      SUM=0.0
      DO 30 J=2,NZM1
      Z=FLOAT(J-1)*DZ
      SUM=SUM+F(J)*COS(XK*PI*Z/XLEN)
   30 CONTINUE
      G(K)=((F(1)+S*F(NZ))+2.0*SUM)*DZ/XLEN
      S=-S
   40 CONTINUE
C
      DZ=XLEN/FLOAT(NUM-1)
```

```
59;C
60;       DO 70 J=1,NUM
61;       ZZ(J)=FLOAT(J-1)*DZ
62;       H(J)=CHAN(Q0,Q1,ZL,ZH,ZZ(J))
63;       SUM=0.0
64;       DO 60 K=2,M
65;       XK=FLOAT(K-1)
66;       SUM=SUM+G(K)*COS(XK*PI*ZZ(J)/XLEN)
67;    60 CONTINUE
68;       F(J)=G(1)/2.0+SUM
69;       F(J)=2.0*COND/(SIGMA*F(J))
70;    70 CONTINUE
71;       CALL SIMP(DZ,F,ANS,NUM)
72;       ANS=ANS/XLEN
73;C
74;       TYPE "QBAR CHECK (KG/M.SEC) ",ANS
75;C      'QBAR CHECK' CHECKS HOW WELL THE CALCULATED FOURIER
76;C      COEFFICIENTS DUPLICATE THE MEAN FLOW ORIGINALLY REQUESTED.
77;C
78;       RETURN
79;       END
```

```
      SUBROUTINE LINV(N,T,FA,V,M)
      DIMENSION V(100),G(0:100),H(100)
C
C     LINV CALCULATES THE NUMERICAL INVERSE OF A LAPLACE
C     TRANSFORM. ALGORITHM 368 (CACM).
C
C     T = REAL SPACE INDEPENDENT VARIABLE
C     N = SOME EVEN INTEGER OF THE ORDER OF THE NUMBER OF DIGITS
C         THE MACHINE IS CAPABLE OF WORKING WITH.
C     M = SOME INTEGER NOT EQUAL TO N AT FIRST CALL TO LINV.
C     FA = THE RETURNED APPROXIMATE VALUE OF F(T).
C     V = AN INTERNAL ARRAY
C     XINV = A FUNCTION REPRESENTING THE TRANSFORM OF F(T)
C
      IF(M.EQ.N) GOTO 100
      G(0)=1.0
      NH=N/2
      DO 10 I=1,N
      G(I)=G(I-1)*FLOAT(I)
   10 CONTINUE
      H(1)=2.0/G(NH-1)
      DO 20 I=2,NH
      H(I)=(FLOAT(I)**NH)*G(2*I)/(G(NH-I)*G(I)*G(I-1))
   20 CONTINUE
      SN=2.0*FLOAT(MOD(NH,2))-1.0
      DO 40 I=1,N
      V(I)=0.0
      NTOP=MIN0(I,NH)
      NBOT=(I+1)/2
      DO 30 K=NBOT,NTOP
      V(I)=V(I)+H(K)/(G(I-K)*G(2*K-I))
   30 CONTINUE
      V(I)=SN*V(I)
      SN=-SN
   40 CONTINUE
C
      M=N
  100 FA=0.0
      A=0.69314/T
      DO 110 I=1,N
      ARG=FLOAT(I)*A
C     ARG = LAPLACE TRANSFORM SPACE INDEPENDENT VARIABLE
      FA=FA+V(I)*XINV(ARG)
  110 CONTINUE
      FA=A*FA
      RETURN
      END
```

```
1;       SUBROUTINE PJINV(EPS,N,A,SUM,ITER,IER)
2;       DIMENSION SUM2(15,15),D(15),A(15,15),SUM(15,15)
3;C
4;C      PJINV CALCULATES THE INVERSE OF AN NXN MATRIX USING
5;C      THE POINT JACOBI METHOD.
6;C
7;C      EPS  = CONVERGENCE CRITERION APPLIED TO EACH ELEMENT OF
8;C             THE RETURNED SOLUTION
9;C      N    = RANK OF MATRIX
10;C     A    = MATRIX TO BE INVERTED (RANK N)
11;C     SUM  = RETURNED INVERSE OF A
12;C     ITER = ITERATIONS REQUIRED TO OBTAIN DESIRED CONVERGENCE
13;C            CRITERION.
14;C
15;      IER=1
16;      DO 10 J=1,N
17;      D(J)=1.0/A(J,J)
18;      A(J,J)=0.0
19;   10 CONTINUE
20;C
21;      DO 30 J=1,N
22;      DO 20 K=1,N
23;      IF(J.EQ.K) F=1.0
24;      IF(J.NE.K) F=0.0
25;      A(J,K)=-D(J)*A(J,K)
26;      SUM(J,K)=A(J,K)+F
27;   20 CONTINUE
28;   30 CONTINUE
29;C
30;      ITER=0
31;   35 ITER=ITER+1
32;      DO 37 J=1,N
33;      DO 36 K=1,N
34;      SUM2(J,K)=SUM(J,K)
35;   36 CONTINUE
36;   37 CONTINUE
37;      IF(ITER.GT.200) GOTO 500
38;      DO 60 J=1,N
39;      DO 50 K=1,N
40;      IF(J.EQ.K) F=1.0
41;      IF(J.NE.K) F=0.0
42;      SS=0.0
43;      DO 40 L=1,N
44;      SS=SS+SUM(J,L)*A(L,K)
45;   40 CONTINUE
46;      SUM(J,K)=SS+F
47;   50 CONTINUE
48;   60 CONTINUE
49;C
50;C     CHECK FOR CONVERGENCE
51;      DO 80 J=1,N
52;      DO 70 K=1,N
53;      DELT=ABS((SUM2(J,K)-SUM(J,K))/SUM(J,K))
54;      IF(DELT.GT.EPS) GOTO 35
55;   70 CONTINUE
56;   80 CONTINUE
57;C
58;C     HAVE CONVERGED ON SOLUTION
```

```
59;       DO 110 J=1,N
60;       DO 100 K=1,N
61;       SUM(J,K)=D(K)*SUM(J,K)
62;   100 CONTINUE
63;   110 CONTINUE
64;       RETURN
65;C
66;   300 IER=0
67;       RETURN
68;       END
```

```
 1;       SUBROUTINE SIMP(H,Y,ANS,NDIM)
 2;C
 3;C      SIMP CALCULATES THE INTEGRAL OF AN EQUIDISTANTLY SPACED
 4;C      TABULATED FUNCTION BY SIMPSON'S RULE.
 5;C
 6;C      H    = INTEGRATION STEP SIZE
 7;C      Y    = INPUT VECTOR OF FUNCTION VALUES
 8;C      ANS  = RETURNED VALUE OF INTEGRAL
 9;C      NDIM = DIMENSION OF Y
10;C      Z    = INTERNAL VECTOR OF INTEGRAL VALUES
11;C
12;C      FROM: IBM SCIENTIFIC SUBROUTINE PACKAGE
13;C
14;       DIMENSION Y(40),Z(40)
15;       HT=0.333333333*H
16;       IF(NDIM-5) 7,8,1
17;C
18;C      NDIM IS GREATER TNAN 5. PREPARATIONS OF INTEGRATION LOOP
19;     1 SUM1=Y(2)+Y(2)
20;       SUM1=SUM1+SUM1
21;       SUM1=HT*(Y(1)+SUM1+Y(3))
22;       AUX1=Y(4)+Y(4)
23;       AUX1=AUX1+AUX1
24;       AUX1=SUM1+HT*(Y(3)+AUX1+Y(5))
25;       AUX2=HT*(Y(1)+3.875*(Y(2)+Y(5))+2.625*(Y(3)+Y(4))+Y(6))
26;       SUM2=Y(5)+Y(5)
27;       SUM2=SUM2+SUM2
28;       SUM2=AUX2-HT*(Y(4)+SUM2+Y(6))
29;       Z(1)=0.0
30;       AUX=Y(3)+Y(3)
31;       AUX=AUX+AUX
32;       Z(2)=SUM2-HT*(Y(2)+AUX+Y(4))
33;       Z(3)=SUM1
34;       Z(4)=SUM2
35;       IF(NDIM-6)5,5,2
36;C
37;C      INTEGRATION LOOP
38;     2 DO 4 I=7,NDIM,2
39;       SUM1=AUX1
40;       SUM2=AUX2
41;       AUX1=Y(I-1)+Y(I-1)
42;       AUX1=AUX1+AUX1
43;       AUX1=SUM1+HT*(Y(I-2)+AUX1+Y(I))
44;       Z(I-2)=SUM1
45;       IF(I-NDIM) 3,6,6
46;     3 AUX2=Y(I)+Y(I)
47;       AUX2=AUX2+AUX2
48;       AUX2=SUM2+HT*(Y(I-1)+AUX2+Y(I+1))
49;     4 Z(I-1)=SUM2
50;     5 Z(NDIM-1)=AUX1
51;       Z(NDIM)=AUX2
52;       ANS=Z(NDIM)
53;       RETURN
54;     6 Z(NDIM-1)=SUM2
55;       Z(NDIM)=AUX1
56;       ANS=Z(NDIM)
57;       RETURN
58;C      END OF INTEGRATION LOOP
```

```
59;C
60;     7 IF(NDIM-3) 12,11,8
61;C
62;C      NDIM IS EQUAL TO 4 OR 5
63;     8 SUM2=1.125*HT*(Y(1)+3.0*Y(2)+3.0*Y(3)+Y(4))
64;       SUM1=Y(2)+Y(2)
65;       SUM1=SUM1+SUM1
66;       SUM1=HT*(Y(1)+SUM1+Y(3))
67;       Z(1)=0.0
68;       AUX1=Y(3)+Y(3)
69;       AUX1=AUX1+AUX1
70;       Z(2)=SUM2-HT*(Y(2)+AUX1+Y(4))
71;       IF(NDIM-5) 10,9,9
72;     9 AUX1=Y(4)+Y(4)
73;       AUX1=AUX1+AUX1
74;       Z(5)=SUM1+HT*(Y(3)+AUX1+Y(5))
75;    10 Z(3)=SUM1
76;       Z(4)=SUM2
77;       ANS=Z(NDIM)
78;       RETURN
79;C
80;C      NDIM IS EQUAL TO 3
81;    11 SUM1=HT*(1.25*Y(1)+2.0*Y(2)-0.25*Y(3))
82;       SUM2=Y(2)+Y(2)
83;       SUM2=SUM2+SUM2
84;       Z(3)=HT*(Y(1)+SUM2+Y(3))
85;       Z(1)=0.0
86;       Z(2)=SUM1
87;       ANS=Z(NDIM)
88;       RETURN
89;C
90;    12 IF(NDIM.EQ.1) GOTO 15
91;       Z(1)=0.0
92;       Z(2)=(Y(1)+(Y(2)-Y(1))*0.5)*HT
93;       ANS=Z(NDIM)
94;       RETURN
95;C
96;    15 Z(1)=0.0
97;       ANS=Z(NDIM)
98;       RETURN
99;       END
```

PAGE 1

```
 1;       SUBROUTINE TMOD(T,X,Q,FLF,TEMP)
 2;       COMMON P(2,9)
 3;       COMMON XK,A,SIGMA,TI,C,D
 4;C
 5;C
 6;C      TMOD CALCULATES PRODUCTION WELL HEAD TEMPERATURE FOR
 7;C      A SIMPLE FRACTURE FLOW MODEL THAT ACCOUNTS FOR A DISPRIB-
 8;C      UTED FLUID LOSS BETWEEN INJECTION AND PRODUCTION PORTS
 9;C      OF THE SYSTEM. THE MODEL ASSUMES A FRACTURE FLOW OF THE
10;C      FORM Q(X) = Q0 + EPS*X WHERE X IS THE DISTANCE FROM THE
11;C      INJECTION PORT IN THE DIRECTION OF FLOW.
12;C
13;C      PARAMETERS
14;C      T.......TIME (YRS)
15;C      X.......DISTANCE FROM INJECTION PORT TO PRODUCTION PORT (KM)
16;C      Q.......PRODUCTION WELL FLOW (KG/M.SEC)
17;C      FLF.....FLUID LOSS PARAMETER
18;C              =(Q(INJ)-Q(PROD))/Q(INJ)
19;C
20;C      XK......ROCK CONDUCTIVITY (W/M.DEG)
21;C      A.......ROCK DIFFUSIVITY (KM**2/YR)
22;C      SIGMA...FLUID SPECIFIC HEAT (J/KG.DEG)
23;C      TI......INJECTION TEMPERATURE
24;C
25;C      INITIAL ROCK FORMATION TEMPERATURE IS C + D*X
26;C
27;C
28;       PI=3.14159
29;       Q0=Q/(1.0-FLF)
30;       EPS=(Q-Q0)/X
31;       ALPHA=2.0*XK/(SIGMA*Q0)
32;       IF(T.EQ.0.0) GOTO 100
33;       IF(EPS.EQ.0.0) GOTO 70
34;       GAM=EPS/Q0
35;       BETA=ALPHA*ALPHA*ALOG(1.0+GAM*X)/(2.0*A*T*GAM*GAM)
36;       TEST=1.0+BETA
37;       A1=GAM*SQRT(A*T)/ALPHA
38;       A2=ALPHA*ALOG(1.0+GAM*X)/(2.0*GAM*SQRT(A*T))
39;       A3=1.0+GAM*X
40;C
41;       C1=1.0-ERF(ABS(A2))
42;       E1=(TI-C)*C1
43;C
44;       E2=D*A3/GAM
45;C
46;       IF(ABS(BETA).LT.0.01) GOTO 40
47;       B1=1.0+ERF(ABS(A1))
48;       IF(TEST.LT.0.0) B2=1.0-ERF(TEST*A1)
49;       IF(TEST.GE.0.0) B2=1.0+ERF(ABS(TEST*A1))
50;       IF(ABS(A1).GT.8.0) A1=8.0
51;       C3=A3*EXP(A1*A1)*(B1-B2)
52;       E3=D*C3/GAM
53;       GOTO 50
54;C
55;    40 E3=-2.0*A2*A3*D/(GAM*SQRT(PI))
56;C
57;    50 E4=(1.0-ERF(A2))*D/GAM
58;C
```

```
      TEMP=E1-E2+E3+E4+C+D*X
C
      RETURN
C
   70 A1=ALPHA*X/(2.0*SQRT(A*T))
      IF(A1.GT.8.0) A1=8.0
      A2=2.0*D*SQRT(A*T/PI)/ALPHA
      B1=(TI-C-D*X)*(1.0-ERF(A1))
      B2=A2*(1.0-EXP(-A1*A1))
      TEMP=B1-B2+C+D*X
      RETURN
  100 TEMP=C+D*X
      RETURN
      END
```

```
      SUBROUTINE XPLOT(N,X,Y,IFLAG,IT,NSYM)
      COMMON/PLABEL/LAB1(1),LAB2(1)
      COMMON P(2,9)
      DIMENSION X(200),Y(200),A(200),B(200)
C
      DATA LAB1/2H X/
      DATA LAB2/2H Y/
      IF(IFLAG.EQ.1) GOTO 100
      IF(IT.EQ.2) GOTO 20
C
      ACCEPT "LENGTH (INCHES) OF ABSICISSA ",P(1,1)
      ACCEPT "HEIGHT (INCHES) OF ORDINATE ",P(1,2)
      ACCEPT "MAX. ABCISSA VALUE ",P(1,3)
      ACCEPT "MIN. ABCISSA VALUE ",P(1,4)
      ACCEPT "MAX. ORDINATE VALUE ",P(1,5)
      ACCEPT "MIN. ORDINATE VALUE ",P(1,6)
      P(1,7)=(P(1,3)-P(1,4))/P(1,1)
      P(1,8)=(P(1,5)-P(1,6))/P(1,2)
      P(1,9)=P(1,1)+1.0
      IF(IT.EQ.1) GOTO 50
      TYPE
   20 TYPE "PARAMETERS FOR PLOT 2"
      ACCEPT "LENGTH (INCHES) OF ABSCISSA ",P(2,1)
      ACCEPT "HEIGHT (INCHES) OF ORDINATE ",P(2,2)
      ACCEPT "MAX. ABCISSA VALUE ",P(2,3)
      ACCEPT "MIN. ABCISSA VALUE ",P(2,4)
      ACCEPT "MAX. ORDINATE VALUE ",P(2,5)
      ACCEPT "MIN. ORDINATE VALUE ",P(2,6)
      P(2,7)=(P(2,3)-P(2,4))/P(2,1)
      P(2,8)=(P(2,5)-P(2,6))/P(2,2)
      P(2,9)=-P(1,9)
C
C
   50 CALL AXIS(0.0,0.0,LAB2,2,P(IT,2),90.0,P(IT,6),P(IT,8),2)
      CALL AXIS(0.0,0.0,LAB1,-2,P(IT,1),0.0,P(IT,4),P(IT,7),2)
C
  100 DO 150 J=1,N
      A(J)=(X(J)-P(IT,4))/P(IT,7)
      B(J)=(Y(J)-P(IT,6))/P(IT,8)
  150 CONTINUE
      NN=N
C
      CALL LINE(A,B,NN,NSYM,1)
      CALL PLOT(0.0,0.0,3)
C
      RETURN
      END
```